The boundary element method : errors and gridding for problems with hot spots

The Boundary Element Method: Errors and gridding for problems with hot spots

CIP-DATA LIBRARY TECHNISCHE UNIVERSITEIT EINDHOVEN

Kakuba, Godwin

The Boundary Element Method:
Errors and gridding for problems with hot spots /
by Godwin Kakuba. -
Eindhoven, Eindhoven University of Technology, 2011.
A catalogue record is available from the Eindhoven University of Technology Library

Proefschrift. - ISBN: 978-90-386-2443-3

NUR 919
Subject headings: boundary element methods / integral equations; numerical methods /
boundary value problems /
boundary elements; numerical methods
2000 Mathematics Subject Classification: 65N38, 65N50, 65N55, 65N06, 74S15, 65R20, 35Q30, 80A25

The Boundary Element Method: Errors and gridding for problems with hot spots

PROEFSCHRIFT

ter verkrijging van de graad van doctor aan de
Technische Universiteit Eindhoven, op gezag van de
rector magnificus, prof.dr.ir. C.J. van Duijn, voor een
commissie aangewezen door het College voor
Promoties in het openbaar te verdedigen
op donderdag 31 maart 2011 om 16.00 uur

door

Godwin Kakuba

geboren te Rwengoma, Oeganda

Dit proefschrift is goedgekeurd door de promotor:

prof.dr. R.M.M. Mattheij

Copromotor:
dr.ir. M.J.H. Anthonissen

Acknowledgements

Having done a general and theoretical maths program in my bachelors degree at Makerere university, I was very curious and interested in applied mathematics when I came to the Netherlands in 2003 for a masters in industrial and applied mathematics. I was not disappointed. I liked and enjoyed the program and therefore the choice of continuing with my PhD at the same University was an easy one for me. I joined the CASA group as a PhD student and my research with the group has led to this thesis. There are a lot of people whose contribution to this cause is indispensable and I would like to register my acknowledgements here to some of them.

In the first place, I would like to express my sincere gratitude to prof.dr. R.M.M. Mattheij my promotor. He has given me tremendous support without which this thesis would not have been a reality. This includes the support to attend the many international conferences which were a delight. Then I would like to thank dr.ir. M. J. H Anthonissen for the great support he has offered me in working on this thesis. I benefited a lot from his expertise in local defect correction techniques plus his comments as he read through my thesis.

I would like to thank the staff at the CASA group who never got tired of my questions. In particular am very grateful to dr.ir. ter Morche, prof Jan de Graaf and dr. M.E. Hochstenbach for the several fruitful discussions we had together. To dr.ir. B.J. van der Linden, thank you for attending to my several IT issues. I thank the CASA secretary mw. Enna van Dijk for the great all round support she has extended to me since the time I got interested in studying at TU/e.

I have generally enjoyed working in the CASA group over the years, and I would like to thank my colleagues for the pleasant working environment. I would like to thank Hans Groot, Zoran Ilievski, Darcy Hou, Maria Ugryumova, Agnieszka Lutowska, Mirela Darau and Roxana Ionotu for being great officemates over the years. I also thank Zoran and dr. Christina Giannopapa for being excellent housemates. I will be haunted if I do not mention having greatly enjoyed the many outings, dinners and poker and sportscentrum games with my fellow PhD students who included: Erwin Vondehoff, Peter in 't pan Huijs, Jan Willem, Hans Groot, Agnieszka Lutowska, Mirela Darau, Zoran Ilievski, Patricio Rosen,

Yves van Genip, Mark van Krij, John Businge, Yeneneh Yimer Yalew, Temesgen Markos, Valeriu Savcenco, Ali Etaati, Maxim Pisarenco, Miguel Patricio, Fan Yabin, Maria Rudnaya, Maria Ugryumova, Kundan Kumar, Tasnim Fatima, Kho Changhi, Sudhir Srivastava, the list goes on and on. I also thank Willem Dijkstra for the several helpful BEM discussions we had. Special thanks to Mirela and Hans for helping me with the printing process.

Finally, I would like to express my great appreciation to my family and friends at home for their support over the years. In particular I would like to register my special thanks to my friends Doreen Karungi, Tumps Ireeta, Asbjorn Atuhaire and John Kitayimbwa for all the support and courage they have always given me. In addition I thank Doreen for reading through and providing lots of grammar corrections. I am very grateful to my colleagues at Makerere; Fred Mayambala, Ismail Mirumbe and David Dumba for helping me get more time to finish up the writing, not forgetting the head Dr. J. Kasozi and the dean of science Prof J. Y. T. Mugisha for their understanding and support in the process. Let me also register my thanks to Dr. B. S. Kato and his family for the several holiday trips I enjoyed with them in London. I totally appreciate the unyielding support of my parents and I hope I have usefully enjoyed the freedom you gave me to do whatever I want in and with my education.

Contents

Ω :	a problem domain	7
$\partial\Omega$:	the boundary of Ω	7
χ :	an arclength coordinate along the boundary $\partial\Omega$	9
$\mathbf{r}$:	coordinates in $\mathbb{R}^2$	9
$H^r(\Omega)$:	the Sobolev space of order r on a domain Ω	15
$C(\Omega)$:	a space of continuous functions on a two dimensional space Ω	15
$\partial\Omega_j$:	a partitioning of $\partial\Omega$ into N elements such that $\bigcup_{j=1}^{N} \partial\Omega_j = \partial\Omega$	21
Γ :	a numerical boundary representing $\partial\Omega$	21
Γ_j :	a partitioning of Γ into N elements each representing $\partial\Omega_j$	21
L, l :	a grid of size L or l	22
$u_j,\ q_j$:	the values $u(\mathbf{r}_j)$ and $q(\mathbf{r}_j)$ respectively in a node $\mathbf{r}_j$	23
$u_j^L,\ q_j^L$:	a BEM approximation of u_j and q_j respectively on a grid of size L	24
l_j :	the length/size of element Γ_j	26
$f_u(\mathbf{r}),\ f_q(\mathbf{r})$:	shape function for $u(\mathbf{r})$ and $q(\mathbf{r})$ respectively	41
$\mathbf{r}(\chi)$:	a coordinate in $\mathbb{R}^2$ at a local coordinate χ	45
$\mathbf{r}_j(\chi)$:	the distance to a point χ on the j-th element	45
Ω_{local} :	a region of Ω where the solution has high activity	88
Γ_{local} :	the boundary of Ω_{local}	89
Γ_{inside} :	a part of Γ_{local} that is contained inside Ω	89
Γ_{active} :	a part of Γ_{local} that contains the high activity and belongs to Γ as well	89
Γ_c :	a part of Γ that is outside of Γ_{active}	89
Γ^L :	a uniform grid discretisation of Γ into elements Γ_j^L of size L	90

Γ^l_{local} :	a uniform grid discretisation of Γ_{local} into elements $\Gamma^l_{\text{local},j}$ each of size l	90
Γ_{local} :	the boundary of Ω_{local}	89
Γ^l_{active} :	part of the uniform grid Γ^l_{local} that belongs to Γ_{inside}	90
$\mathbf{r}^l_{\text{local}}$:	nodes of the local fine grid of size l	90
$\mathbf{r}^l_{\text{active}}$:	nodes of the local fine grid that belong to Γ_{active}	90
$\mathbf{r}^l_{\text{inside}}$:	nodes of the local fine grid that belong to Γ_{inside}	90
$\Gamma^{l,L}$:	a composite grid discretisation of Γ into elements of size l in Γ_{active} and size L in Γ_c	91
$\mathbf{r}^{l,L}$:	nodes of the composite grid	91

Chapter 1

Introduction

1.1 Background

The boundary element method (BEM) is a numerical method for approximating solutions of boundary value problems (BVPs). The most important and unique feature of BEM is that only the boundary of a domain needs to be discretised. This is also its most important advantage over its main competitor *finite element methods* (FEM) and other methods like *finite difference methods*(FDM). It makes BEM suitable for exterior problems. Also problems in which singularities or discontinuities occur in the domain can be handled efficiently by BEM solving is at the boundary. Another advantage of the BEM is that the functions at the boundary and their normal derivatives are solved for at the same time and with the same degree of accuracy.

The main disadvantage of BEM is that it requires the knowledge of fundamental solutions for a problem partial differential equations in order to be used and these are not readily available for all problems. This factor contributed to the initially relatively slower development of BEM. The method also involves computing singular integrals. However, today these fundamental solutions and the singular integrals involved with the method are well understood and the BEM has undergone rapid advancement in recent years [16]. The basic foundation for BEM are integral equations. It has been known for well over a century that BVPs whose fundamental solutions are known such as the Laplace equation and the equations of linear elastostatics can be formulated as a boundary integral equation (BIE), see for instance [36]. The unknown boundary data then depends on the prescribed data in the BIE. Once all the data becomes available through the solution of the BIE, then the solution to the BVP is obtained through the application of Green's identity.

A BEM formulation can be classified as either a *direct* formulation or *indirect* formulation. The basis for the indirect formulation can be credited to Fredholm. In 1903 he already used discretised integral equations for potential problems [20]. The basis of the direct formulation can be credited to Somigliana who in 1886 presented an integral equation relating displacements and stresses [69]. Since then a number of books and papers have been published including Kellog [36], Mushkhelishvili [55], Mikhlin [50] and Kupradze [42]. Their results are, however, limited to simple problems as the integral equations had to be solved with analytical procedures and without the aid of computers.

The real breakthrough came in the nineteen sixties when the integral equations for two dimensional potential problems were discretised using rectilinear elements [27, 75] by Jawson and Symm. At each line element the functions are approximated by constants. Their method cannot be classified as exactly a direct formulation because the functions needed to be differentiated or integrated to obtain physical quantities [16]. A direct formulation was introduced by Rizzo [63], who also used discretised integral equations to relate displacements and tractions in two-dimensional elasticity theory. The extension to three dimensions was given by Cruse [14], using triangular elements to describe the domain boundary. In 1963 Jawson and Symm [27, 75] demonstrated that the associated integral equation can be solved accurately and reliably using the numerical methods. In 1978, CA Brebbia formally introduced the terminology boundary-element method (BEM) for the first time in contrast to what had already been established terminology, finite element method.

Presently, the BEM is well established as an effective alternative in the solution of engineering problems from a variety of application fields which include acoustics, fracture mechanics, potential theory, elasticity theory and viscous flows. However, estimating the BIEs numerically raises the need for error and convergence analysis. For BEM, the mathematical foundation for such analysis was laid down in Hsiao and Wendland [26], who performed such error and convergence analysis for the *Galerkin* formulation. Error analyses for the collocation formulation were pioneered by Arnold, Saranen and Wendland [2, 3, 64] during the eighties. They mostly provide an indirect way of measuring error and are usually based on the Galerkin formulation. Techniques include using solutions obtained by using different collocation points or different formulations, [22, 29, 44].

In this thesis direct error estimates for collocation BEM are derived and moreover in the maximum norm. Starting from its basic formulation, error estimates for collocation BEM are derived by tracking down the *interpolation error* committed at the elements.

The issue of error analysis becomes even more crucial when considering problems with hot spots where specialised gridding is necessary. *Hot spots* refers to small regions of high activity. Hot spots appear in a variety of problems. For

example in combustion problems [1] or in corrosion problems, which often exhibit regions of high activity where the corrosion is taking place, the microwave heating problem [62], antenna transmissions [46], [82] and also in fluid dynamics [80]. If these spots are located well inside the domain, then standard BEM has no problem since it is the boundary that is discretised. However such spots can be in or very close to the boundary and as such require special attention in a BEM discretisation. In this thesis we consider one such problem, viz corrosion, and look at the potential problem of impressed current cathodic protection system.

In particular, functions with hot spots are an instant of multi-scales problems, that is, the problem is such that there is a large region where the variation is relatively benign and small regions of rapid variation. This poses the problem of forming a grid that accurately captures all the activity but with a high degree of computational efficiency. The distribution of the elements therefore becomes a very important decision. In the competing field of finite elements such a need has generated a large amount of literature of which a good review can be found in [71] and [72]. While adaptive meshing in finite elements is quite advanced, in boundary element methods the research is only at the beginning. Quite a few approaches, including element residual methods, flux projection estimates, extrapolation error estimates and estimates measuring the sensitivity of the numerical solution to a shift in collocation points have been considered. A good review of the various approaches is presented in [45]. In this thesis a new form of gridding for problems with hot spots in the name of *Local Defect Correction* (LDC) is presented. This method has been tested and is well documented in the other numerical methods such as Finite Difference Methods and Finite Volume Methods [1, 21, 51]. It is a proven efficient approach for solving problems with hot spots with a control on complexity. An approach for using LDC in BEM is presented here.

1.2 Outline of this thesis

The basis for the boundary element method is a boundary integral equation. In Chapter 2, boundary integral equations for boundary value problems using the direct formulation are discussed. As is elaborated there, the BEM operator has different properties depending on the kind of boundary conditions, that is either Dirichlet, Neumann or mixed boundary conditions. In this chapter properties of these operators that are helpful for the work covered in this thesis are introduced and discussed. A boundary element discretisation uses either constant elements, linear elements, quadratic elements or even higher order elements depending on the assumptions followed on the given functions during the formulation. In Chapter 3, constant and linear elements formulations are introduced and discussused. These are the formulations we analyse and use throughout this thesis. They also turn out to be the most used formulations in

literature for the direct approach. Also in this chapter a set of examples that will be used to verify our findings in this thesis are discussed.

Chapter 4 is dedicated to discussing local errors in BEM for both the constant and linear elements formulations. The question of local errors in BEM is an interesting one because by its nature, the boundary integral is a global method. However, we show that we are able to define and use the error committed on each element to define the local error in a point at the boundary. For the first time we derive direct error estimates, that is, we start from the exact assumptions made in the formulation of BEM for a local error analysis in this chapter. Local error behaviour for the constant and linear element formulations is predicted and verified. A *sublocal* error is introduced and it is shown that it is third order in grid size. Using this sublocal error it is shown that the local error is second order in grid size for constant elements as well as linear elements. Then this can be exploited to obtain an error equidistributing grid.

In any numerical solution, the error that the user is interested in is the *global error*. Having understood the local error in Chapter 4, good information is now available to go on and analyse the global error. This is the subject of Chapter 5. The problem on a circle is considered since in this case, all the analytical eigenfunctions and eigenvectors of the integral operators are available. Therefore a spectral analysis and the information on local errors is used to derive bounds for the global error.

Now that information on both the local and global errors is available, we present in Chapter 6 a local defect correction (LDC) formulation for the boundary element method. It is shown here that LDC for BEM is a reliable strategy for obtaining solutions on a composite grid but with less complexity. This is entertaining news since BEM matrices are usually full matrices that would rather require more memory and computation time as compared to when LDC is used.

The local Local defect correction formulation discussed here can be applied to several problems with hot spots where BEM is used such as in electromagnetics, fluid mechanics and structural mechanics. Chapter 7 discusses such an application to a potential problem for an *impressed current cathodic protection (ICCP)* system. ICCP is a system used to protect steel structures from corrosion. Such structures include submarines such as ships, underground pipes, over ground storage tanks. Chapter 7 discusses an LDC model for ICCP for a storage tank.

"But those who hope in the Lord will renew their strength. They will soar on wings like eagles; they will run and not grow weary, they will walk and not be faint."–Isaiah 40:31

Chapter 2

The boundary integral equations

2.1 Introduction

Consider a closed domain Ω with boundary $\partial\Omega$. On Ω, consider the potential equation

$$\nabla^2 u(\mathbf{r}) = f(\mathbf{r}), \ \mathbf{r} \in \Omega. \tag{2.1.1}$$

The solution $u = u(\mathbf{r})$ of (2.1.1) represents the potential produced at a point $\mathbf{r}$ in a domain Ω due to a source $f(\mathbf{r})$ distributed over Ω. Denote by $\mathbf{n}$ the outward unit normal at $\partial\Omega$.

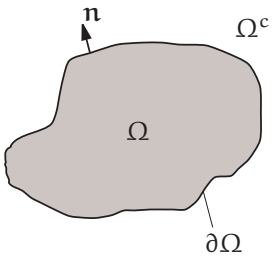

(a) Domain illustration for a Dirichlet or Neumann problem

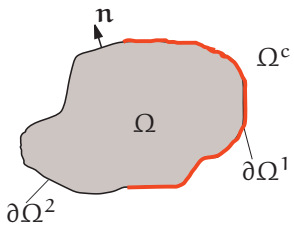

(b) Domain illustration for a mixed problem

Figure 2.1: Definition of terms for the potential problems given in (2.1.3a) to (2.1.3c).

Throughout this thesis we consider the Laplace equation for which $f(\mathbf{r}) = 0$, that is,

$$\nabla^2 u(\mathbf{r}) = 0, \ \mathbf{r} \in \Omega, \tag{2.1.2}$$

for which the following boundary conditions may be defined on $\partial\Omega$:

(1) *Dirichlet boundary conditions*;

$$u(\mathbf{r}) = g(\mathbf{r}), \ \mathbf{r} \in \partial\Omega, \tag{2.1.3a}$$

where g is a given function.

(2) *Neumann boundary conditions*;

$$\frac{\partial u}{\partial n}(\mathbf{r}) = \mathbf{n} \cdot \nabla u(\mathbf{r}) = h(\mathbf{r}), \ \mathbf{r} \in \partial\Omega, \tag{2.1.3b}$$

where h is a given function.

(3) *Mixed boundary conditions*;

$$\begin{cases} u(\mathbf{r}) = g(\mathbf{r}) & \mathbf{r} \in \partial\Omega^1 \\ \\ \dfrac{\partial u}{\partial n}(\mathbf{r}) = h(\mathbf{r}) & \mathbf{r} \in \partial\Omega^2 \end{cases} \tag{2.1.3c}$$

where $\partial\Omega^1 \cup \partial\Omega^2 = \partial\Omega$ and $\partial\Omega^1 \cap \partial\Omega^2 = \emptyset$ and g and h are given functions.

Subsequently a problem with Neumann boundary conditions will be referred to as a *Neumann problem*, that with Dirichlet boundary conditions a *Dirichlet problem* and that with mixed boundary conditions a *Mixed problem*. The fundamental solution of the Laplace equation is the solution of the singularly forced Laplace equation

$$\nabla^2_{\mathbf{r}} v(\mathbf{s};\mathbf{r}) + \delta(\mathbf{s};\mathbf{r}) = 0, \quad \mathbf{s}, \mathbf{r} \in \Omega^\infty, \tag{2.1.4}$$

where $\mathbf{r}$ is the variable field point, $\mathbf{s}$ is the fixed location of the source point or pole and Ω^∞ denotes the infinite domain which is the whole plane in 2D. The subscript $\mathbf{r}$ on the operator ∇ means differentiation is with respect to $\mathbf{r}$.

The *Dirac delta distribution* $\delta(\mathbf{s};\mathbf{r})$ satisfies the following properties [60, p 12], [35, p 21]:

$$\int_\Omega \delta(\mathbf{s};\mathbf{r}) \, d\Omega = \begin{cases} 1, & \text{if } \mathbf{s} \in \Omega, \\ \\ 0, & \text{if } \mathbf{s} \notin \Omega. \end{cases} \tag{2.1.5}$$

The Dirac delta is not truly a function but rather a generalised function. For example, any function that is zero everywhere except in a single point has total

integral zero but the Dirac delta has integral one [39, p 271]. It is used to model phenomena with sufficiently concentrated properties such as a point charge or point force.

For a two-dimensional case, introducing polar coordinates and using the properties of the Dirac delta distribution, the solution of (2.1.4) is found to be

$$v(\mathbf{s};\mathbf{r}) = \frac{1}{2\pi}\log\frac{1}{r} \tag{2.1.6}$$

where $\mathbf{r} = (x, y)$, $\mathbf{s} = (x_s, y_s)$ and $r := \sqrt{(x-x_s)^2 + (y-y_s)^2}$ is the Euclidean distance from $\mathbf{s}$ to $\mathbf{r}$. Let us also introduce a boundary *arclength coordinate* defined along $\partial\Omega$ is shown in Figure 2.2.

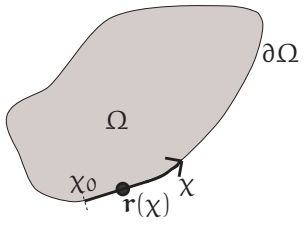

Figure 2.2: Definition of arclength coordinate χ and the position $\mathbf{r}(\chi)$ which is $\mathbf{r}$ at χ, χ_0 is the origin.

In this chapter we derive integral relations for the potential $u(\mathbf{s})$ for $\mathbf{s}$ at different locations of the domain Ω. These relations have been abundantly derived in literature and are readily available in various books on boundary element methods such as [57, p. 38], [35, p. 28], [59]. They are presented here for completeness. The relations are derived starting from the following Green's identity:

Theorem 2.1.1 (Green's second identity) *Let ϕ, defined in Ω, and ψ, defined in $\Omega \times \Omega$, be two scalar functions which are continuous and admit continuous partial derivatives, then*

$$\int_\Omega \left(\phi(\mathbf{z})\nabla_z^2\psi(\mathbf{s};\mathbf{z}) - \psi(\mathbf{s};\mathbf{z})\nabla^2\phi(\mathbf{z})\right)\, d\Omega(\mathbf{z}) = \int_{\partial\Omega}\left(\phi(\mathbf{r}(\chi))\frac{\partial\psi}{\partial n}(\mathbf{s};\mathbf{r}(\chi)) - \psi(\mathbf{s};\mathbf{r}(\chi))\frac{\partial\phi}{\partial n}(\mathbf{r}(\chi))\right)\, d\chi,\ \mathbf{s}\in\Omega, \tag{2.1.7}$$

where χ is an arc length coordinate in $\partial\Omega$.

In (2.1.7), $\mathbf{n}$ is the outward unit normal at $\partial\Omega$ as shown in Figure 2.1. To derive the integral relations for the Laplace equation, use is made of the iden-

tity (2.1.7). We take ϕ as the unknown function u and ψ the fundamental solution (2.1.6).

2.2 Integral equation for points inside Ω

Starting from Green's second identity (2.1.7), an integral relation for a point $\mathbf{s} \in \Omega$ is derived, see Figure 2.3. Since the fundamental solution v is singular at the point $\mathbf{s}$, the domain of integration where Green's second identity is applied must be defined isolating the point $\mathbf{s}$. We construct a ball Ω_ϵ of radius ϵ around it. Then the new domain of integration is now $\Omega - \Omega_\epsilon$ with boundary $\partial\Omega + \partial\Omega_\epsilon$, see Figure 2.3.

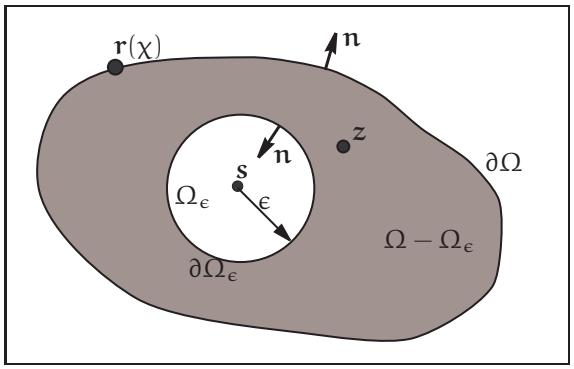

Figure 2.3: Definition of the domain of integration for internal points.

Then apply (2.1.7) on $\Omega - \Omega_\epsilon$ and take the limit as $\epsilon \to 0$. Thus, with $\mathbf{z} \in \Omega - \Omega_\epsilon$ and $\mathbf{s} \in \Omega_\epsilon$, we have

$$\begin{aligned}
&\lim_{\epsilon\to 0} \int_{\Omega-\Omega_\epsilon} \Big(u(\mathbf{z})\nabla_{\mathbf{z}}^2 v(\mathbf{s};\mathbf{z}) - v(\mathbf{s};\mathbf{z})\nabla^2 u(\mathbf{z}) \Big)\, d\Omega(\mathbf{z}) \\
&= \int_{\partial\Omega} \left(u(\mathbf{r}(\chi))\frac{\partial v}{\partial n}(\mathbf{s};\mathbf{r}(\chi)) - v(\mathbf{s};\mathbf{r}(\chi))\frac{\partial u}{\partial n}(\mathbf{r}(\chi)) \right) d\chi \\
&\qquad + \lim_{\epsilon\to 0} \int_{\partial\Omega_\epsilon} \left(u(\mathbf{r}(\chi))\frac{\partial v}{\partial n}(\mathbf{s};\mathbf{r}(\chi)) - v(\mathbf{s};\mathbf{r}(\chi))\frac{\partial u}{\partial n}(\mathbf{r}(\chi)) \right) d\chi. \quad (2.2.1)
\end{aligned}$$

Since the point $\mathbf{s}$ is outside $\Omega - \Omega_\epsilon$, use (2.1.5) to conclude that integrating the first term on the left hand side yields 0. For the integral of the second term on

the left hand side, note that

$$v(\mathbf{s};\mathbf{z}) = v(\mathbf{z};\mathbf{s})$$

and for the Laplacian

$$\nabla^2 u(\mathbf{z}) = f(\mathbf{z}) = 0$$

so that

$$\lim_{\epsilon\to 0} \int_{\Omega-\Omega_\epsilon} v(\mathbf{s};\mathbf{z})\nabla^2 u(\mathbf{z})\mathrm{d}\Omega(\mathbf{z}) = \lim_{\epsilon\to 0} \int_{\Omega-\Omega_\epsilon} v(\mathbf{z};\mathbf{s})f(\mathbf{z})\mathrm{d}\Omega(\mathbf{z}) = \int_{\Omega} v(\mathbf{z};\mathbf{s})f(\mathbf{z})\mathrm{d}\Omega(\mathbf{z}) = 0. \tag{2.2.2}$$

Now consider the second integral on the right hand side of (2.2.1). The boundary $\partial\Omega_\epsilon$ is a circumference of radius ϵ, the normal $\mathbf{n}$ is along the radius of Ω_ϵ and towards the point $\mathbf{s}$. So

$$\mathrm{d}\chi = \epsilon\mathrm{d}\theta, \quad \frac{\partial v}{\partial n} = -\left.\frac{\partial v}{\partial r}\right|_{r=\epsilon} = \frac{1}{2\pi\epsilon}.$$

Then

$$\lim_{\epsilon\to 0} \int_{\partial\Omega_\epsilon} \left(u(\mathbf{r}(\chi))\frac{\partial v}{\partial n}(\mathbf{s};\mathbf{r}(\chi)) - v(\mathbf{s};\mathbf{r}(\chi))\frac{\partial u}{\partial n}(\mathbf{r}(\chi)) \right) \mathrm{d}\chi$$

$$= \lim_{\epsilon\to 0} \int_0^{2\pi} \left(u(\mathbf{r}(\chi))\frac{1}{2\pi\epsilon}\epsilon + \frac{1}{2\pi}\epsilon\log\epsilon \right) \mathrm{d}\theta = u(\mathbf{s}). \tag{2.2.3}$$

Therefore (2.2.1) becomes

$$u(\mathbf{s}) = \int_{\partial\Omega} \left[v(\mathbf{s};\mathbf{r}(\chi))\frac{\partial u}{\partial n}(\mathbf{r}(\chi)) - u(\mathbf{r}(\chi))\frac{\partial v}{\partial n}(\mathbf{s};\mathbf{r}(\chi)) \right] \mathrm{d}\chi, \quad \mathbf{s}\in\Omega. \tag{2.2.4}$$

The integral relation (2.2.4) expresses the value of u at any point $\mathbf{s}$ in the domain Ω in terms of its values and normal derivatives at the boundary. Thus if u and $\partial u/\partial n$ are known at the boundary, u can be computed at any point in the domain.

2.3 Integral equation for boundary points

Consider the case $\mathbf{s}\in\partial\Omega$. In a similar fashion as above, draw a ball of radius ϵ around the point $\mathbf{s}$ in $\partial\Omega$, see Figure 2.4. Note that only part of the ball lies within Ω; denote this intersection by Ω_ϵ. For generality, consider a point $\mathbf{s}$ located at a corner. Let $\partial\Omega_\epsilon^1$ be the part of $\partial\Omega$ from point A to $\mathbf{s}$ and $\mathbf{s}$ to B. Let

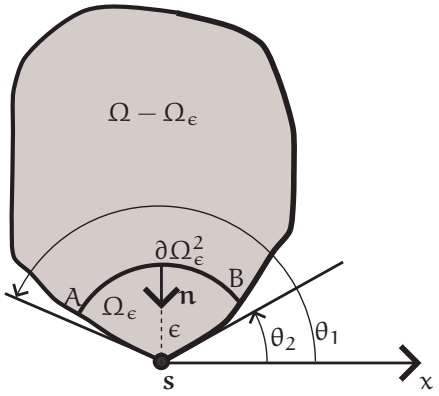

Figure 2.4: Definition of the domain of integration for boundary points.

$\partial\Omega_\epsilon^2$ be the arc AB. Applying Green's identity (2.1.7) in $\Omega - \Omega_\epsilon$, the left hand side is zero since the Laplace equation is considered and the singular point for the fundamental solution is outside $\Omega - \Omega_\epsilon$. Then

$$0 = \lim_{\epsilon\to 0}\int_{\partial\Omega-\partial\Omega_\epsilon^1}\left[u(\mathbf{r}(\chi))\frac{\partial v}{\partial n}(\mathbf{s};\mathbf{r}(\chi)) - v(\mathbf{s};\mathbf{r}(\chi))\frac{\partial u}{\partial n}(\mathbf{r}(\chi))\right]d\chi$$

$$+\lim_{\epsilon\to 0}\int_{\partial\Omega_\epsilon^2}\left[u(\mathbf{r}(\chi))\frac{\partial v}{\partial n}(\mathbf{s};\mathbf{r}(\chi)) - v(\mathbf{s};\mathbf{r}(\chi))\frac{\partial u}{\partial n}(\mathbf{r}(\chi))\right]d\chi. \quad (2.3.1)$$

The limit of the first integral of (2.3.1) is the integral over the whole of $\partial\Omega$. Consider the first term of the second integral, we have

$$\frac{\partial v}{\partial n}(\mathbf{s};\mathbf{r}(\chi)) = -\frac{1}{2\pi r}\frac{\partial r}{\partial n} = \frac{1}{2\pi r}. \quad (2.3.2)$$

In this case $r = \epsilon$ and $d\chi = -\epsilon d\theta$. So

$$\lim_{\epsilon\to 0}\int\limits_{\partial\Omega_\epsilon} u(\mathbf{r}(\chi))\frac{\partial v}{\partial n}\,d\chi = \lim_{\epsilon\to 0}\int\limits_{\theta_1}^{\theta_2} u(\mathbf{r}(\theta))\frac{1}{2\pi\epsilon}(-\epsilon d\theta) = \frac{\theta_1-\theta_2}{2\pi}u(\mathbf{s}) \quad (2.3.3)$$

because the point $\mathbf{r}(\chi)$ approaches $\mathbf{s}$ as $\epsilon \to 0$.

The second term of the second integral of (2.3.1) gives,

$$\lim_{\epsilon\to 0}\int_{\partial\Omega_\epsilon} v(\mathbf{s};\mathbf{r}(\chi))\frac{\partial u}{\partial n}(\mathbf{r}(\chi))\,d\chi = \lim_{\epsilon\to 0}\left(\frac{\epsilon\ln\epsilon}{2\pi}\int_{\theta_1}^{\theta_2}\frac{\partial u}{\partial n}(\mathbf{r}(\theta))\,d\theta\right) = 0. \quad (2.3.4)$$

Substituting (2.3.3) and (2.3.4) in (2.3.1) gives the integral relation

$$\frac{\theta_1-\theta_2}{2\pi}u(\mathbf{s})=\int_{\partial\Omega}\left[v(\mathbf{s};\mathbf{r}(\chi))\frac{\partial u}{\partial n}(\mathbf{r}(\chi))-u(\mathbf{r}(\chi))\frac{\partial v}{\partial n}(\mathbf{s};\mathbf{r}(\chi))\right]d\chi. \tag{2.3.5}$$

In the limit as $\epsilon\to 0$ the angle $(\theta_1-\theta_2)$ is the internal angle at $\mathbf{s}$ which we denote $\alpha(\mathbf{s})$. For a flat surface this angle is π and therefore the coefficient $(\theta_1-\theta_2)/2\pi$ in (2.3.5) is $1/2$.

2.4 Integral equation for points outside Ω

If the point $\mathbf{s}$ is outside Ω, again due to the properties of $v(\mathbf{s};\mathbf{r})$ and since the singularity point is now outside Ω then the left hand side of (2.1.7) is zero. So we have

$$0=\int_{\partial\Omega}\left[v(\mathbf{s};\mathbf{r}(\chi))\frac{\partial u}{\partial n}(\mathbf{r}(\chi))-u(\mathbf{r}(\chi))\frac{\partial v}{\partial n}(\mathbf{s};\mathbf{r}(\chi))\right]d\chi,\quad \mathbf{s}\in\Omega^c. \tag{2.4.1}$$

Equations (2.2.4), (2.3.5) and (2.4.1) can be summarised as

$$c(\mathbf{s})u(\mathbf{s})=\int_{\partial\Omega}\left[v(\mathbf{s};\mathbf{r}(\chi))\frac{\partial u}{\partial n}(\mathbf{r}(\chi))-u(\mathbf{r}(\chi))\frac{\partial v}{\partial n}(\mathbf{s};\mathbf{r}(\chi))\right]d\chi, \tag{2.4.2}$$

where the coefficient $c(\mathbf{s})$ is given by

$$c(\mathbf{s}):=\begin{cases}1, & \mathbf{s}\in\Omega,\\ \dfrac{\alpha(\mathbf{s})}{2\pi}, & \mathbf{s}\in\partial\Omega,\\ 0, & \mathbf{s}\in\Omega^c.\end{cases} \tag{2.4.3}$$

Using the properties of the fundamental solution v introduced in Section 2.1 it can be shown that

$$\int_{\partial\Omega}\frac{\partial v}{\partial n}(\mathbf{s};\mathbf{r}(\chi))\,d\chi=\begin{cases}-1, & \mathbf{s}\in\Omega,\\ -1/2, & \mathbf{s}\in\partial\Omega,\\ 0, & \mathbf{s}\in\Omega^c,\end{cases} \tag{2.4.4}$$

where $\mathbf{n}$, Ω and $\partial\Omega$ are as defined in Figure 2.1. We now introduce the following definitions of the *single* and *double layer potentials* respectively:

$$\mathcal{K}^s q(\mathbf{s}):=\int_{\partial\Omega}v(\mathbf{s};\mathbf{r}(\chi))q(\mathbf{r}(\chi))d\chi, \tag{2.4.5a}$$

$$\mathcal{K}^d u(\mathbf{s}):=\int_{\partial\Omega}\frac{\partial v}{\partial n}(\mathbf{s};\mathbf{r}(\chi))u(\mathbf{r}(\chi))d\chi. \tag{2.4.5b}$$

These integrals are called single and double layer potentials respectively by making an analogy with the corresponding boundary distributions of electric charges and charge dipoles in electrostatics, see [5, p 319], [31, p 42], [38, p 67], [60, p 21], [66]. Using (2.4.5), the integral equation (2.4.2) can be written as

$$(c\mathcal{I} + \mathcal{K}^d)u(\mathbf{s}) = \mathcal{K}^s q(\mathbf{s}). \tag{2.4.6}$$

The operators $\mathcal{K}^s$ and $\mathcal{K}^d$ are called the *single* and *double layer* operator respectively and $\mathcal{I}$ is the identity operator. When $\mathbf{s}$ is located at the boundary the integral equation is referred to as a *boundary integral equation (BIE)*. The functions

$$k^s(\mathbf{s};\mathbf{r}) := v(\mathbf{s};\mathbf{r}), \tag{2.4.7a}$$

$$k^d(\mathbf{s};\mathbf{r}) := \frac{\partial v}{\partial n}(\mathbf{s};\mathbf{r}), \tag{2.4.7b}$$

are called the *kernel* of the integral operators $\mathcal{K}^s$ and $\mathcal{K}^d$ respectively.

The operators $\mathcal{K}^s$ and $\mathcal{K}^d$ together with their kernels are popular and have been extensively studied. In Section 2.5, some of their properties that will be helpful for the topics studied in this thesis are presented.

2.5 Operator theory

In this section, some properties of the operators $\mathcal{K}^s$ and $\mathcal{K}^d$ that will be needed in later chapters are presented. Most important, we discuss their spectral properties and present proven theorems on their compactness and continuity. As discussed below, properties of $\mathcal{K}^s$ are important in the solution for a Dirichlet as those of $\mathcal{K}^d$ are for a Neumann problem. We show that the operator $\mathcal{K}^d$ has a zero eigenvalue, which results in a singular system and hence a non unique solution. Here we discuss how to circumvent this problem to obtain a unique solution. These properties will be helpful in the investigation of local and global errors in Chapters 4 and 5. The continuity and boundedness properties will also be helpful in the investigation of the local defect correction algorithm introduced in Chapter 6.

Consider the integral equation (2.4.6). If the function $q(\mathbf{r})$ at the boundary is known, then the right hand side is known. Define

$$f(\mathbf{s}) := \mathcal{K}^s q(\mathbf{s}),$$

then (2.4.6) becomes

$$(c\mathcal{I} + \mathcal{K}^d)u(\mathbf{s}) = f(\mathbf{s}). \tag{2.5.1}$$

Equation (2.5.1) is known as a *Fredholm integral equation of the second kind*, see for instance [5, 3], [24, 42], [38, 1]. Therefore, a Neumann problem results into a Fredholm integral equation of the second kind, which sometimes is simply known as a second kind integral equation.

On the other hand, if the function $u(\mathbf{r})$ is known at the boundary, then define $g(\mathbf{s}) := (c\mathcal{I} + \mathcal{K}^d)u(\mathbf{s})$ and equation (2.4.6) becomes

$$\mathcal{K}^s q(\mathbf{s}) = g(\mathbf{s}). \tag{2.5.2}$$

Equation (2.5.2) is a *Fredholm integral equation of the first kind* which is sometimes simply called a first kind integral equation.

A considerable amount of theory for both the first and second kind integral equations has already been established. Also, several numerical methods for determining the unknowns approximately have been discussed, an increasingly popular one being BEM. In contrast to the properties possessed by the second kind integral equation, many of the properties of the first kind integral equation are "very unpleasant and often surprising to even mathematicians," [81, pp 1,2]. These properties are determined by the corresponding operators and in this section a few of them are highlighted.

Introduce $H^r(\Omega)$ which denotes the *Sobolev space* $V^{r,2}(\Omega)$ which is given by

$$V^{r,2} = \{f : \Omega \to \mathbb{R} \,\big|\, \|f\|_{k,2} < \infty\}$$

where

$$\|f\|_{k,2} = \left(\sum_{|\alpha| \le k} \int_\Omega |D^\alpha f|^2 \, dx \right)^{1/2}$$

and $D^\alpha f$ denotes the mixed partial derivatives of f of order α. The integer k is the largest order derivative that the functions in $W^{k,2}(\Omega)$ all admit. This discussion and in more detail is presented in [9, pp. 19-21].

Theorem 2.5.1 *For Ω a simply connected bounded domain in $\mathbb{R}^2$ with smooth boundary $\partial\Omega$, the operators $\mathcal{K}^s$ and $\mathcal{K}^d$ map functions from the* Sobolev space $H^r(\partial\Omega)$ *to* $H^{r+1}(\partial\Omega)$, $r \in \mathbb{R}$.

Proof. See [9, pp. 249, 286-287]. ■

In fact, for Ω smooth, Theorem 2.5.1 can actually be strengthened to mapping from $H^r(\partial\Omega)$ to $C^\infty(\partial\Omega)$ for any $r \in \mathbb{R}$, see [9, p. 249].

In this thesis, we restrict ourselves to $C(\Omega)$, a space of continuous functions on a two dimensional space Ω with a positive measure μ such that

$$(f, g) = \int_\Omega f(\mathbf{r}) g(\mathbf{r}) \, d\mu. \tag{2.5.3}$$

So over the boundary $\partial\Omega$, the *inner product* (2.5.3) is defined as

$$(f, g) := \int_{\partial\Omega} f(\mathbf{r}(\chi))g(\mathbf{r}(\chi))\, d\chi. \tag{2.5.4}$$

For vectors, we use the median 2-norm which for a vector $\mathbf{u} \in \mathbb{R}^M$ is defined as, [48, p. 98],

$$\|\mathbf{u}\|_{2,M} := \frac{1}{\sqrt{M}} \left(\sum_{i=1}^{M} u_i^2 \right)^{1/2} \tag{2.5.5}$$

and the infinity norm $\|\mathbf{d}\|_\infty = \max_{i=1,\ldots,M} |d_i|$ where $\mathbf{d} = (d_1, d_2, \ldots, d_M)^T$. These norms are used in Chapters 4 and 5 to estimate and compare local and global errors in BEM solutions.

Theorem 2.5.2 (Compactness) *The single layer operator $\mathcal{K}^s$ is a compact and self-adjoint operator.*

Proof. See [16, p. 16], [30, p. 121]. ■

From the spectral theory of compact operators, it follows that the eigenvalues of $\mathcal{K}^s$ have an accumulation point at zero. In fact, on a smooth boundary, both the double layer and the single layer are compact operators, see [5, p. 439], [38, Theorem 2.22]. Thus, the possibility of a zero eigenvalue implies the need for regularisation in the solution of the integral equations. Section 2.5.1 uses the particular case of a circle to demonstrate the eigenvalues of the single and double layer operators. In Section 2.5.2 it is shown that the operator associated with the second kind integral equation of the Neumann problem has a zero eigenvalue and thus is singular. A regularisation strategy used to obtain a unique solution is discussed.

First the following theorem implies that an integral operators can be expanded in terms of its eigenvalues and eigenfunctions. This will be helpful in the regularisation strategy discussed here and in the analysis of global errors in Chapter5.

Theorem 2.5.3 *Let $\mathcal{A} \neq 0$ be a compact operator in a Hilbert space H and (λ_n) its ordered sequence of eigenvalues. Then there exists an orthonormal sequence of eigenvectors a_j corresponding to the λ_j. For every $u \in H$ the expression*

$$u = u_0 + \sum_j (u, a_j)a_j$$

holds where u_0 is in the null space of $\mathcal{A}$ and

$$\mathcal{A}u = \sum_j \lambda_j (u, a_j)a_j.$$

Proof. See [30, pp. 121,122]. ■

2.5.1 Eigenvalues of $\mathcal{K}^s$ and $\mathcal{K}^d$: A circular boundary example

A number λ is an eigenvalue of an operator K with eigenfunction f if

$$\lambda f = K f. \tag{2.5.6}$$

In what follows in this section we establish the eigenvalues and eigenfunctions for the integral operators $\mathcal{K}^s$ and $\mathcal{K}^d$. The case of a general boundary is rather complicated and we consider here the case of a circular boundary. Consider a circle of radius R. Let us introduce polar coordinates so that the distance r between two points, a fixed point $\mathbf{s}$ and any other point $\mathbf{r}$, at polar angles θ_s and θ respectively is given by

$$r^2 = \|\mathbf{s} - \mathbf{r}\|^2 = 2R^2[1 - \cos(\theta_s - \theta)]. \tag{2.5.7}$$

Also the normal at $\mathbf{r}$ is given by $[\cos\theta,\ \sin\theta]^T$. So we have

$$\mathcal{K}^s(\mathbf{s};\mathbf{r}) = -\frac{1}{2\pi}\log r = -\frac{1}{4\pi}[2\log R + \log(2 - 2\cos(\theta_s - \theta))], \tag{2.5.8}$$

$$\mathcal{K}^d(\mathbf{s};\mathbf{r}) = -\frac{1}{4\pi R}. \tag{2.5.9}$$

Then using the Fourier series for the function $f(\theta) = \log(2 - 2\cos\theta)$ gives [16, p 25]:

$$\mathcal{K}^s q(\theta_s) = -\frac{R}{4\pi}\int_0^{2\pi}\left[2\log R - \sum_{n=1}^{\infty}\frac{2}{n}\left(\cos(n\theta_s)\cos(n\theta) + \sin(n\theta_s)\sin(n\theta)\right)\right] q(\theta)\,d\theta. \tag{2.5.10}$$

So

$$\mathcal{K}^s 1 = -\frac{R}{4\pi}\int_0^{2\pi} 2\log R\,d\theta = -R\log R, \tag{2.5.11}$$

$$\mathcal{K}^s \cos k\theta_s = -\frac{R}{2\pi}\log R\int_0^{2\pi}\cos(k\theta)\,d\theta + \frac{R}{2\pi k}\int_0^{2\pi}\cos(k\theta_s)\cos^2(k\theta)\,d\theta + \frac{R}{2\pi k}\int_0^{2\pi}\sin(k\theta_s)\sin(k\theta)\cos(k\theta)\,d\theta. \tag{2.5.12}$$

Carrying out the integrals in (2.5.12) yields zero for the first and third integrals and the second one yields $R\pi\cos(k\theta_s)/(2\pi k)$. So

$$\mathcal{K}^s \cos k\theta_s = \frac{R}{2k}\cos(k\theta_s). \tag{2.5.13}$$

$$\mathcal{K}^s \sin k\theta_s = -\frac{R}{2\pi}\log R\int_0^{2\pi}\sin(k\theta)\,d\theta + \frac{R}{2\pi k}\int_0^{2\pi}\cos(k\theta_s)\cos(k\theta)\sin(k\theta)\,d\theta + \frac{R}{2\pi k}\int_0^{2\pi}\sin(k\theta_s)\sin^2(k\theta)\,d\theta \tag{2.5.14}$$

The first and second integrals in (2.5.14) yield zero where as the third integral yields $R\pi \sin(k\theta_s)/(2\pi k)$. Then

$$\mathcal{K}^s \sin k\theta_s = \frac{R}{2k} \sin(k\theta_s). \tag{2.5.15}$$

For the double layer

$$\mathcal{K}^d 1 = -\frac{1}{4\pi} \int_0^{2\pi} d\theta = -1/2, \tag{2.5.16a}$$

$$\mathcal{K}^d \cos k\theta_s = -\frac{1}{4\pi} \int_0^{2\pi} \cos k\theta \, d\theta = 0, \tag{2.5.16b}$$

$$\mathcal{K}^d \sin k\theta_s = -\frac{1}{4\pi} \int_0^{2\pi} \sin k\theta \, d\theta = 0. \tag{2.5.16c}$$

From (2.5.11), (2.5.13) and (2.5.15) we conclude that $-R \log R$ is an *eigenvalue* of $\mathcal{K}^s$ with *eigenfunction* 1 and $R/2k$ is an eigenvalue of $\mathcal{K}^s$ with eigenfunctions $\cos k\theta$ and $\sin k\theta$. The later eigenvalue indeed shows that the eigenvalues of $\mathcal{K}^s$ converge at zero. From (2.5.16a) to (2.5.16c) we conclude that $-1/2$ is an eigenvalue of $\mathcal{K}^d$ with eigenfunction 1 and 0 is an eigenvalue of $\mathcal{K}^d$ with eigenfunctions $\cos k\theta$ and $\sin k\theta$. In Section 2.5.2 it is shown that $-1/2$ is always an eigenvalue of the double layer operator making the second kind integral equation on smooth boundaries always singular. How to go around this to obtain unique solutions is also discussed.

2.5.2 Uniqueness of the solution to the Neumann problem

Result (2.4.4) implies that $-1/2$ is an eigenvalue of the double layer operator $\mathcal{K}^d$ with eigenfunction 1. From (2.4.6), the Neumann problem can be represented as the second kind integral equation

$$(\frac{1}{2}\mathcal{I} + \mathcal{K}^d)u(\mathbf{s}) = \mathcal{K}^s q(\mathbf{s}) =: f(\mathbf{s}), \tag{2.5.17}$$

where $f(\mathbf{r})$ is a known function at $\partial\Omega$. Since $-1/2$ is an eigenvalue of $\mathcal{K}^d$ with eigenfunction 1, it implies that 0 is an eigenvalue of the operator $(\frac{1}{2}\mathcal{I} + \mathcal{K}^d)$ with eigenfunction 1. Thus the space of functions spanned by 1, that is the constant functions, form the eigenspace of the operator $(\frac{1}{2}\mathcal{I}+\mathcal{K}^d)$ corresponding to eigenvalue 0. Let us denote this space by W_0, that is,

$$W_0 := \text{span}\{1\}. \tag{2.5.18}$$

Let

$$W_1 := W_0^{\perp} \tag{2.5.19}$$

be the orthogonal complement of W_0 in $C^2(\Omega) \cap C^1(\bar{\Omega})$.

Consider the operator

$$\mathcal{K} := \frac{1}{2}\mathcal{I} + \mathcal{K}^d,$$

which is also compact and Hermitian with a zero eigenvalue.

Consider the result of Theorem 2.5.3. Let $\{\phi_j\}$ be an orthonormal basis for the eigenspace of $\mathcal{K}$ corresponding to the eigenvalues λ_j. Then expanding u in terms of the basis $\{\phi_j\}$ and substituting into (2.5.17) gives,

$$\sum_j \lambda_j (u, \phi_j)\phi_j = \sum_j \lambda_j \alpha_j \phi_j = f,$$

where

$$\alpha_j := (u, \phi_j).$$

Each α_j can then be computed as

$$\alpha_j = \frac{(f, \phi_j)}{\lambda_j}, \ \lambda_j \neq 0.$$

Now,

$$\lambda_0 \alpha_0 \phi_0 + \sum_{j=1}^{\infty} \lambda_j \alpha_j \phi_j = f. \tag{2.5.20}$$

Since λ_0 is chosen to be zero, we have the freedom to choose $u_0 = (u, \phi_0)\phi_0$, the component of u in the direction of ϕ_0. This is responsible for the nonuniqueness of the solution. Fixing α_0 would imply fixing u and thus we obtain a unique solution. The easiest option is to choose $\alpha_0 = 0$. What is more general and used in practice is to choose $u(s) = u_s$ for some s a point at the boundary, see for instance [9, p 13]. Suppose it is given that $u(s) = u_s$ for some point s at the boundary. Then

$$\alpha_0 \phi_0(s) + \sum_{j=1}^{\infty} \alpha_s \phi_j(s) = u_s. \tag{2.5.21}$$

So we have

$$\alpha_0 = \frac{1}{\phi_0}(u_s - \sum_{j=1}^{\infty} \alpha_j \phi_j(s)). \tag{2.5.22}$$

The solution is the original solution but shifted.

"The purpose of computation is insight, not numbers. "–Richard Hamming

Chapter 3

The boundary element method

3.1 Introduction

The integral equation (2.4.2) expresses the value of the potential u at any point s in terms of its values and normal derivative at the boundary. A discretisation of this equation leads to the *Boundary Element Method (BEM)* system of algebraic equations. To this end, the physical boundary $\partial\Omega$ is partitioned into N parts $\partial\Omega_j$, $j = 1, 2, \ldots, N$, see Figure 3.1. Each physical partition $\partial\Omega_j$ is represented

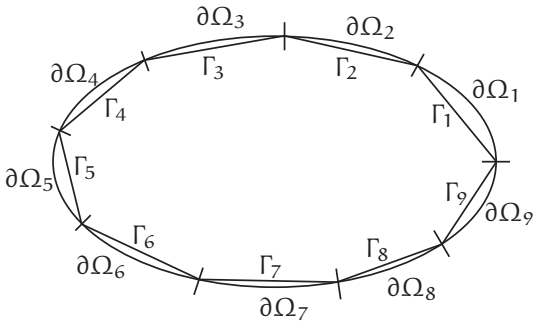

Figure 3.1: A discretisation of an ellipse into $N = 9$ elements.

by a numerical partition Γ_j. The union $\Gamma := \bigcup_{j=1}^{N} \Gamma_j$ is what is called a *numerical boundary*. For Γ_j we use rectilinear *elements* in which the ends of each partition

$\partial\Omega_j$ are connected by a straight line of length l_j to be called a *boundary element*, here simply called element and l_j the *element size*. A grid that has the same element size l for all the elements is called a *uniform grid* of size l .

The elements are numbered according to the standard BEM convention: increasing in the anticlockwise sense. On each of the elements Γ_j an assumption is made on the functions u and q. Basically these functions are assumed to vary as polynomials which are called *shape functions*. Depending on the order of the shape functions on each element, the type of elements used is said to be either constant, linear or even higher order. In this thesis examples in both *constant elements* and *linear elements* are considered. In constant elements, constant shape functions are used, that is, the functions on each element are assumed constant. In linear elements linear shape functions are used, that is, the functions on each element are assumed to vary linearly. In other cases, quadratic or even higher order shape functions may be used.

3.2 Constant elements

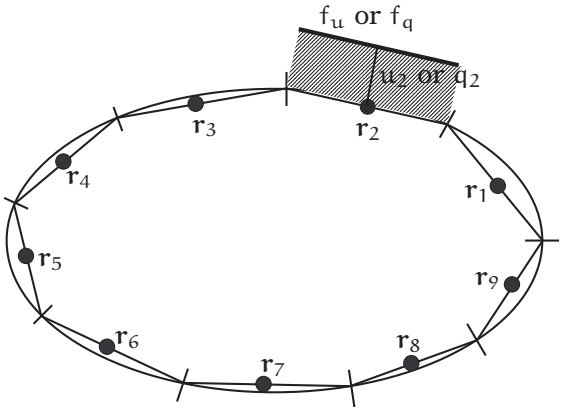

Figure 3.2: Constant elements nodes $r_1, \ldots, r_9$ corresponding to the discretisation in Figure 3.1 and discretisation of functions, f_u, f_q are the shape functions.

For constant elements an element is represented by a single node placed at the midpoint of the element. The element containing the j-th node is denoted Γ_j. These nodes are also used as the *collocation points*, that is, the points where the integral equation is applied. The BIE is then applied at the i-th node and integration over $\partial\Omega$ is estimated by the sum of the integrations on all the N

elements. That is,

$$c(\mathbf{r}_i)u(\mathbf{r}_i) + \sum_{j=1}^{N} \int_{\Gamma_j} u(\mathbf{r}(\chi)) \frac{\partial v}{\partial n}(\mathbf{r}_i; \mathbf{r}(\chi))\, d\chi = \sum_{j=1}^{N} \int_{\Gamma_j} q(\mathbf{r}(\chi)) v(\mathbf{r}_i; \mathbf{r}(\chi))\, d\chi. \quad (3.2.1)$$

Here the nodes $\mathbf{r}_i$, $i = 1, 2, \ldots, N$, are the midpoints of the elements, see Figure 3.2. Next is the discretisation of the functions u and q. These functions are assumed to be constant on each element and equal to their nodal values where the nodes are the midpoints of the elements. So let us introduce the definitions

$$u_j := u(\mathbf{r}_j), \qquad q_j := q(\mathbf{r}_j), \quad (3.2.2)$$

where $\mathbf{r}_j$ is the midpoint of Γ_j. Then assume that

$$u(\mathbf{r}) = u_j \ \text{ and } \ q(\mathbf{r}) = q_j \ \text{ for } \ \mathbf{r} \in \Gamma_j. \quad (3.2.3)$$

Then using (3.2.3) in (3.2.1) gives

$$c_i u_i + \sum_{j=1}^{N} u_j \int_{\Gamma_j} \frac{\partial v}{\partial n}(\mathbf{r}_i; \mathbf{r}(\chi))\, d\chi = \sum_{j=1}^{N} q_j \int_{\Gamma_j} v(\mathbf{r}_i; \mathbf{r}(\chi))\, d\chi, \quad (3.2.4)$$

for all the collocation points $i = 1, 2, \ldots, N$. Define

$$\hat{H}_{ij} := \int_{\Gamma_j} \frac{\partial v}{\partial n}(\mathbf{r}_i; \mathbf{r}(\chi))\, d\chi, \ \text{ and } \ G_{ij} := \int_{\Gamma_j} v(\mathbf{r}_i; \mathbf{r}(\chi))\, d\chi. \quad (3.2.5)$$

These are called influence coefficients because their values express the contribution of the nodal values u_j and q_j to the formation of $c_i u_i$, [35, p. 49]. With this notation equation (3.2.4) becomes

$$c_i u_i + \sum_{j=1}^{N} \hat{H}_{ij} u_j = \sum_{j=1}^{N} G_{ij} q_j. \quad (3.2.6)$$

Setting

$$H_{ij} := c_i \delta_{ij} + \hat{H}_{ij}, \quad (3.2.7)$$

where δ_{ij} is the Kronecker delta, (3.2.6) can be written as

$$\sum_{j=1}^{N} H_{ij} u_j = \sum_{j=1}^{N} G_{ij} q_j. \quad (3.2.8)$$

Let $\mathbf{H}$ and $\mathbf{G}$ be $N \times N$ matrices whose elements are given by (3.2.7) and (3.2.5). Also introduce the following vectors of length N :

$$\mathbf{u} := (u_1,\ u_2, \ldots, u_N)^T, \ \ \mathbf{q} := (q_1,\ q_2, \ldots, q_N)^T. \quad (3.2.9)$$

Then applying equation (3.2.8) for all the collocation points $\mathbf{r}_i$, $i = 1, 2, \ldots, N$, yields

$$\mathbf{Hu} = \mathbf{Gq}. \tag{3.2.10}$$

In (3.2.10) we have a system of N algebraic equations in $2N$ unknowns u_j and q_j, $j = 1, 2, \ldots, N$, which, as it is now, is an underdetermined system. The extra N relations needed to solve the system uniquely must come from the boundary conditions. For each element j, either u_j or q_j is known through boundary conditions.

For generality, let us assume a part $\partial\Omega^1$ of the boundary on which $u(\mathbf{r})$ is given and a part $\partial\Omega^2$ on which $q(\mathbf{r})$ is given. Let these two parts be discretised into N_1 and N_2 constant elements respectively such that $N_1 + N_2 = N$. Thus, there are still N unknowns, $N - N_1$ values of $u(\mathbf{r})$ on $\partial\Omega^2$ and $N - N_2$ values of $q(\mathbf{r})$ on $\partial\Omega^1$ which are to be determined from the system (3.2.10). Before solving the system, the unknown need to be separated from the known quantities. To this end, partition the matrices $\mathbf{H}$ and $\mathbf{G}$ and write (3.2.10) as

$$\begin{pmatrix} \mathbf{H}_1 & \mathbf{H}_2 \end{pmatrix} \begin{pmatrix} \tilde{\mathbf{u}}_1 \\ \mathbf{u}_2 \end{pmatrix} = \begin{pmatrix} \mathbf{G}_1 & \mathbf{G}_2 \end{pmatrix} \begin{pmatrix} \mathbf{q}_1 \\ \tilde{\mathbf{q}}_2 \end{pmatrix}, \tag{3.2.11}$$

where $\tilde{\mathbf{u}}_1$ and $\tilde{\mathbf{q}}_2$ denote the known quantities on Γ^1 (representing $\partial\Omega^1$) and Γ^2 (representing $\partial\Omega^2$) respectively. Then carry out the multiplications and move all the unknowns to the left hand side of the equation to obtain

$$\mathbf{Ax} = \mathbf{b} \tag{3.2.12}$$

where

$$\mathbf{A} := \begin{pmatrix} -\mathbf{G}_1 & \mathbf{H}_2 \end{pmatrix}, \ \mathbf{x} := \begin{pmatrix} \mathbf{q}_1 \\ \mathbf{u}_2 \end{pmatrix}, \mathbf{b} := -\mathbf{H}_1\tilde{\mathbf{u}}_1 + \mathbf{G}_2\tilde{\mathbf{q}}_2. \tag{3.2.13}$$

The solution of the system (3.2.12) gives a BEM approximation of the unknowns in $\mathbf{x}$ in the grid nodes $\mathbf{r}_j$. We denote by $\mathbf{x}^L$ a BEM approximation on a grid of size L. Thus u_j^L (or q_j^L) is a BEM approximation of u_j (or q_j) using a grid of size L.

If the N_1 points and the N_2 points where the values of u and respectively q are prescribed are not consecutive then the partitioning of the matrices in (3.2.11) is preceded by an appropriate rearrangement of columns in $\mathbf{H}$ and $\mathbf{G}$. Solving (3.2.12) gives the unknown boundary quantities of u and q. Therefore we now have all the boundary quantities. The solution $u(\mathbf{r})$ can then be computet at any point $\mathbf{r} \in \Omega$ using (3.2.4) with $c(\mathbf{r}) = 1$.

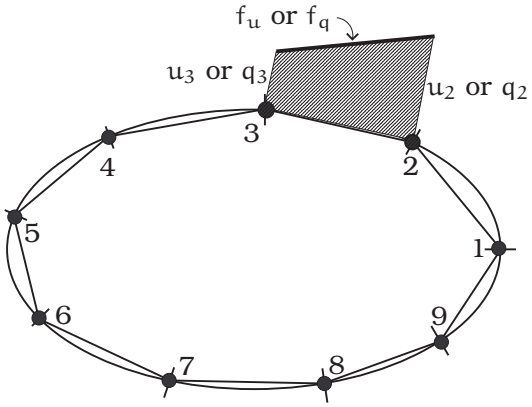

Figure 3.3: Linear elements nodes and discretisation of the functions, f_u and f_q are shape functions.

3.3 Linear elements

In the case of linear elements the potential and its derivative are assumed to vary linearly over each element. This thesis discusses *continuous linear elements* in which the nodes are placed at the extremes of the element, see Figure 3.3. So f_u and f_q are linear interpolation functions expressed in terms of the values of u and q respectively at the extremes of the element. That is

$$f_u(\xi) = a + b\xi, \qquad f_q(\xi) = c + d\xi, \tag{3.3.1}$$

where ξ is a local coordinate on an element (see (3.5.4)) and a, b and c, d are constants to be determined by substituting the values of u and q respectively at the extremes of the elements. For details on obtaining the system of equations (3.2.12) when linear elements are used see [35, p. 111], [57, p. 78].

3.4 Boundary corner singularities

Most of this thesis is devoted to discussing errors in BEM. In Chapter 4 we discuss sources of error that are due to the approximations that we make in a BEM formulation. One inherent source of error in BEM solutions may be due to the boundary on which we are solving. In particular boundaries with corners, in two dimensions, and edges, in three dimensions, deserve special attention due to the errors that occur in these regions. These errors are due to the singular behaviour of the functions involved in these locations, see for

instance [13], [54], [70]. Of course the potential at any point, be it a corner or otherwise, can only have one value. However, there are two distinct normal gradients at every corner, and several combinations of boundary conditions at a corner are now possible, see [78].

The spatial derivative of the potential field governed by the Laplace and Poisson equations can become infinite at corners and edges rendering the standard BEM as discussed in this thesis to give inaccurate results [24, p 282], [28, p 164], [56]. In [65] the authors have suggested a formulation of mixed elements to overcome this problem. Due to this corner problem, in the course of measuring error order in the subsequent chapters of this thesis we avoid boundaries with corners. This is because any results obtained with such boundaries will also reflect how well this corner problem is being circumvented.

3.5 Matrix elements

Forming the system (3.2.12) requires the formation of the matrices $\hat{\mathbf{H}}$ and $\mathbf{G}$ for which we need to evaluate the integrals in (3.2.5). In two dimensions we have

$$G_{ij} = \int_{\Gamma_j} v(\mathbf{r}_i; \mathbf{r}(\chi))\, d\chi = -\frac{1}{2\pi} \int_{\Gamma_j} \log \|\mathbf{r}_i - \mathbf{r}(\chi)\|\, d\chi \tag{3.5.1a}$$

and

$$\hat{H}_{ij} = \frac{1}{2\pi} \int_{\Gamma_j} \frac{\partial v}{\partial n}(\mathbf{r}_i; \mathbf{r}(\chi))\, d\chi = \frac{1}{2\pi} \int_{\Gamma_j} \frac{(\mathbf{r}_i - \mathbf{r}(\chi), \mathbf{n}(\chi))}{\|\mathbf{r}_i - \mathbf{r}(\chi)\|^2}\, d\chi. \tag{3.5.1b}$$

We note that the integrals are singular when $\mathbf{r} \to \mathbf{r}_i$ and therefore need special treatment when $i = j$. For $i \neq j$, the integrals are nonsingular and are evaluated numerically using Gaussian quadrature. To this end suppose we use rectilinear elements and $\mathbf{r}_{j-\frac{1}{2}}$ and $\mathbf{r}_{j+\frac{1}{2}}$ are the extremes of element j of length l_j as shown in Figure 3.4. We denote the *grid size* of element Γ_j by

$$l_j := \|\mathbf{r}_{j+1/2} - \mathbf{r}_{j-1/2}\|. \tag{3.5.2}$$

We do a parameterization of the element j in terms of a local coordinate ξ on Γ_j, that is

$$\mathbf{r}(\xi) := \frac{1}{2}(\mathbf{r}_{j-\frac{1}{2}} + \mathbf{r}_{j+\frac{1}{2}}) + \frac{(\mathbf{r}_{j+\frac{1}{2}} - \mathbf{r}_{j-\frac{1}{2}})}{l_j}\xi, \tag{3.5.3}$$

where

$$-l_j/2 \leq \xi \leq l_j/2. \tag{3.5.4}$$

The Jacobian of this transformation is

$$J(\xi) = \sqrt{\left(\frac{dx}{d\xi}\right)^2 + \left(\frac{dy}{d\xi}\right)^2} = 1,$$

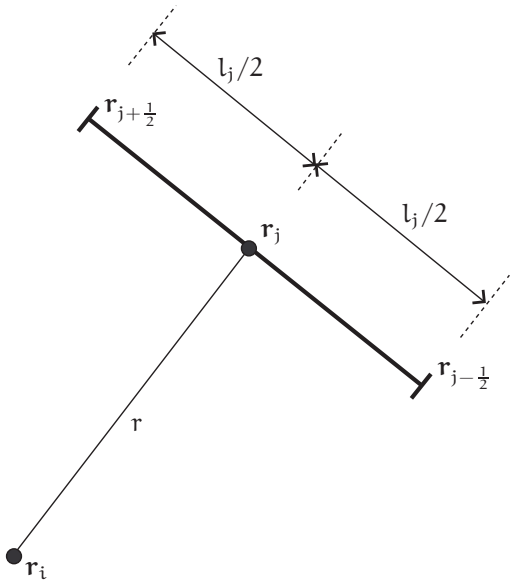

Figure 3.4: Illustration of integration terms on element Γ_j

where, from (3.5.3),

$$x(\xi) = \frac{1}{2}(x_{j-\frac{1}{2}} + x_{j+\frac{1}{2}}) + \frac{(x_{j+\frac{1}{2}} - x_{j-\frac{1}{2}})}{l_j}\xi,$$
$$y(\xi) = \frac{1}{2}(y_{j-\frac{1}{2}} + y_{j+\frac{1}{2}}) + \frac{(y_{j+\frac{1}{2}} - y_{j-\frac{1}{2}})}{l_j}\xi.$$

Then using the above parameterization the integrals (3.5.1) become

$$G_{ij} = -\frac{1}{2\pi}\int_{-l_j/2}^{l_j/2} \log\|\mathbf{r}_i - \mathbf{r}(\xi)\|\,d\xi \tag{3.5.5a}$$

$$\hat{H}_{ij} = \frac{1}{2\pi}\int_{-l_j/2}^{l_j/2} \frac{(\mathbf{r}_i - \mathbf{r}(\xi), \mathbf{n})}{\|\mathbf{r}_i - \mathbf{r}(\xi)\|^2}\,d\xi. \tag{3.5.5b}$$

Since Gaussian quadrature points are given for the interval $[-1, 1]$ introduce a new coordinate η defined as $\eta := \xi/(l_j/2)$. Then the integrals (3.5.5) become

$$G_{ij} = -\frac{l_j}{4\pi}\int_{-1}^{1} \log\|\mathbf{r}_i - \mathbf{r}(\eta)\|\,d\eta \tag{3.5.6a}$$

$$\hat{H}_{ij} = \frac{l_j}{4\pi}\int_{-1}^{1} \frac{(\mathbf{r}_i - \mathbf{r}(\eta), \mathbf{n})}{\|\mathbf{r}_i - \mathbf{r}(\eta)\|^2}\,d\eta, \tag{3.5.6b}$$

where

$$\mathbf{r}(\eta) := \frac{1}{2}(\mathbf{r}_{j-\frac{1}{2}} + \mathbf{r}_{j+\frac{1}{2}}) + \frac{1}{2}(\mathbf{r}_{j+\frac{1}{2}} - \mathbf{r}_{j-\frac{1}{2}})\eta \tag{3.5.7}$$

and η is a local coordinate on the element such that $-1 \leq \eta \leq 1$.

When $i \neq j$ the integrands in (3.5.6) are nonsingular and the integrals can be evaluated using standard Gaussian quadrature. However for $i = j$ the integrands are singular and the integrals are evaluated analytically. We have

$$\int_{-l_j/2}^{l_j/2} \log \|\mathbf{r}_i - \mathbf{r}(\xi)\| \, d\xi = 2 \lim_{\epsilon \to 0} \int_{\epsilon}^{l_j/2} \log \xi \, d\xi = l_j(\log(l_j/2) - 1).$$

So (3.5.5a) becomes

$$G_{ii} = -\frac{l_i}{2\pi}(\log(l_i/2) - 1). \tag{3.5.8}$$

The integrand of $\hat{H}_{ij}$ has the inner product $(\mathbf{r}_i - \mathbf{r}, \mathbf{n})$ in the numerator. When $i = j$ the vector $\mathbf{r}_i - \mathbf{r}$ is in the same element as the normal $\mathbf{n}$ and the two are perpendicular. Consequently $(\mathbf{r}_i - \mathbf{r}, \mathbf{n}) = 0$ and hence

$$\hat{H}_{ii} = \frac{1}{2\pi} \int_{\Gamma_i} \frac{(\mathbf{r}_i - \mathbf{r}(\chi), \mathbf{n})}{\|\mathbf{r}_i - \mathbf{r}(\chi)\|^2} \, d\chi = 0. \tag{3.5.9}$$

3.6 Numerical integration

To complete the system of equations to be solved in BEM, the integrals in (3.5.6) have to be evaluated. When the integrands are singular the integrals are evaluated analytically as shown in (3.5.8) and (3.5.9). However, the nonsingular integrals can be approximated using standard *Gauss-Legendre quadrature*. After parametrisation in (3.5.6) the integrals are of the form

$$\int_{-1}^{1} f(\eta) \, d\eta. \tag{3.6.1}$$

For $f(\eta)$ nonsingular, the standard Gauss-Legendre quadrature gives

$$\int_{-1}^{1} f(\eta) \, d\eta \approx \sum_{i=1}^{m} \omega_i f(\eta_i), \tag{3.6.2}$$

where η_i are the *knots* and ω_i the *weights*, see [73] for tables of knots and their corresponding weights.

Other than resorting to analytical expressions, if f has a weak or logarithmic singularity over the interval $[-1, 1]$, the integral can also be evaluated using

special numerical integration schemes for integrals with a weak or logarithmic singularity. For an integral with a logarithmic singularity the following Gauss-log approximation is used [15, 73],

$$\int_0^1 f(\eta)\log(\eta)\,d\eta \approx \sum_{i=1}^{m} \tilde{\omega}_i f(\tilde{\eta}_i), \tag{3.6.3}$$

where $\tilde{\eta}_i$ are the *knots* and $\tilde{\omega}_i$ the *weights* for the quadrature rule with a logarithmic singularity. In addition to [15, 73], the weights can also be found in [43, p. 513]. More on numerical computation of integrals with a logarithmic singularity can be found in [67].

3.7 Examples

In this thesis we like to use some reference cases. They are given by Examples 3.7.1 to 3.7.4. For the problem domain, either a disc or a square is used.

Example 3.7.1 (Problem (a): Dirichlet problem, smooth solution)

$$\begin{cases} \nabla^2 u(\mathbf{r}) = 0, & \mathbf{r} \in \Omega, \\ \\ u(\mathbf{r}) = x^2 - y^2, & \mathbf{r} \in \partial\Omega. \end{cases} \tag{3.7.1}$$

Taking $\Omega = \{\mathbf{r} \in \mathbb{R}^2 : \|\mathbf{r}\| \leq 1.2\}$, Example 3.7.1 has the continuous solution shown in Figure 3.5b. Figure 3.5a shows the domain considered: a circular disc of radius $R = 1.2$ centred at the origin. Since $u(x, y)$ itself satisfies the Laplace equation in Ω we can easily compute the analytic solution $q(x, y) = \mathbf{n} \cdot \nabla u(x, y)$. The boundary function $u(x, y)$ in polar coordinates centred at the origin is given by $u(R, \theta) = R^2 \cos 2\theta$ and the analytic solution is $q(R, \theta) = 2R \cos 2\theta$. Figure 3.5b shows the solution plotted against the polar angle.

Example 3.7.2 (Problem (b): Dirichlet problem, locally active solution)

$$\begin{cases} \nabla^2 u(\mathbf{r}) = 0, & \mathbf{r} \in \Omega, \\ \\ u(\mathbf{r}) = \log(\|\mathbf{r} - \mathbf{r}_0\|), & \mathbf{r} \in \partial\Omega, \end{cases} \tag{3.7.2}$$

where $\mathbf{r}_0$ is a fixed point outside Ω. Again taking the disc shown in Figure 3.6a as the domain and $\mathbf{r}_0 = (0.36, 1.8)$, Example 3.7.2 can be solved analytically. The continuous solution, shown in Figure 3.6b, is $q(\mathbf{r}) = (\mathbf{r} - \mathbf{r}_0) \cdot \mathbf{n}(\mathbf{r})/\|\mathbf{r} - \mathbf{r}_0\|^2$ where $\mathbf{n}(\mathbf{r})$ is the unit outward normal at $\mathbf{r}$. The solution is plotted against the angle θ around the circle, note the local high activity near $\theta = 1.4$.

Example 3.7.3 (Problem (c): Neumann problem, smooth solution)

$$\begin{cases} \nabla^2 u(\mathbf{r}) = 0, & \mathbf{r} \in \Omega, \\ \\ q(\mathbf{r}) = \dfrac{2(x^2 - y^2)}{\sqrt{x^2 + y^2}}, & \mathbf{r} \in \partial\Omega. \end{cases} \tag{3.7.3}$$

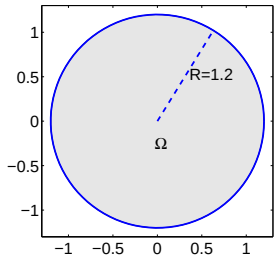

(a) Disc domain.

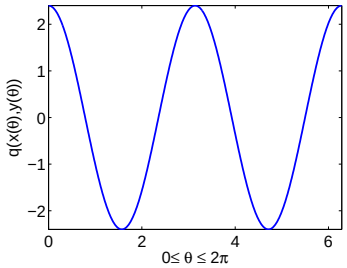

(b) Solution on circle

Figure 3.5: A disc domain and solution to Example 3.7.1 on the circular boundary of radius $R = 1.2$.

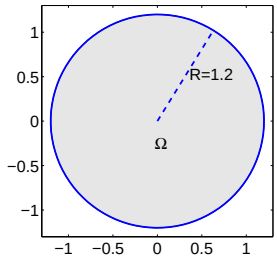

(a) Disc domain.

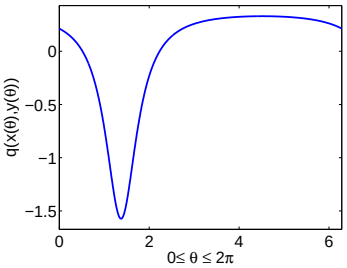

(b) Solution on circle

Figure 3.6: A disc domain and solution to Example 3.7.2 with $r_0 = (0.36, 1.8)$ on the circular boundary of radius $R = 1.2$.

Take again as domain the disc of radius $R = 1.2$ shown in Figure 3.7a. The solution to this problem can be computed analytically. For our circular domain the solution is easily expressed in polar coordinates centred at the origin and is given by $u(R, \theta) = R^2 \cos 2\theta$. Figure 3.7b is a plot of this solution against θ.

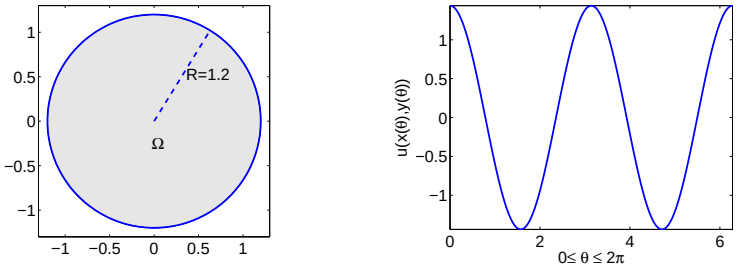

(a) Disc domain. (b) Solution on circle

Figure 3.7: A disc domain and solution to Example 3.7.3 on the circular boundary of radius $R = 1.2$.

Example 3.7.4 (Problem (d): Neumann problem, locally active solution)

$$\begin{cases} \nabla^2 u(\mathbf{r}) = 0, & \mathbf{r} \in \Omega, \\ q(\mathbf{r}) = \dfrac{(\mathbf{r} - \mathbf{r}_0) \cdot \mathbf{n}(\mathbf{r})}{\|\mathbf{r} - \mathbf{r}_0\|^2}, & \mathbf{r} \in \partial\Omega, \end{cases} \tag{3.7.4}$$

where $\mathbf{r}_0$ is a fixed point outside Ω and $\mathbf{n}(\mathbf{r})$ is the outward normal at $\mathbf{r}$. The solution to this problem can be computed analytically. Again for the disc shown in Figure 3.8a as domain and $\mathbf{r}_0 = (0.36, 1.8)$, Example 3.7.4 has the continuous solution shown in Figure 3.8 where θ is the angle around the circle. Note again the relatively high local activity near $\theta = 1.4$.

For these examples, the analytic expressions for the solutions are known. This will help us compare exact analytic and numerical solutions and thus compute global and local errors as we will see in Chapters 4 and 5. Observe in these examples that the solution to Dirichlet problem 1 is the boundary condition in Neumann problem 1 and vice-versa. Also the solution to Dirichlet problem 2 is the boundary condition in Neumann problem 2 and vice-versa.

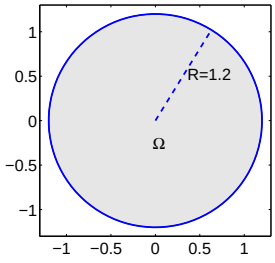

(a) Disc domain.

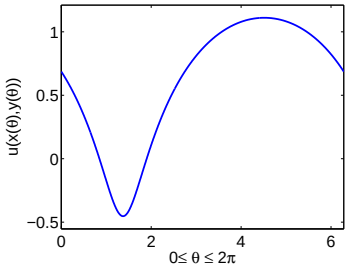

(b) Solution on circle

Figure 3.8: A disc domain and solution to Example 3.7.4 with $r_0 = (0.36, 1.8)$ on the circular boundary of radius $R = 1.2$.

"The study of error is not only in the highest degree prophylatic, but it serves as a stimulating introduction to the study of truth." – Walter Lipmann

Chapter 4

Local errors in BEM for potential problems

4.1 Introduction

The BEM results from a numerical discretisation of a BIE. The subject of errors in BEM is still a very interesting one and some aspects have not yet been as explored as they are in other numerical methods like finite element methods (FEM) and finite difference methods (FDM). Errors in BEM solutions may be due to discretisation or to inaccuracies in the solver that involves the use of BEM matrices with high condition numbers. Although a BIE is an exact representation for the solution of a BVP, errors will occur in BEM because the BIE is applied at only a selected set of collocation points.

For a given discretisation, there are several ways to implement BEM because of the choice in collocation and nodal points and the shape functions. These will all influence the resulting error in the solution. Amongst the error sources also is the fact that the choice of shape functions at the boundary elements may not satisfy the smoothness requirements of the original BIE. In most cases where error measurement has been performed, like in adaptive refinement, the main focus has been a guiding measure of the error. In this chapter we present recent results on an analysis of actual local errors in BEM solutions. The results presented will not only be helpful in choosing an implementation strategy but also in guiding adaptive refinement techniques. We focus our attention to obtaining infinity norm estimates of the error.

Several techniques have been used to measure BEM errors in the area of adaptive refinement. In [45] and [37] a review of error estimation and adaptive

methods can be found. Most of these methods are *a posteriori* providing an indirect way of estimating the error. For instance the discretisation error is estimated by the difference between two solutions obtained using different collocation points but the same discretisation [22]. Another technique uses the first (singular integral equation) and the second (hypersingular integral equation) kind formulations to provide an error estimate [44]. Data from the first kind of equation is substituted into the second kind to obtain a residual which is then used to estimate the error. In [29] the authors have used a so called gradient recovery procedure to develop a local error estimate. The error function is generated from differences between smoothed and non-smoothed rates of change of boundary variables in a local tangent direction. Some authors have used a posteriori error estimation in FEM as a guiding tool to develop error estimates for BEM [8]. In [66] residual based estimators are used in the case of Galerkin solutions. An error estimator is also obtained by solving an error equation as accurately as possible, see [66]. Unfortunately usually such techniques are restricted to Galerkin BEM and literature is scarce for collocation BEM formulations and BEM in general as compared to FEM [8, 17, 29, 45]. In our case we would like to start from the basics of the BIE discretisation to develop error analyses for collocation BEM for potential problems. Though the ideas could easily be adapted to 3D, 2D problems and the Laplace equation in particular are discussed.

When a value x_j is approximated by x_j^L using BEM, a *global error* e_j, which is the difference between the exact solution x_j and its BEM approximation x_j^L, is committed. That is,

$$\mathbf{e} := \mathbf{x} - \mathbf{x}^L. \tag{4.1.1}$$

For instance for a Dirichlet problem the BEM solution is a vector of values of the normal derivative $\mathbf{q}^L$ and the global error is given by

$$\mathbf{e} := \mathbf{q} - \mathbf{q}^L. \tag{4.1.2}$$

To assess this we first have to investigate the *local discretisation error*. Local discretisation errors are usually defined as the residual that remains if the exact solution is substituted into the discretised equation. In operator notation, suppose we have an operator $\mathcal{A}$ and a discretisation of $\mathcal{A}$, say $\mathcal{A}^L$, both defined on the same space. Let the continuous solution u satisfy

$$\mathcal{A}u = b. \tag{4.1.3}$$

Let the discretised problem be

$$\mathcal{A}^L u^L = b^L, \tag{4.1.4}$$

where u^L is the discrete approximation of u. Then the *local error* d^L is defined by

$$\mathcal{A}^L u = b^L + d^L, \tag{4.1.5}$$

where u is the projection of the full exact solution on the grid. As a consequence, the global error satisfies

$$\mathcal{A}^L e = d^L. \tag{4.1.6}$$

Alternatively we can define the local error through

$$\mathcal{A}u^L = b + d, \tag{4.1.7}$$

that is, by substituting the approximation into the exact problem. This gives

$$\mathcal{A}e = d. \tag{4.1.8}$$

Both (4.1.6) and (4.1.8) can be useful to estimate global error. However, inversion in order to get the global error in (4.1.8) is hampered by the fact that we need information of the solutions everywhere. Nevertheless (4.1.7) is appealing as it is based on the original operator.

In this chapter local errors are discussed. Global errors will be discussed in Chapter 5. Section 4.2 presents a brief survey of error sources in BEM and Section 4.2.1 presents a discussion on local errors due to interpolation in BEM and a theory for the expected convergence rates of the local error for both constant and linear elements. It is shown here that the local errors for both formulations are of second order. Numerical results for both Dirichlet and Neumann examples are presented to verify the theory presented on local errors.

For the theories on local errors we assume a uniform grid. However it might not always be necessary to have uniform grids. For problems with localised regions of high activity, a composite coarse-fine grid is useful. In Section 4.7 the process of *equidistribution* in BEM for problems whose solutions have small regions of high activity is discussed.

4.2 A survey of error sources

In a BEM implementation, the first step is to discretise the boundary of the domain. Then in the application of the integral equation we have the freedom to choose collocation points and the nodal points. This suggests that for a given discretisation there is more than one way one can choose to implement the BEM, each of which will have its own advantages and disadvantages. Throughout this thesis we consider discretisations using rectilinear elements. This results into the numerical boundary being a polygon, see for instance Figure 4.1 in the case of a circular boundary.

Besides choosing the position of collocation and nodal points on the numerical boundary, the way boundary conditions are treated is also important. In the traditional constant elements for example, the nodes are the midpoints of the

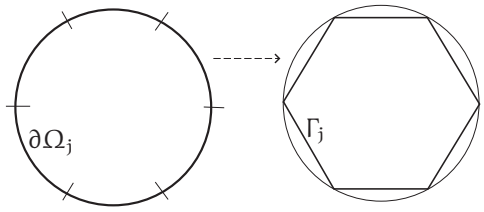

Figure 4.1: Discretisation of a circle into a six elements polygon.

elements and are also the collocation points. For the discretisation shown in Figure 4.1, the numerical boundary does not coincide with the physical boundary and so we may talk of exact points $\mathbf{r}_i$ on $\partial\Omega$ and their numerical representations $\bar{\mathbf{r}}_i$ on Γ as shown in Figure 4.2. One may thus choose collocation points

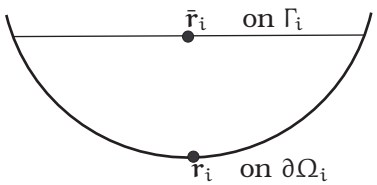

Figure 4.2: Numerical representation of boundary points; $\mathbf{r}_i$ the exact point and $\bar{\mathbf{r}}_i$ its numerical representation.

on the physical boundary or on the numerical boundary. Likewise one may choose to compute the integrals of the known functions on the exact physical boundary or on the numerical boundary. In Table 4.1 we give a summary of the possibilities one may consider in the case of a Dirichlet problem when implementing constant elements. Similar choices arise in the case of a Neumann or mixed problem.

The different cases arise from the location of collocation points on either the numerical boundary or the physical boundary, treatment of boundary conditions and the choice between the numerical and physical boundary for the integrals involved in the formation of the matrix $\mathbf{A}$ and vector $\mathbf{b}$ in (3.2.12).

Consider for instance, cases (1) and (5) in Table 4.1. In case (1) the collocation points are on the numerical boundary Γ_j, the boundary function u is assumed constant on Γ_j taking on the midpoint value $u(\mathbf{r}_j)$, the right hand side $\mathbf{b}$ and the matrix $\mathbf{A}$ are formed by integrating on Γ_j. This is the traditional implementation

position of collocation points	boundary condition on the element	form **b** by integrating either on $\partial\Omega_j$ or Γ_j	form **A** by integrating either on $\partial\Omega_j$ or Γ_j	
on Γ_i	$u(\mathbf{r}_j)$	Γ_j	Γ_j	(1)
			$\partial\Omega_j$	(2)
		$\partial\Omega_j$	Γ_j	(3)
			$\partial\Omega_j$	(4)
	$u(\mathbf{r})$	Γ_j	Γ_j	(5)
			$\partial\Omega_j$	(6)
		$\partial\Omega_j$	Γ_j	(7)
			$\partial\Omega_j$	(8)
on $\partial\Omega_i$	$u(\mathbf{r}_j)$	-	-	(9)
			-	(10)
		$\partial\Omega_j$	-	(11)
			$\partial\Omega_j$	(12)
	$u(\mathbf{r})$	-	-	(13)
			-	(14)
		$\partial\Omega_j$	-	(15)
			$\partial\Omega_j$	(16)

Table 4.1: Summary of possibilities on how one could implement constant elements BEM.

of constant elements. That is,

$$b_i := -\frac{1}{2}u_i - \sum_{j=1}^{N} u_j \int_{\Gamma_j} \frac{\partial \nu}{\partial n}(\bar{\mathbf{r}}_i; \mathbf{r}(\chi))\, d\chi, \tag{4.2.1}$$

$$A_{ij} := -\int_{\Gamma_j} \nu(\bar{\mathbf{r}}_i; \mathbf{r}(\chi))\, d\chi. \tag{4.2.2}$$

In case (5) the collocation points are on the numerical boundary, the boundary function $u(\mathbf{r})$ is not assumed constant on Γ_j but used directly as given in the formation of **b**, the right hand side **b** and the matrix **A** are formed by integrating on Γ_j. That is

$$b_i := -\frac{1}{2}u(\bar{\mathbf{r}}_i) - \sum_{j=1}^{N} \int_{\Gamma_j} u(\mathbf{r}(\chi)) \frac{\partial \nu}{\partial n}(\bar{\mathbf{r}}_i; \mathbf{r}(\chi))\, d\chi, \tag{4.2.3}$$

$$A_{ij} := -\int_{\Gamma_j} \nu(\bar{\mathbf{r}}_i; \mathbf{r}(\chi))\, d\chi. \tag{4.2.4}$$

The other cases can also be explained by following their respective trends in the table. Cases (9) to (16) are obtained by choosing collocation on the physical boundary. The dashes in the table are for cases that are not feasible in the sense that once we have chosen to collocate on the physical boundary then we should implement the integral equation on the physical boundary by carrying out the integrations in the formation of **b** and **A** on the same boundary.

In Table 4.2 results for some of the cases in Table 4.1 are presented. In particular, in Table 4.2a is a comparison of cases (1) and (5) and in Table 4.2b a

comparison of cases (12) and (16).

	$\|\|\mathbf{d}\|\|_\infty$	
N	*case (1)*	*case (5)*
5	1.20	1.02E-01
15	1.66E-01	3.87E-02
45	1.90E-02	5.12E-03
135	2.13E-03	5.98E-04
405	2.38E-04	6.75E-05
1215	2.65E-05	7.57E-06

(a)

	$\|\|\mathbf{d}\|\|_\infty$	
N	*case (12)*	*case (16)*
5	1.76E-02	1.81E-01
15	3.53E-02	2.86E-02
45	4.99E-03	4.74E-03
135	5.93E-04	5.84E-04
405	6.73E-05	6.70E-05
1215	7.54E-06	7.52E-06

(b)

Table 4.2: Local errors in cases (1) and (5) in (a) and cases (12) and (16) in (b) when the problem in Example 3.7.1, which is a Dirichlet problem, is solved on a disc domain. The local error $\mathbf{d}$ is defined in (4.1.5).

	$\|\|\mathbf{d}\|\|_\infty$	
N	*case (1)*	*case (5)*
5	3.11E-01	2.63E-02
15	4.81E-02	1.12E-02
45	5.67E-03	1.52E-03
135	6.39E-04	1.79E-04
405	7.13E-05	2.02E-05
1215	7.93E-06	2.26E-06

(a)

	$\|\|\mathbf{d}\|\|_\infty$	
N	*case (12)*	*case (16)*
5	5.34E-03	5.49E-02
15	1.04E-02	8.40E-03
45	1.49E-03	1.42E-03
135	1.78E-04	1.75E-04
405	2.02E-05	2.01E-05
1215	2.26E-06	2.26E-06

(b)

Table 4.3: Local errors in cases (1) and (5) in (a) and cases (12) and (16) in (b) when we the problem in Example 3.7.1, which is a Dirichlet problem, is solved on a disc domain. The local error $\mathbf{d}$ is defined in (4.1.5).

It is expected that the results of case (5) are better than those of case (1), since case (5) should capture the variation of the boundary function better. For the same reasons, the results of case (16) are expected to be better than those of case (12). Since in cases (12) and (16) the numerical boundary coincides with the physical boundary, the corresponding results should be better than those of cases (1) and (5). The results in Table 4.2 agree with this observation. Although the difference in results might seem not that much, we note that the problems in real life will usually involve more complicated geometries for the physical boundary and more wild boundary conditions. This will make the difference between the choices in Table 4.1 more important than it looks in the above example.

Although some work has already been done in estimating errors in BEM, there is not yet an error analysis that traces down all the error sources above. In [28,

p. 141] the authors have remarked that: "any error analysis which seeks to trace the accumulation of error as it arises from the approximation of the physical boundary by a numerical boundary, approximation of the boundary quantities by interpolation and approximation of the integrals by quadrature rules is likely to be very complicated, if indeed it is possible at all." In the next sections we concentrate on analysing the error that is due to the approximation of the boundary quantities by interpolation in constant and linear elements.

4.2.1 Defining local errors

Section 4.2 above introduced different ways in which BEM can be implemented. These induce sources of error in BEM for potential problems: approximation of the physical boundary by a numerical boundary, approximation of the boundary quantities by interpolation, and approximation of the integrals by quadrature rules. Thus, the local error in BEM will be an accumulation of the following errors from each of the above sources respectively:

(i) *Boundary discretisation error*: This error is not there if Γ_j and $\partial\Omega_j$ coincide.

(ii) *Interpolation error*: This is the most important one. The unknown functions are assumed to vary as certain interpolation polynomials, the so called shape functions $f_u(\mathbf{r})$ and $f_q(\mathbf{r})$ for $u(\mathbf{r})$ and $q(\mathbf{r})$ respectively. For instance for constant elements, assuming the functions $u(\mathbf{r})$ and $q(\mathbf{r})$ are assumed piecewise constant on each Γ_j.

(iii) *Quadrature error*: This error is also very important since all the integrals in (3.2.5) are usually evaluated using numerical quadrature. However, it can be minimised by choosing suitable high order quadrature rules.

Let us again consider a general point $\mathbf{s}$ at the boundary where the integral equation is applied. Then constant elements assumes:

$$\int_{\partial\Omega_j} u(\mathbf{r}(\chi))\frac{\partial v}{\partial n}(\mathbf{s};\mathbf{r}(\chi))\,d\chi \doteq \int_{\Gamma_j} u(\mathbf{r}(\chi))\frac{\partial v}{\partial n}(\mathbf{s};\mathbf{r}(\chi))\,d\chi, \tag{4.2.5a}$$

$$\int_{\Gamma_j} u(\mathbf{r}(\chi))\frac{\partial v}{\partial n}(\mathbf{s};\mathbf{r}(\chi))\,d\chi \doteq \int_{\Gamma_j} f_u(\mathbf{r}(\chi))\frac{\partial v}{\partial n}(\mathbf{s};\mathbf{r}(\chi))\,d\chi = u_j \int_{\Gamma_j} \frac{\partial v}{\partial n}(\mathbf{s};\mathbf{r}(\chi))\,d\chi, \tag{4.2.5b}$$

$$u_j \int_{\Gamma_j} \frac{\partial v}{\partial n}(\mathbf{s};\mathbf{r}(\chi))\,d\chi \doteq u_j Q_j\left(\frac{\partial v}{\partial n}(\mathbf{s};\mathbf{r}(\chi))\right). \tag{4.2.5c}$$

Here $Q_j\left\{\frac{\partial v}{\partial n}(\mathbf{s};\mathbf{r}(\chi))\right\}$ denotes a quadrature approximation of the integral. Likewise for the single layer integrals we have

$$\int_{\partial\Omega_j} q(\mathbf{r}(\chi))v(\mathbf{s};\mathbf{r}(\chi))\,d\chi \doteq \int_{\Gamma_j} q(\mathbf{r}(\chi))v(\mathbf{s};\mathbf{r}(\chi))\,d\chi, \tag{4.2.6a}$$

$$\int_{\Gamma_j} q(\mathbf{r}(\chi))v(\mathbf{s};\mathbf{r}(\chi))\,d\chi \doteq \int_{\Gamma_j} f_q(\mathbf{r}(\chi))v(\mathbf{s};\mathbf{r}(\chi))\,d\chi = q_j\int_{\Gamma_j} v(\mathbf{s};\mathbf{r}(\chi))\,d\chi, \tag{4.2.6b}$$

$$q_j\int_{\Gamma_j} v(\mathbf{s};\mathbf{r}(\chi))\,d\chi \doteq q_j Q_j\left(v(\mathbf{s};\mathbf{r}(\chi))\right). \tag{4.2.6c}$$

If Dirichlet boundary conditions are given on Γ_j, then $u_j = u(\mathbf{r}_j)$ in (4.2.5b) and likewise $q_j = q(\mathbf{r}_j)$ in (4.2.6b), in the case of Neumann boundary conditions.

Note that the expressions in (4.2.5) and (4.2.6) will be similar in linear elements except that now the functions f_u and f_q will be order one polynomials as introduced in (3.3.1). The local error per element is an accumulation of the local errors in (4.2.5) and/or (4.2.6), depending on the boundary conditions given and how they are treated. So we define the errors on the j-th element for a source node $\mathbf{s}$ as:

$$d_j^u(\mathbf{s}) := \int_{\partial\Omega_j} u(\mathbf{r}(\chi))\frac{\partial v}{\partial n}(\mathbf{s};\mathbf{r}(\chi))\,d\chi - u_j Q_j\left(\frac{\partial v}{\partial n}(\mathbf{s};\mathbf{r}(\chi))\right), \tag{4.2.7a}$$

$$d_j^q(\mathbf{s}) := \int_{\partial\Omega_j} q(\mathbf{r}(\chi))v(\mathbf{s};\mathbf{r}(\chi))\,d\chi - q_j Q_j\left(v(\mathbf{s};\mathbf{r}(\chi))\right). \tag{4.2.7b}$$

The errors d_j^u and d_j^q in (4.2.7) are what we will call the *sublocal errors*. Then the local error at $\mathbf{s}$ due to contributions from all the elements is defined as

$$d(\mathbf{s}) := -\sum_{j=1}^{N} d_j^u(\mathbf{s}) + \sum_{j=1}^{N} d_j^q(\mathbf{s}). \tag{4.2.8}$$

When $\mathbf{s} = \mathbf{r}_i$ in the discretisation introduced in Section 3.2, then the error $d(\mathbf{r}_i)$ given by (4.2.8) is the local error in the i-th equation. That is if we were to write the exact equation of (3.2.1) using BEM approximations u_j and q_j we would obtain

$$c(\mathbf{r}_i)u(\mathbf{r}_i) + \sum_{j=1}^{N} u_j\int_{\partial\Omega_j}\frac{\partial v}{\partial n}(\mathbf{r}_i;\mathbf{r}(\chi))\,d\chi = \sum_{j=1}^{N} q_j\int_{\partial\Omega_j} v(\mathbf{r}_i;\mathbf{r}(\chi))\,d\chi + d(\mathbf{r}_i). \tag{4.2.9}$$

We will mainly be interested in the error due to interpolation and will minimise the error due to quadrature by using high order adaptive quadrature rules. It is also important to note that in some problems the physical boundary is

quite regular or indeed coincides exactly with the numerical boundary hence eliminating one inherent source of error.

The treatment of boundary conditions also has a significant contribution to the local error we are assessing. Consider the case of a Dirichlet problem. Although in this case the continuous function u is known, usually u is still assumed to be constant like in (4.2.5b). Although this leaves the method cheaper and easier to implement, it introduces an error in the right hand side that could have rather been avoided. The contribution d_{ij}^{u} in (4.2.7a) to the local error can be skipped by avoiding this assumption on u and thus have an *"exact right hand side"*.

In what follows we assess further local errors for both the constant and linear element formulations and in Chapter 5 global errors are assessed. Out of the possibilities presented in Table 4.1, we concentrate on the traditional constant elements. However, the constant u assumption is avoided on elements where the continuous function is known. Thus, possibility (5) in the table is examined. We use here a better in depth approach than that used in [33] by using the local arc coordinate and sublocal error.

4.3 Dirichlet problems

Consider the case of Dirichlet boundary conditions. This case results in the first kind integral equation

$$\mathcal{K}^{s}(\mathbf{s};\mathbf{r})q(\mathbf{r}) = f(\mathbf{r}) \tag{4.3.1}$$

where the right hand side

$$f(\mathbf{r}) = \frac{1}{2}\mathcal{I} + \mathcal{K}^{d}(\mathbf{s};\mathbf{r})u(\mathbf{r}) \tag{4.3.2}$$

is known since u is given. The solution of (4.3.1) in BEM therefore involves estimating integrals of the form

$$I := \frac{1}{2\pi}\int_{\partial\Omega_j} v(\mathbf{s};\mathbf{r}(\chi))q(\mathbf{r}(\chi))\,d\chi. \tag{4.3.3}$$

The following two sections discuss local errors due to a BEM solution of (4.3.1) using constant elements and linear elements.

4.3.1 Constant elements

In this section attention is focussed on constant elements and assess the interpolation error. As one may expect the error will depend on the size of the

elements where the interpolation is done. We will derive a relation between the local error and the grid size.

Suppose the boundary Γ is discretised into elements Γ_j each of size l_j. For an element with Dirichlet boundary conditions, if we perform exact integration for u, then the only contribution to the sublocal error (4.2.7) is that due to interpolation of q. Let us introduce $d_{0j}(\mathbf{s})$, the error due to interpolation on the j-th element when the source node is $\mathbf{s}$, which is defined as:

$$d_{0j}(\mathbf{s}) := \int_{\Gamma_j} q(\mathbf{r}(\chi))v(\mathbf{s};\mathbf{r}(\chi))\,d\chi - q_j \int_{\Gamma_j} v(\mathbf{s};\mathbf{r}(\chi))\,d\chi. \tag{4.3.4}$$

The subscript $_0$ is used to denote constant elements where a zeroth order polynomial is used for interpolation. The error $d_{0j}(\mathbf{s})$ is the sublocal error due to interpolation and the local error $d_0(\mathbf{s})$ due to interpolation is the sum of all the sublocal errors. That is,

$$d_0(\mathbf{s}) = \sum_j d_{0j}(\mathbf{s}). \tag{4.3.5}$$

The following lemma is based on a discretisation of the boundary into a polygon, that is, the element Γ_j is a straight line of length l_j say.

Lemma 4.3.1 *The truncation error in* (4.3.4) *is third order in grid size* l_j *and is given by*

$$d_{0j}(\mathbf{s}) = \begin{cases} -\dfrac{1}{24\pi}\dfrac{\partial q}{\partial \chi}(\chi_j)\dfrac{1}{r_j(\chi_j)}\dfrac{\partial r_j}{\partial \chi}(\chi_j)l_j^3 - \dfrac{1}{48\pi}\dfrac{\partial^2 q}{\partial \chi^2}(\mathbf{r}_j)l_j^3\log\left(\|\mathbf{s}-\mathbf{r}_j\|_2\right) + \mathcal{O}(l_j^4), \mathbf{s} \notin \partial\Omega_j, \\ -\dfrac{1}{48\pi}\dfrac{\partial^2 q}{\partial \chi^2}(\mathbf{r}_i)l_i^3(1/3-\log(l_i/2)) + \mathcal{O}(l_i^4), \mathbf{s} \in \partial\Omega_j, j = i. \end{cases} \tag{4.3.6}$$

where χ *is an arc length coordinate in* $\partial\Omega$ *and* $\partial q/\partial\chi$ *is the tangential derivative of* q.

Proof. Let χ_j be the midpoint of $\partial\Omega_j$, see Figure 4.3.

Consider the "exact" integral in (4.3.4), that is,

$$I := \int_{\Gamma_j} v(\mathbf{s};\mathbf{r}(\chi))q(\mathbf{r}(\chi))\,d\chi. \tag{4.3.7}$$

This integral can be rewritten in terms of χ. Suppose we have a Taylor series expansion of $q(\chi)$ about χ_j within the element Γ_j, that is,

$$q(\chi) = q(\chi_j) + \frac{\partial q}{\partial \chi}(\chi_j)(\chi-\chi_j) + \frac{1}{2}\frac{\partial^2 q}{\partial \chi^2}(\chi_j)(\chi-\chi_j)^2 + \frac{1}{6}\frac{\partial^3 q}{\partial \chi^3}(\chi_j)(\chi-\chi_j)^3 + \cdots, \tag{4.3.8}$$

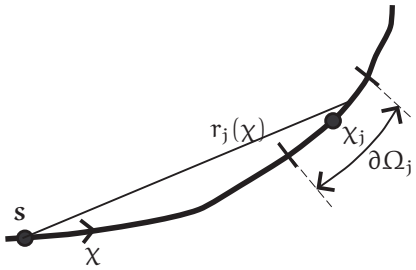

Figure 4.3: Distance $r_j(\chi)$ from $\mathbf{s}$ to an element Γ_j of length l_j on a boundary curve.

For simplicity we may write $q'(\chi_j)$ instead of $\dfrac{\partial q}{\partial \chi}$, $q''(\chi_j)$ instead of $\dfrac{\partial^2 q}{\partial \chi^2}$, etcetera, so that $q'(\chi_j)$, $q''(\chi_j)$, and so on, on $\partial\Omega_j$ are actually the *tangential derivatives* of q at χ_j. In general we shall use the notation

$$r(\chi) := \|\mathbf{s} - \mathbf{r}(\chi)\| \tag{4.3.9}$$

for a fixed point $\mathbf{s}$ and any point $\chi \in \partial\Omega$. We also define the distance $r_j(\chi)$ from a point $\mathbf{s}$ to $\partial\Omega_j$ as

$$r_j(\chi) := \|\mathbf{s} - \mathbf{r}(\chi)\|, \quad \chi \in \partial\Omega_j. \tag{4.3.10}$$

If $\mathbf{r}(\chi)$ is a point on $\partial\Omega_j$, we write

$$r_j(\chi_j) = \|\mathbf{s} - \mathbf{r}(\chi_j)\| = \|\mathbf{s} - \mathbf{r}_j\| \quad \text{since} \quad \mathbf{r}(\chi_j) = \mathbf{r}_j, \tag{4.3.11}$$

see Figure 4.3. Using (4.3.8) in (4.3.7) and substituting the expression for $\nu(\mathbf{s};\mathbf{r})$ gives

$$-2\pi I = \int_{-l_j/2}^{l_j/2} \log[r_j(\chi)]\, q(\chi_j)\, d\chi + \int_{-l_j/2}^{l_j/2} \log[r_j(\chi)] \frac{\partial q}{\partial \chi}(\chi_j)(\chi - \chi_j)\, d\chi + \int_{-l_j/2}^{l_j/2} \log[r_j(\chi)] \frac{1}{2} \frac{\partial^2 q}{\partial \chi^2}(\chi_j)(\chi - \chi_j)^2\, d\chi + \cdots . \tag{4.3.12}$$

In constant elements BEM only the first term of (4.3.12) is used, that is,

$$I \doteq -\frac{1}{2\pi} \int_{-l_j/2}^{l_j/2} \log[r_j(\chi)]\, q(\chi_j)\, d\chi. \tag{4.3.13}$$

This results in a truncation error given by

$$d_{0j}(\mathbf{s}) = -\frac{1}{2\pi} \int_{-l_j/2}^{l_j/2} \log[r_j(\chi)] \frac{\partial q}{\partial \chi}(\chi_j)(\chi - \chi_j)\, d\chi - \frac{1}{2\pi} \int_{-l_j/2}^{l_j/2} \log[r_j(\chi)] \frac{1}{2} \frac{\partial^2 q}{\partial \chi^2}(\chi_j)(\chi - \chi_j)^2\, d\chi + \cdots . \tag{4.3.14}$$

Consider the first term of (4.3.14). That is,

$$T1 := -\frac{1}{2\pi}\int_{-l_j/2}^{l_j/2} \frac{\partial q}{\partial \chi}(\chi_j)\log[r_j(\chi)](\chi-\chi_j)\,d\chi. \tag{4.3.15}$$

For $\mathbf{s} \in \partial\Omega_j, j = i$, then $\mathbf{s} = \mathbf{r}_i$, $r(\chi) = |\chi|$ and we see that the cauchy principal value integral in (4.3.15) evaluates to zero. Otherwise, for $\chi - \chi_j$ small, or equivalently l_j small, the distance $r_j(\chi)$ can be expanded about the point χ_j as,

$$r_j(\chi) = r_j(\chi_j) + r_j'(\chi_j)(\chi-\chi_j) + \mathcal{O}((\chi-\chi_j)^2). \tag{4.3.16}$$

Since $r_j(\chi_j) \neq 0$ we can write (4.3.16) as

$$r_j(\chi) \doteq r_j(\chi_j)\left(1 + \frac{1}{r_j(\chi_j)}\frac{\partial r_j}{\partial \chi}(\chi_j)(\chi-\chi_j)\right) + \mathcal{O}((\chi-\chi_j)^2). \tag{4.3.17}$$

Substituting (4.3.17) in (4.3.15) gives

$$\begin{aligned} T1 \doteq & -\frac{1}{2\pi}\int_{-l_j/2}^{l_j/2} \frac{\partial q}{\partial \chi}(\chi_j)\log(r_j(\chi_j))(\chi-\chi_j)\,d\chi \\ & -\frac{1}{2\pi}\int_{-l_j/2}^{l_j/2} \frac{\partial q}{\partial \chi}(\chi_j)\log\left(1 + \frac{1}{r_j(\chi_j)}\frac{\partial r_j}{\partial \chi}(\chi_j)(\chi-\chi_j)\right)(\chi-\chi_j)\,d\chi \end{aligned} \tag{4.3.18}$$

Consider ξ a local coordinate in $\partial\Omega_j$ such that, see Figure 4.4a,

$$\chi = \chi_j + \xi, \quad -l_j/2 \leq \xi \leq l_j/2. \tag{4.3.19}$$

Then the first integral on the right of (4.3.18) becomes

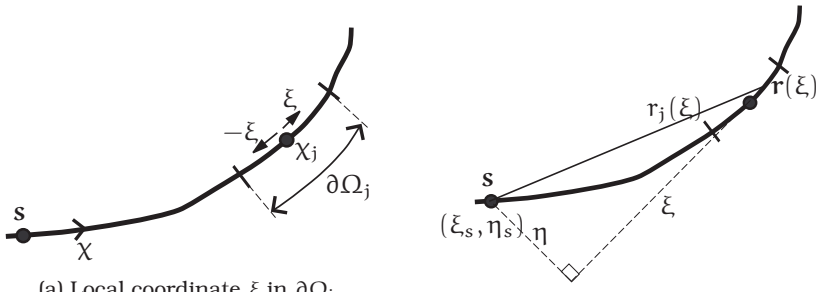

(a) Local coordinate ξ in $\partial\Omega_j$.

(b) Local coordinates ξ and η.

Figure 4.4: Local coordinates in (ξ, η) at the boundary.

$$\int_{-l_j/2}^{l_j/2} \frac{\partial q}{\partial \chi}(\chi_j)\log(r_j(\chi_j))\xi\,d\xi = 0. \tag{4.3.20}$$

Define ξ as a local coordinate in $\partial\Omega_j$ and η the inward normal coordinate, see the illustration in Figure 4.4. The distance $r_j(\xi)$ introduced in (4.3.10) is then

given by

$$r_j(\xi) = [(\xi - \xi_s)^2 + \eta_j^2]^{1/2} \quad \text{so} \quad r_j'(\xi) = \frac{\xi - \xi_s}{[(\xi - \xi_s)^2 + \eta_s^2]^{1/2}}.$$

Then we have, since $\xi_j = 0$,

$$\frac{r_j'(\xi_j)}{r_j(\xi_j)}(\xi - \xi_j) = \frac{-\xi_s \xi}{\xi_s^2 + \eta_s^2}.$$

Note that $\xi \in \partial\Omega_j$ so that $|\xi| \leq l_j/2$. Hence, since $\eta_s^2 \geq 0$ we find

$$\left| \frac{r_j'(\xi_j)}{r_j(\xi_j)}(\xi - \xi_j) \right| = \left| \frac{\xi_s \xi}{\xi_s^2 + \eta_s^2} \right| < 1. \tag{4.3.21}$$

A natural logarithm series expansion can therefore be used for the logarithm term in the second integral on the right hand side of (4.3.18). Therefore, the second integral, with the help of natural logarithm series for $\log(1+x)$, becomes

$$-\frac{1}{2\pi} \int_{-l_j/2}^{l_j/2} \frac{\partial q}{\partial \chi}(\chi_j) \log\left(1 + \frac{1}{r_j(\chi_j)} \frac{\partial r_j}{\partial \chi}(\chi_j)(\chi - \chi_j)\right) (\chi - \chi_j)\, d\chi =$$

$$-\frac{1}{2\pi} \int_{-l_j/2}^{l_j/2} \frac{\partial q}{\partial \chi}(\chi_j) \frac{1}{r_j(\chi_j)} \frac{\partial r_j}{\partial \chi}(\chi_j) \xi^2\, d\xi = -\frac{1}{24\pi} \frac{\partial q}{\partial \chi}(\chi_j) \frac{1}{r_j(\chi_j)} \frac{\partial r_j}{\partial \chi}(\chi_j) l_j^3.$$

Hence, we have

$$T1 \doteq -\frac{1}{24\pi} \frac{\partial q}{\partial \chi}(\chi_j) \frac{1}{r_j(\chi_j)} \frac{\partial r_j}{\partial \chi}(\chi_j) l_j^3 + \mathcal{O}(l_j^4). \tag{4.3.22}$$

Now consider the second order term of (4.3.14),

$$T2 := -\frac{1}{2\pi} \int_{-l_j/2}^{l_j/2} \frac{1}{2} \frac{\partial^2 q}{\partial \chi^2}(\chi_j) \log[r_j(\chi)](\chi - \chi_j)^2\, d\chi. \tag{4.3.23}$$

Recall that since $r_j(\chi_j) > 0$, the distance $r_j(\chi)$ introduced in (4.3.10) can be written as

$$r_j(\chi) \doteq r_j(\chi_j) \left(1 + \frac{1}{r_j(\chi_j)} \frac{\partial r_j}{\partial \chi}(\chi_j)(\chi - \chi_j)\right). \tag{4.3.24}$$

Using the local coordinate notation introduced in Figure 4.4 and the result (4.3.21) , we can again use natural logarithm series for the term in parentheses in (4.3.24) to obtain

$$\log(r_j(\xi)) = \log(r_j(\xi_j)) + \frac{r_j'(\xi_j)}{r_j(\xi_j)}(\xi - \xi_j) + \mathcal{O}((\xi - \xi_j)^2). \tag{4.3.25}$$

Using (4.3.25) and (4.3.21) in (4.3.23) we have

$$T2 = -\frac{1}{4\pi}\frac{\partial^2 q}{\partial \chi^2}(\xi_j)\int_{-l_j/2}^{l_j/2}(\xi-\xi_j)^2\left(\log(r_j(\xi_j)) + \frac{-\xi_s\xi}{\xi_s^2+\eta_s^2}\right)\,d\xi.$$

Finally, if the original $\partial\Omega_j$ is not a straight line but a curve then it is easy to see that the midpoint of the approximate Γ_j (a straight line) is only $\mathcal{O}(l_j^2)$ away from $\mathbf{r}_j$ and so are the derivatives of q. Hence we may conclude that $q''(\xi_j)$ is equal to $\dfrac{\partial^2 q}{\partial \chi^2}(\mathbf{r}_j)$ up to $\mathcal{O}(l_j^2)$ and conclude that, for a general point $\mathbf{s}$ and using the notation in (4.3.11),

$$T2 \doteq -\frac{1}{48\pi}\frac{\partial^2 q}{\partial \chi^2}(\mathbf{r}_j)l_j^3\log(\|\mathbf{s}-\mathbf{r}_j\|) + \mathcal{O}(l_j^4), \tag{4.3.26}$$

which is third order in grid size l_j.

When $\mathbf{s}\in\partial\Omega_j,\ j=i$, $r=|\xi|$ and this integral becomes

$$\begin{aligned} T2 &\doteq -\frac{1}{4\pi}\int_{-l_i/2}^{l_i/2}\frac{\partial^2 q}{\partial \chi^2}(\mathbf{r}_i)\log[r_i(\xi)](\xi-\xi_i)^2\,d\xi, &(4.3.27)\\ &= -\frac{1}{4\pi}\frac{\partial^2 q}{\partial \chi^2}(\mathbf{s})\int_{-l_i/2}^{l_i/2}\log[|\xi|]\xi^2\,d\xi = -\frac{1}{8\pi}\frac{\partial^2 q}{\partial \chi^2}(\mathbf{s})\int_{-l_i/2}^{l_i/2}\log(\xi^2)\xi^2\,d\xi,\\ &= -\frac{1}{4\pi}\frac{\partial^2 q}{\partial \chi^2}(\mathbf{s})\lim_{\epsilon\to 0}\int_{\epsilon}^{l_j/2}\log(\xi^2)\xi^2\,d\xi,\\ &= -\frac{1}{48\pi}\frac{\partial^2 q}{\partial \chi^2}(\mathbf{s})l_i^3(\log(l_i/2)-1/3). &(4.3.28)\end{aligned}$$

Putting (4.3.22), (4.3.26), and (4.3.28) in (4.3.14) gives the result (4.3.6). ■

Apparently, the sublocal error is third order in grid size. Moreover for a mild $\dfrac{\partial^2 q}{\partial \chi^2}$ and a given grid size, the most important factor in the sublocal error is $\log[r_j(\chi_j)]$, the log of the distance $\|\mathbf{s}-\mathbf{r}_j\|$. The sublocal error is large close to the source node $\mathbf{s}$ and decays logarithmically away from this point. This way, the most important contributions to the local error $d_0(\mathbf{s})$ will be those from elements close to $\mathbf{s}$. Since the local error is a sum of the sublocal errors, Lemma 4.3.1 puts us in a position to state the following theorems for the local error:

Theorem 4.3.1 (Constant elements local error) *The local error* (4.3.5) *in constant elements BEM applied to a boundary curve $\partial\Omega$ with midpoint collocation on a grid of size l_j, $j=1,2,\ldots,N$, where N is the number of elements used, is given by*

$$\begin{aligned} d_0(\mathbf{s}) = -\frac{1}{24\pi}\sum_j \frac{\partial q}{\partial \chi}(\chi_j)\frac{1}{r_j(\chi_j)}\frac{\partial r_j}{\partial \chi}(\chi_j)l_j^3 - \frac{1}{48\pi}\sum_{\mathbf{s}\notin\partial\Omega_j} l_j^3\frac{\partial^2 q}{\partial \chi^2}(\mathbf{r}_j)\log(\|\mathbf{s}-\mathbf{r}_j\|)\\ - \frac{1}{48\pi}\frac{\partial^2 q}{\partial \chi^2}(\mathbf{s})l_i^3(\log(l_i/2)-1/3) + \mathcal{O}(l_j^4). \end{aligned}\tag{4.3.29}$$

Proof. The local error over $\partial\Omega$ is the sum of all the sublocal errors (4.3.6). So we have

$$d_0(\mathbf{s}) = -\frac{1}{24\pi}\sum_{\mathbf{s}\notin\partial\Omega_j}\frac{\partial q}{\partial\chi}(\chi_j)\frac{1}{r_j(\chi_j)}\frac{\partial r_j}{\partial\chi}(\chi_j)l_j^3 - \frac{1}{48\pi}\sum_{\mathbf{s}\notin\partial\Omega_j} l_j^3\frac{\partial^2 q}{\partial\chi^2}(\mathbf{r}_j)\log(\|\mathbf{s}-\mathbf{r}_j\|)$$
$$- \frac{1}{48\pi}\frac{\partial^2 q}{\partial\chi^2}(\mathbf{s})l_i^3(\log(l_i/2)-1/3), \quad (4.3.30)$$

which is (4.3.29). ■

Corollary 4.3.1 *The local error* (4.3.29) *is second order in grid size and is given by*

$$d_0(\mathbf{s}) \doteq \frac{1}{48\pi}D\int_{\partial\Omega}\frac{1}{\log(\|\mathbf{s}-\mathbf{r}(\chi)\|)}\,d\chi. \quad (4.3.31)$$

where D *is second order in grid size.*

Proof. Consider the contribution from the first order derivative term in (4.3.29). Let

$$S1 := -\frac{1}{24\pi}\sum_j\frac{\partial q}{\partial\chi}(\chi_j)\frac{1}{r_j(\chi_j)}\frac{\partial r_j}{\partial\chi}(\chi_j)l_j^3. \quad (4.3.32)$$

Suppose $l_j^2\dfrac{\partial q}{\partial\chi}(\chi_j)$ is constant, that is, $l_j^2\dfrac{\partial q}{\partial\chi}(\chi_j) = C$ over $\partial\Omega$ for some constant C. Further, if Ω is convex, then there is an extremal point $\hat{\mathbf{s}}\in\partial\Omega$ such that $\hat{\mathbf{s}}-\mathbf{s}$ is in the direction of the normal, see Figure 4.5. Then the sum $S1$ can be computed as follows:

$$\begin{aligned} S1 &= -\frac{1}{24\pi}\sum_j\frac{\partial q}{\partial\chi}(\chi_j)\frac{1}{r_j(\chi_j)}\frac{\partial r_j}{\partial\chi}(\chi_j)l_j^3 \\ &\doteq D\sum_j\frac{1}{r_j(\chi_j)}\frac{\partial r_j}{\partial\chi}(\chi_j)l_j \doteq D\left\{\int_{l_i/2}^{\chi(\hat{\mathbf{s}})}\frac{1}{r(\chi)}\frac{\partial r}{\partial\chi}(\chi)\,d\chi - \int_{l_i/2}^{\chi(\hat{\mathbf{s}})}\frac{1}{r(\chi)}\frac{\partial r}{\partial\chi}(\chi)\,d\chi\right\} = 0, \end{aligned} \quad (4.3.33)$$

where $D = -C/(24\pi)$. So if $l_j^2\dfrac{\partial q}{\partial\chi}(\chi_j) = C$, then the local error (4.3.30) becomes

$$d_0(\mathbf{s}) \doteq -\frac{1}{48\pi}\sum_{\mathbf{s}\notin\partial\Omega_j} l_j^3\frac{\partial^2 q}{\partial\chi^2}(\mathbf{r}_j)\log(\|\mathbf{s}-\mathbf{r}_j\|)$$
$$- \frac{1}{48\pi}\frac{\partial^2 q}{\partial\chi^2}(\mathbf{s})l_i^3(\log(l_i/2)-1/3). \quad (4.3.34)$$

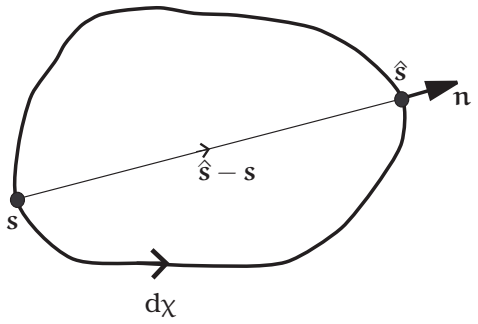

Figure 4.5: Extremal point $\hat{\mathbf{s}}$ corresponding to point $\mathbf{s}$ on a convex boundary.

Let us assume Ω has a radius less than one half, that is, $\rho(\Omega) < 1/2$. This is a nonrestrictive assumption since if not, we can introduce a scaling α such that $\mathbf{r} \to \alpha\mathbf{r}$ for all $\mathbf{r} \in \bar{\Omega}$ and α chosen small enough. Then we will have $\log(\|\mathbf{s}-\mathbf{r}\|) < 0$ for all $\mathbf{s}, \mathbf{r} \in \partial\Omega$. Suppose in addition that $l_j^2 \dfrac{\partial^2 q}{\partial \chi^2}(\chi_j) = D$ over $\partial\Omega$ for some constant D, then we have

$$d_0(\mathbf{s}) \doteq -\frac{1}{48\pi} D \sum_{\mathbf{s} \notin \partial\Omega_j} l_j \log(\|\mathbf{s} - \mathbf{r}(\chi_j)\|) - \frac{1}{48\pi} \frac{\partial^2 q}{\partial \chi^2}(\mathbf{s}) l_i^3 (\log(l_i/2) - 1/3). \quad (4.3.35)$$

Using Riemann integral interpretation for the sum and since $\log(\|\mathbf{s}-\mathbf{r}\|) < 0$, we have

$$d_0(\mathbf{s}) \doteq -\frac{1}{48\pi} D \lim_{l_i \to 0} \int_{\partial\Omega - l_i} \log(\|\mathbf{s} - \mathbf{r}(\chi)\|)\, d\chi - \frac{1}{48\pi} \frac{\partial^2 q}{\partial \chi^2}(\mathbf{s}) \lim_{l_i \to 0} l_i^3 (\log(l_i/2) - 1/3), \quad (4.3.36)$$

which yields

$$d_0(\mathbf{s}) \doteq \frac{1}{48\pi} D \int_{\partial\Omega} \frac{1}{\log(\|\mathbf{s} - \mathbf{r}(\chi)\|)}\, d\chi. \quad (4.3.37)$$

If $l_j^2 \dfrac{\partial^2 q}{\partial \chi^2}(\chi_j)$ is not constant over $\partial\Omega$, then we take D as the average of $l_j^2 \dfrac{\partial^2 q}{\partial \chi^2}(\chi_j)$ over $\partial\Omega$, that is, some value between $\max(l_j^2 \dfrac{\partial^2 q}{\partial \chi^2}(\chi_j))$ and $\min(l_j^2 \dfrac{\partial^2 q}{\partial \chi^2}(\chi_j))$.

If $l_j^2 \dfrac{\partial q}{\partial \chi}(\chi_j)$ is not constant over $\partial\Omega$, then let D' be the average of $l_j^2 \dfrac{\partial q}{\partial \chi}(\chi_j)$ over $\partial\Omega$. So the sum $S1$ in (4.3.32) becomes, using the same argument as in (4.3.33),

$$\begin{aligned} S1 &= -\frac{1}{24\pi} \sum_j \frac{\partial q}{\partial \chi}(\chi_j) \frac{1}{r_j(\chi_j)} \frac{\partial r_j}{\partial \chi}(\chi_j) l_j^3 \\ &\doteq D' \sum_j \frac{1}{r_j(\chi_j)} \frac{\partial r_j}{\partial \chi}(\chi_j) l_j \doteq D' \int_{\partial\Omega} \frac{1}{r(\chi)} \frac{\partial r}{\partial \chi}(\chi)\, d\chi = 0. \end{aligned} \tag{4.3.38}$$

■

The contour integral in (4.3.37) is rather complicated and of course depends on the type of geometry under consideration. The result of Theorem (4.3.1) can be used to derive error expressions for some regular geometries. In particular we consider here the cases of a circle and a square. Note that we do not consider a circle of radius unity. This is because we have existence and uniqueness of the Dirichlet problem if and only if the logarithmic capacity of $\partial\Omega$, which is equal to its radius in the case of a circle, is not equal to unity. Then the BEM equation leads to a singular system, see [11, 12, 16, 68, 76].

Corollary 4.3.2 (Constant elements local error: Circle) *For $\partial\Omega$ a circle of radius R, the local error* (4.3.5) *is second order in grid size l and is given by*

$$d_0(\mathbf{s}) = \frac{1}{48\pi} D(2\pi R) \log(1/R) + \mathcal{O}(l^4) \tag{4.3.39}$$

where D is second order in grid size and is as defined in Corollary 4.3.1.

Proof. Let us express the distance $\|\mathbf{s} - \mathbf{r}_j\|$ in terms of the angle α and radius R as shown in Figure 4.6. The contour integral over $\partial\Omega$ is now

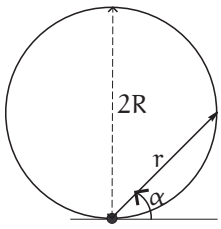

Figure 4.6: Parameterisation of a circle for evaluating the integral in (4.3.37).

$$\begin{aligned}\int_{\partial\Omega} \log\left(\frac{1}{\|\mathbf{s}-\mathbf{r}(\chi)\|}\right) d\chi &= -\int_{\partial\Omega} \log(r(\alpha))\, d\alpha = -\int_0^{\pi} \log(2R\sin\alpha)(2R d\alpha),\\ &= -2\pi R\log(2R) - 2R\int_0^{\pi}\log(\sin\alpha)\, d\alpha\\ &= (2\pi R)\log(1/R). \end{aligned} \tag{4.3.40}$$

So we obtain

$$d_0(\mathbf{s}) = \frac{1}{48\pi} D(2\pi R)\log(1/R) + \mathcal{O}(l^4), \tag{4.3.41}$$

where $2\pi R$ is the circumference of the circle. ■

Corollary 4.3.3 (Constant elements local error: Square) *For $\partial\Omega$ a square of length L, the local error (4.3.5) is second order in grid size l and is given by*

$$d_0(\mathbf{s}) = \frac{1}{48\pi} D(4L)(1 - \log(2^{1/4}L) - \pi/8) + \mathcal{O}(l^4), \tag{4.3.42}$$

where D is second order in grid size and is as defined in Corollary 4.3.1.

Proof. Likewise let us start from the result of Theorem 4.3.1. We need to compute the contour integral in (4.3.37). Now,

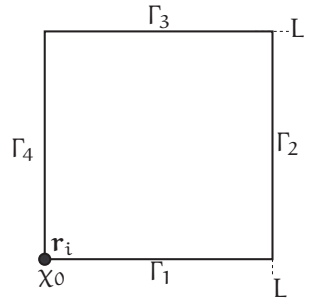

Figure 4.7: A square boundary Γ with source point $s_0 = \mathbf{r}_i$ at the origin.

$$\begin{aligned}\int_{\partial\Omega} \log\left(\frac{1}{\|\mathbf{s}-\mathbf{r}(\chi)\|}\right) d\chi &= -\int_{\partial\Omega} \log(\|\mathbf{s}-\mathbf{r}(\chi)\|)\, d\chi\\ &= -\sum_{i=1}^{4}\int_{\Gamma_i} \log(\|\mathbf{s}-\mathbf{r}(\chi)\|)\, d\chi,\\ &= -4L(\log(2^{1/4}L) - 1 + \pi/8). \end{aligned} \tag{4.3.43}$$

Thus we obtain

$$d_0(\mathbf{s}) = \frac{1}{48\pi}\frac{\partial^2 q}{\partial \chi^2}(\eta) l^2 (4L)(1 - \log(2^{1/4}L) - \pi/8) + \mathcal{O}(l^4), \tag{4.3.44}$$

where $4L$ is the perimeter of the square. ■

The results above show that indeed the local error in constant elements BEM is second order in grid size and the numerical computations in Section 4.6 agree with these findings.

4.3.2 Linear elements

In this section we develop similar estimates for the local error due to interpolation for linear elements.

Again consider an element with Dirichlet boundary conditions and assume that all integrals involving u are computed exactly since $u(\mathbf{r})$ is known. Then the only contribution to the interpolation error is that from interpolation of $q(\mathbf{r})$. Let us introduce $d_{1j}(\mathbf{s})$, the error due to interpolation on the j-th element when the source node is $\mathbf{s}$, which is defined as:

$$d_{1j}(\mathbf{s}) := \int_{\Gamma_j} q(\mathbf{r}(\chi))v(\mathbf{s};\mathbf{r}(\chi))\,d\chi - \int_{\Gamma_j} f_q(\mathbf{r}(\chi))v(\mathbf{s};\mathbf{r}(\chi))\,d\chi \tag{4.3.45}$$

where $f_q(\mathbf{r})$ is an order one polynomial. The subscript $_1$ is used to denote linear elements where an order one polynomial is used for interpolation. The error $d_{1j}(\mathbf{s})$ is the sublocal error due to interpolation in linear elements and the local error $d_1(\mathbf{s})$ due to interpolation for a node $\mathbf{s}$ is the sum of all these sublocal errors, that is,

$$d_1(\mathbf{s}) = \sum_j d_{1j}(\mathbf{s}). \tag{4.3.46}$$

Lemma 4.3.2 (Linear elements sublocal error) *Let l_j be the grid size of element Γ_j. The sublocal error* (4.3.46) *is third order in l_j and is given by*

$$d_{1j}(\mathbf{s}) = \begin{cases} \dfrac{1}{24\pi}\dfrac{\partial^2 q}{\partial \chi^2}(\zeta_j) l_j^3 \log(\|\mathbf{s} - \mathbf{r}_j\|) + \mathcal{O}(l_j^4),\ \zeta_j \in \Gamma_j,\ \ \mathbf{s} \notin \Gamma_j, \\ \dfrac{1}{24\pi}\dfrac{\partial^2 q}{\partial \chi^2}(\zeta_j) l_j^3 (\log(l_j) - 5/6) + \mathcal{O}(l_j^4),\ \zeta_j \in \Gamma_j,\ \ \mathbf{s} \in \Gamma_j. \end{cases} \tag{4.3.47}$$

where $\dfrac{\partial^2 q}{\partial \chi^2}(\zeta_j)$ is the tangential double derivative of q at ζ_j.

Proof. Consider the error due to interpolation by a linear polynomial $f_q(\mathbf{r})$. The *interpolation error* is given by, see [25, p. 324],

$$q(\xi) - f_q(\xi) = \frac{1}{2}\frac{\partial^2 q}{\partial \chi^2}(\zeta)(\xi - \xi_0)(\xi - \xi_1), \zeta \in (\xi_0, \xi_1), \tag{4.3.48}$$

where ξ_0 and ξ_1 are the points of interpolation and $\frac{\partial^2 q}{\partial \chi^2}(\zeta)$ is the tangential double derivative of q at ζ. Since we are considering continuous linear elements in which we interpolate at the end points of $\partial\Omega_j$, we have $\xi_0 =: \xi^{\text{left}} = -l_j/2$ and $\xi_1 =: \xi^{\text{right}} = l_j/2$ where ξ^{left} and ξ^{right} are the left and right boundary points of the element respectively. So the local truncation error is given by

$$\begin{aligned} d_{1j}(\mathbf{s}) &= -\frac{1}{2\pi}\int_{\partial\Omega_j} (q(\mathbf{r}) - f_q(\mathbf{r}(\chi)))\log(\|\mathbf{s} - \mathbf{r}(\xi)\|)\,d\xi \\ &\doteq -\frac{1}{4\pi}\frac{\partial^2 q}{\partial \chi^2}(\zeta)\int_{-l_j/2}^{l_j/2} \log(\|\mathbf{s} - \mathbf{r}(\xi)\|)(\xi + l_j/2)(\xi - l_j/2)\,d\xi. \end{aligned} \tag{4.3.49}$$

Of course, in (4.3.48), the point ζ is unknown. So at best (4.3.49) will give us a bound on the error if the bound for $\partial^2 q/\partial\chi^2$ on Γ_j is known. Let

$$I := \int_{-l_j/2}^{l_j/2} \log(\|\mathbf{s} - \mathbf{r}(\xi)\|)(\xi + l_j/2)(\xi - l_j/2)\,d\xi.$$

For source points outside $\partial\Omega_j$ the expansion (4.3.16) is used for $r(\xi)$ and (4.3.25) for $\log(\|\mathbf{s} - \mathbf{r}(\xi)\|)$ to obtain

$$\begin{aligned} I &= \int_{-l_j/2}^{l_j/2} \left(\log(\|\mathbf{s} - \mathbf{r}_j\|)(\xi + l_j/2)(\xi - l_j/2) + \mathcal{O}(\xi - \xi_j)^3\right) d\xi \\ &= -\frac{l_j^3}{6}\log(\|\mathbf{s} - \mathbf{r}_j\|) + \mathcal{O}(l_j^4). \end{aligned} \tag{4.3.50}$$

As remarked in Lemma 4.3.1, if the original $\partial\Omega_j$ is not a straight line but a curve then it is easy to see that the midpoint of the approximate Γ_j (a straight line) is only $\mathcal{O}(l_j^2)$ away from $\mathbf{r}_j$ and so are the derivatives of q. Hence we may conclude that $\partial^2 q(\xi_j)/\partial\chi^2$ is equal to $\dfrac{\partial^2 q}{\partial \chi^2}(\mathbf{r}_j)$ up to $\mathcal{O}(l_j^2)$. So from (4.3.49) we get

$$d_{1j}(\mathbf{s}) = \frac{1}{24\pi}\frac{\partial^2 q}{\partial \chi^2}(\zeta_j) l_j^3 \log(\|\mathbf{s} - \mathbf{r}_j\|) + \mathcal{O}(l_j^4) \tag{4.3.51}$$

which is third order in grid size. For $\mathbf{s} \in \Gamma_j$; $r = \xi$, $\xi^{\text{left}} = 0$, $\xi^{\text{right}} = l_j$, so we have

$$I = \int_0^{l_j} \xi(\xi - l_j)\log(\xi)\,d\xi = -\frac{l_j^3}{6}(\log(l_j) - 5/6). \tag{4.3.52}$$

Thus

$$d_{1j}(\mathbf{s}) = \begin{cases} \dfrac{1}{24\pi}\dfrac{\partial^2 q}{\partial \chi^2}(\zeta_j) l_j^3 \log(\|\mathbf{s}-\mathbf{r}_j\|) + \mathcal{O}(l_j^4), & \mathbf{s} \notin \partial\Omega_j, \\ \dfrac{1}{24\pi}\dfrac{\partial^2 q}{\partial \chi^2}(\zeta_j) l_j^3 (\log(l_j) - 5/6) + \mathcal{O}(l_j^4), & \mathbf{s} \in \partial\Omega_j. \end{cases} \tag{4.3.53}$$

■

The same remarks that were made about the sublocal error in Lemma 4.3.1 hold for the result in (4.3.53). For a mild $\partial^2 q/\partial\chi^2$ and a given discretisation, the most important factor for the sublocal error is $\log\|\mathbf{s}-\mathbf{r}_j\|$. The sublocal error is large close to the source node $\mathbf{s}$ and decays off logarithmically away from this point. So the most important contributions to the local error $d_1(\mathbf{s})$ will be those from elements close to a source point.

Since the local error is a sum of sublocal errors, Lemma 4.3.2 puts us in a position to state the following theorems about the local error in linear elements.

Theorem 4.3.2 (Linear elements local error) *The local error* (4.3.46) *in linear elements applied to a boundary curve* $\partial\Omega$ *with a discretisation of size* l_j, $j = 1, 2, \ldots, N$, *where* N *is the number of elements is given by*

$$d_1(\mathbf{s}) \doteq \frac{1}{24\pi} \sum_{\mathbf{s}\notin\Gamma_j} \frac{\partial^2 q}{\partial \chi^2}(\chi_j) l_j^3 \log(\|\mathbf{s}-\mathbf{r}_j\|) + \frac{1}{24\pi}\frac{\partial^2 q}{\partial \chi^2}(\chi_j) l_j^3 (\log(l_j) - 5/6). \tag{4.3.54}$$

Proof. The instruments for the proof of this theorem are similar to those for Theorem 4.3.1. The local error is the sum of the sublocal errors so

$$d_1(\mathbf{s}) \doteq \sum_j d_{1j}(\mathbf{s}) = \sum_{\mathbf{s}\notin\Gamma_j} \frac{1}{24\pi}\frac{\partial^2 q}{\partial \chi^2}(\chi_j) l_j^2 \log(\|\mathbf{s}-\mathbf{r}_j\|) + \frac{1}{24\pi}\frac{\partial^2 q}{\partial \chi^2}(\chi_j) l_j^3 (\log(l_j) - 5/6), \tag{4.3.55}$$

which is the result. ■

Corollary 4.3.4 *The local error* (4.3.54) *is second order in grid size and is given by*

$$d_1(\mathbf{s}) \doteq \frac{1}{24\pi} D \int_{\partial\Omega} \log(\|\mathbf{s} - \mathbf{r}(\chi)\|)\, d\chi, \tag{4.3.56}$$

where D *is a constant second order in grid size.*

Proof. Suppose $l_j^2 \dfrac{\partial^2 q}{\partial \chi^2}(\chi_j) = D$ over $\partial\Omega$ for some constant D. Then

$$\begin{aligned} d_1(\mathbf{s}) &\doteq \sum_{\mathbf{s}\notin\partial\Omega_j} \frac{1}{24\pi}\frac{\partial^2 q}{\partial \chi^2}(\zeta_j) l^3 \log(\|\mathbf{s}-\mathbf{r}_j\|) + \frac{1}{24\pi}\frac{\partial^2 q}{\partial \chi^2}(\zeta_j) l^3(\log(l) - 5/6), \\ &\doteq \frac{1}{24\pi} D \sum_{\mathbf{s}\notin\partial\Omega_j} l_j \log(\|\mathbf{s}-\mathbf{r}_j\|) + \frac{1}{24\pi} D l_i(\log(l_i) - 5/6), \\ &\doteq \frac{1}{24\pi} D \lim_{l_i\to 0} \int_{\partial\Omega - l_i} \log(\|\mathbf{s}-\mathbf{r}(\chi)\|)\, d\chi + \frac{1}{24\pi} D \lim_{l_i\to 0} l_i(\log(l_i) - 5/6), \\ &= \frac{1}{24\pi} D \int_{\partial\Omega} \log(\|\mathbf{s}-\mathbf{r}(\chi)\|)\, d\chi, \end{aligned} \tag{4.3.57}$$

where χ is the arc length coordinate in $\partial\Omega$. If $l_j^2 \dfrac{\partial^2 q}{\partial \chi^2}(\chi_j)$ is not constant over $\partial\Omega$, then we take D as the average of $l_j^2 \dfrac{\partial^2 q}{\partial \chi^2}(\chi_j)$ over $\partial\Omega$, that is, some value between $\max(l_j^2 \dfrac{\partial^2 q}{\partial \chi^2}(\chi_j))$ and $\min(l_j^2 \dfrac{\partial^2 q}{\partial \chi^2}(\chi_j))$. ■

Corollary 4.3.5 (Linear elements local error: Circle) *For $\partial\Omega$ a circle of radius R, the local error in linear elements BEM is second order in grid size and is given by*

$$d_1(\mathbf{s}) \doteq \frac{1}{24\pi} D(2\pi R)\log R, \tag{4.3.58}$$

where D is second order in grid size and is as defined in Corollary 4.3.4.

Proof. Using the result (4.3.40) for the contour integral in (4.3.57) on a circle of radius R yields the result

$$d_1(\mathbf{s}) \doteq \frac{1}{24\pi} D(2\pi R)\log R. \tag{4.3.59}$$

■

Corollary 4.3.6 (Linear elements local error: Square) *For $\partial\Omega$ a square of length L, the local error using linear elements BEM is second order in grid size and is given by*

$$d_1(\mathbf{s}) \doteq \frac{1}{24\pi} D(4L)(\log(2^{1/4}L) - 1 + \pi/8). \tag{4.3.60}$$

where D is second order in grid size and is as defined in Corollary 4.3.4.

Proof. Likewise, using the result (4.3.43) for the contour integral in (4.3.57) on a square gives the result. ■

4.4 Neumann problems

Consider the case of Neumann boundary conditions. This case results in the second kind integral equation

$$\left(\frac{1}{2} + \mathcal{K}^d(\mathbf{s};\mathbf{r})\right) u(\mathbf{r}) = g(\mathbf{r}) \tag{4.4.1}$$

where the right hand side

$$g(\mathbf{r}) = \mathcal{K}^s(\mathbf{s};\mathbf{r})q(\mathbf{r}) \tag{4.4.2}$$

is known since q is given. The solution of (4.4.1) in BEM therefore involves estimating integrals of the form

$$I := \frac{1}{2\pi}\int_{\partial\Omega_j} \frac{\partial\nu}{\partial n}(\mathbf{s};\mathbf{r})u(\mathbf{r})\,d\chi. \tag{4.4.3}$$

In the following two sections, local errors in the BEM solution of (4.4.1) using constant elements and linear elements are discussed.

4.4.1 Constant elements

In the case the unknown function u in (4.4.3) is assumed to be constant over $\partial\Omega_j$ and takes on the value of u at a point $\mathbf{r}_j \in \partial\Omega_j$. That is,

$$I \doteq \frac{1}{2\pi}\int_{\partial\Omega_j} \frac{\partial\nu}{\partial n}(\mathbf{s};\mathbf{r})u(\mathbf{r}_j)\,d\chi, \tag{4.4.4}$$

and thus the truncation error committed is given by

$$d_{0j}(\mathbf{s}) := \frac{1}{2\pi}\int_{\partial\Omega_j} \frac{\partial\nu}{\partial n}(\mathbf{s};\mathbf{r})u(\mathbf{r})\,d\chi - \frac{1}{2\pi}\int_{\partial\Omega_j} \frac{\partial\nu}{\partial n}(\mathbf{s};\mathbf{r})u(\mathbf{r}_j)\,d\chi. \tag{4.4.5}$$

Suppose we have a Taylor series expansion of $u(\chi)$ about χ_j within the element $\partial\Omega_j$, that is,

$$u(\chi) = u(\chi_j) + \frac{\partial u}{\partial\chi}(\chi_j)(\chi-\chi_j) + \frac{1}{2}\frac{\partial^2 u}{\partial\chi^2}(\chi_j)(\chi-\chi_j)^2 + \frac{1}{6}\frac{\partial^3 u}{\partial\chi^3}(\chi_j)(\chi-\chi_j)^3 + \cdots. \tag{4.4.6}$$

Then using (4.4.6) in (4.4.5) yields the truncation error

$$d_{0j}(\mathbf{s}) \doteq \frac{1}{2\pi}\int_{\partial\Omega_j} \frac{\partial\nu}{\partial n}(\chi)\frac{\partial u}{\partial\chi}(\chi_j)(\chi-\chi_j)\,d\chi + \frac{1}{2\pi}\int_{\partial\Omega_j} \frac{\partial\nu}{\partial n}(\chi)\frac{1}{2}\frac{\partial^2 u}{\partial\chi^2}(\chi_j)(\chi-\chi_j)^2\,d\chi + \cdots. \tag{4.4.7}$$

Recall that

$$\frac{\partial \nu}{\partial n}(\chi) = \frac{(\mathbf{s} - \mathbf{r}(\chi)) \cdot \mathbf{n}(\chi)}{\|\mathbf{s} - \mathbf{r}(\chi)\|^2} \tag{4.4.8}$$

where $\mathbf{n}(\chi)$ is the outward normal at $\mathbf{r}(\chi)$. To obtain the explicit dependency on grid size we will need to obtain the dependency of the kernel (4.4.8) on the grid size as in Sections 4.3. This is a more complicated process but our results show that indeed the local error is second order in grid size.

4.4.2 Linear elements

In this case the function u in the integral

$$I = \frac{1}{2\pi} \int_{\partial\Omega_j} \frac{\partial \nu}{\partial n}(\mathbf{s};\mathbf{r}) u(\mathbf{r})\, d\gamma(\mathbf{r}). \tag{4.4.9}$$

is assumed to vary as an order one polynomial over $\partial\Omega_j$ and in so doing, the so called sublocal error $d_{1j}(\mathbf{s})$ over $\partial\Omega_j$ is committed. That is,

$$d_{1j}(\mathbf{s}) := \frac{1}{2\pi} \int_{\partial\Omega_j} \frac{\partial \nu}{\partial n}(\mathbf{s};\mathbf{r}) u(\mathbf{r})\, d\gamma(\mathbf{r}) - \frac{1}{2\pi} \int_{\partial\Omega_j} \frac{\partial \nu}{\partial n}(\mathbf{s};\mathbf{r}) f_u(\mathbf{r})\, d\gamma(\mathbf{r}) \tag{4.4.10}$$

where $f_u(\mathbf{r})$ is the order one polynomial approximating u.

Lemma 4.4.1 (Neumann linear elements sublocal error) *Let l_j be the grid size of element $\partial\Omega_j$. The sublocal error* (4.4.10) *is third order in l_j and is given by*

$$d_{1j}(\mathbf{s}) \doteq \frac{1}{24\pi} \frac{\partial^2 u}{\partial \chi^2}(\zeta_j) \frac{\partial \nu}{\partial n}(r_j) l_j^3. \tag{4.4.11}$$

where $\dfrac{\partial^2 u}{\partial \chi^2}(\zeta_j)$ is the tangential double derivative of u at ζ_j a point in $\partial\Omega$.

Proof. Let ξ be the local coordinate in $\partial\Omega_j$, see Figure 4.8. Then express (4.4.9) in terms of ξ so that,

$$I := \frac{1}{2\pi} \int_0^{l_j} \frac{\partial \nu}{\partial n}(r(\xi)) u(\xi)\, d\xi. \tag{4.4.12}$$

Next, replace u by an order one polynomial, that is,

$$u(\xi) \doteq \frac{\xi}{l_j} u(\xi_j) + \frac{l_j - \xi}{l_j} u(\xi_0), \tag{4.4.13}$$

to obtain

$$I \doteq \frac{1}{2\pi} \int_0^{l_j} \frac{\partial \nu}{\partial n}(r(\xi)) \left[\frac{\xi}{l_j} u(\xi_j) + \frac{l_j - \xi}{l_j} u(\xi_0) \right] d\xi + \frac{1}{2\pi} \int_0^{l_j} \frac{\partial \nu}{\partial n}(r(\xi)) \frac{1}{2} (l_j - \xi) \xi \frac{\partial^2 u}{\partial \chi^2}(\zeta(\xi))\, d\xi.$$

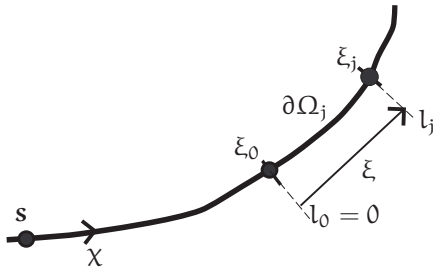

Figure 4.8: Local coordinates on an element in linear boundary elements.

(4.4.14)

The second integral on the right hand side of (4.4.14) is an error term due to interpolation. Therefore the error when only the first term of (4.4.14) is used to estimate the integrals in linear elements is

$$d_{1j}(\mathbf{s}) := \frac{1}{2\pi}\int_0^{l_j} \frac{\partial v}{\partial n}(\xi)\frac{1}{2}(l_j - \xi)\xi\frac{\partial^2 u}{\partial \chi^2}(\zeta(\xi))\,d\xi. \tag{4.4.15}$$

Using the mean value theorem we obtain

$$d_{1j}(\mathbf{s}) \doteq \frac{1}{24\pi}\frac{\partial^2 u}{\partial \chi^2}(\zeta_j)\frac{\partial v}{\partial n}(r_j)l_j^3. \tag{4.4.16}$$

Note that when $\mathbf{s} \in \partial\Omega_j$, $\partial v/\partial n = 0$ and so there is no need to worry about singular elements. ■

Corollary 4.4.1 *If* $\frac{\partial^2 u}{\partial \chi^2}(\zeta_j)l_j^2 = C$ *over* $\partial\Omega$ *for some constant* C*, then the local error is second order in grid size and is given by*

$$d_1(\mathbf{s}) = \frac{1}{24\pi}C\int_{\partial\Omega}\frac{\partial v}{\partial n}(\chi)\,d\chi, \tag{4.4.17}$$

where C *is second order in grid size.*

Proof. The local error is the sum of all the sublocal errors. So,

$$d_1(\mathbf{s}) = \sum_j d_{1j}(\mathbf{s}) \doteq \sum_j \frac{1}{24\pi}\frac{\partial^2 u}{\partial \chi^2}(\zeta_j)\frac{\partial v}{\partial n}(\chi_j)l_j^3 \doteq \frac{1}{24\pi}C\sum_j \frac{\partial v}{\partial n}(\chi_j)l_j. \tag{4.4.18}$$

Then using Riemann integral interpretation for the sum in (4.4.18) yields

$$d_1(\mathbf{s}) \doteq \frac{1}{24\pi}C\int_{\partial\Omega}\frac{\partial v}{\partial n}(\chi)\,d\chi. \tag{4.4.19}$$

■

Corollary 4.4.2 *Using the properties* (2.4.4) *of* $\partial v/\partial n$, *the local error in* (4.4.19) *is*

$$d_1(s) \doteq -C/48\pi. \tag{4.4.20}$$

Proof. From (2.4.4), the integral in (4.4.19) is $-1/2$ hence the result. ■

4.5 Mixed boundary conditions

For a mixed problem, there is a part $\partial\Omega^1$ of the boundary $\partial\Omega$ where u is given and a part $\partial\Omega^2$ where q is given, see Figure 4.9.

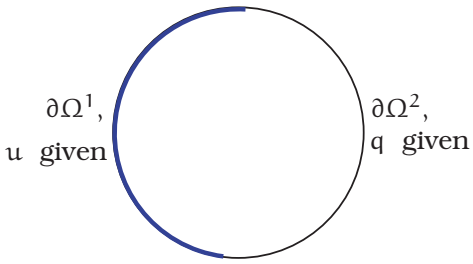

Figure 4.9:

Thus we have to estimate integrals of the form (4.3.3) on the part where u is given and (4.4.3) on the part where q is known. Therefore, when using constant elements, the truncation error committed per element is given by (4.3.6) in the part where u is known and (4.4.7) in the Neumann part. When linear elements are used, the sublocal error is given by (4.3.47) in the Dirichlet part and (4.4.11) in the Neumann part.

Corollary 4.5.1 (Mixed problem linear elements local error) *Let the Dirichlet part* $\partial\Omega^1$ *be discretised using* M *elements and the Neumann part be discretised using* N *elements. Then the local error for a mixed problem when using linear elements BEM is given by*

$$d_1(s) \doteq \frac{1}{24\pi}\sum_{j=1,s\notin\Gamma_j}^{M}\frac{\partial^2 q}{\partial\chi^2}(\chi_j)l_j^3\log(\|s-r_j\|)+\frac{1}{24\pi}\frac{\partial^2 q}{\partial\chi^2}(\chi_j)l_j^3(\log(l_j)-5/6)$$
$$+\frac{1}{24\pi}\sum_{j=M+1}^{N}\frac{\partial^2 u}{\partial\chi^2}(\zeta_j)\frac{\partial v}{\partial n}(r_j)l_j^3, \tag{4.5.1}$$

when the point $\mathbf{s} \in \partial\Omega^1$ *and*

$$d_1(\mathbf{s}) \doteq \frac{1}{24\pi} \sum_{j=1, \mathbf{s}\notin\Gamma_j}^{M} \frac{\partial^2 q}{\partial \chi^2}(\chi_j) l_j^3 \log(\|\mathbf{s}-\mathbf{r}_j\|) + \frac{1}{24\pi} \sum_{j=M+1}^{N} \frac{\partial^2 u}{\partial \chi^2}(\zeta_j) \frac{\partial v}{\partial n}(r_j) l_j^3, \quad (4.5.2)$$

when the point $\mathbf{s} \in \partial\Omega^2$.

Proof. The local error is the sum of all the local errors per element. Then

$$d(\mathbf{s}) = \sum_{j=1,\ \partial\Omega_j\in\partial\Omega^1}^{M} d_{1j} + \sum_{j=M+1,\ \partial\Omega_j\in\partial\Omega^2}^{N} d_{1j}. \quad (4.5.3)$$

Then using the results (4.3.47) and (4.4.11) in (4.5.3) gives the result. ■

Corollary 4.5.2 *The local error* (4.5.1) *is second order in grid size and is given by*

$$d_1(\mathbf{s}) \doteq \frac{1}{24\pi} D \int_{\partial\Omega^1} \log(\|\mathbf{s}-\mathbf{r}(\chi)\|)\, d\chi + \frac{1}{24\pi} D \int_{\partial\Omega^2} \frac{\partial v}{\partial n}(\chi)\, d\chi, \quad (4.5.4)$$

where D *is a constant second order in grid size.*

Proof. Suppose $l_j^2 \frac{\partial^2 q}{\partial \chi^2}(\chi_j) = D$ over $\partial\Omega^1$ and $l_j^2 \frac{\partial^2 u}{\partial \chi^2}(\chi_j) = D$ over $\partial\Omega^2$ for some constant D. Then we have, on $\partial\Omega^1$,

$$\begin{aligned} d_1(\mathbf{s}) &\doteq \sum_{j=1,\ \mathbf{s}\notin\partial\Omega_j}^{N} \frac{1}{24\pi}\frac{\partial^2 q}{\partial \chi^2}(\chi_j) l_j^3 \log(\|\mathbf{s}-\mathbf{r}_j\|) + \frac{1}{24\pi}\frac{\partial^2 q}{\partial \chi^2}(\chi_i) l_i^3 (\log(l_i) - 5/6), \\ &\doteq \frac{1}{24\pi} D \sum_{j=1,\ \mathbf{s}\notin\partial\Omega_j}^{N} l_j \log(\|\mathbf{s}-\mathbf{r}_j\|) + \frac{1}{24\pi} D l_i (\log(l_i) - 5/6), \\ &\doteq \frac{1}{24\pi} D \lim_{l_i\to 0} \int_{\partial\Omega^1 - l_i} \log(\|\mathbf{s}-\mathbf{r}(\chi)\|)\, d\chi + \frac{1}{24\pi} D \lim_{l_i\to 0} l_i(\log(l_i) - 5/6), \\ &= \frac{1}{24\pi} D \int_{\partial\Omega^1} \log(\|\mathbf{s}-\mathbf{r}(\chi)\|)\, d\chi. \end{aligned} \quad (4.5.5)$$

On $\partial\Omega^2$,

$$d_1(\mathbf{s}) = \sum_{j=1}^{N} d_{1j}(\mathbf{s}) \doteq \sum_{j=M+1}^{N} \frac{1}{24\pi}\frac{\partial^2 u}{\partial \chi^2}(\chi_j)\frac{\partial v}{\partial n}(\chi_j) l_j^3 \doteq \frac{1}{24\pi} D \sum_j \frac{\partial v}{\partial n}(\chi_j) l_j. \quad (4.5.6)$$

Using Riemann integral interpretation for the sum in (4.5.6) leads to

$$d_1(\mathbf{s}) \doteq \frac{1}{24\pi} D \int_{\partial\Omega} \frac{\partial v}{\partial n}(\chi)\, d\chi. \tag{4.5.7}$$

Putting (4.5.5) and (4.5.7) together gives the result in (4.5.4).

If $l_j^2 \frac{\partial^2 q}{\partial \chi^2}(\chi_j)/l_j^2 \frac{\partial^2 u}{\partial \chi^2}(\chi_j)$ is not constant over $\partial\Omega^1/\partial\Omega^2$, then take D as the average of $l_j^2 \frac{\partial^2 q}{\partial \chi^2}(\chi_j)/l_j^2 \frac{\partial^2 u}{\partial \chi^2}(\chi_j)$ over $\partial\Omega^1/\partial\Omega^2$. ■

4.6 Examples

Below we present results to illustrate the estimates derived above using Problems (a) and (c) of Examples 3.7.1 and 3.7.3. Since in each example analytic expression for the unknown is available, for each node $\mathbf{r}_i$ we can compute the exact value q_i or u_i of the unknown. Then the local error defined in (4.1.5) can be computed. That is

$$\mathbf{d} := \mathbf{Aq} - \mathbf{b} \quad \text{or} \quad \mathbf{d} := \mathbf{Au} - \mathbf{b}.$$

We refine by a factor three and, to see what happens to the error after each refinement, the ratios of the errors at consecutive grids are computed. That is,

$$\text{error ratio} = \|\mathbf{d}\|_\infty(N)/\|\mathbf{d}\|_\infty(3N), \tag{4.6.1}$$

where $\|\mathbf{d}\|_\infty(N)$ denotes the infinity norm of $\mathbf{d}$ of length N. In the formulation of the BEM systems for each example, the right hand side is computed "exactly" as explained in Section 4.2.1.

Example 4.6.1 (Dirichlet Problem (a) using constant elements) *The problem in Example 3.7.1 is solved using constant elements. The results are shown in Figure 4.10.*

N	$\|\mathbf{d}\|_\infty$	error ratios
5	2.63E-02	2.34
15	1.13E-02	7.37
45	1.52E-03	8.53
135	1.79E-04	8.85
405	2.03E-05	8.95
1215	2.26E-06	-

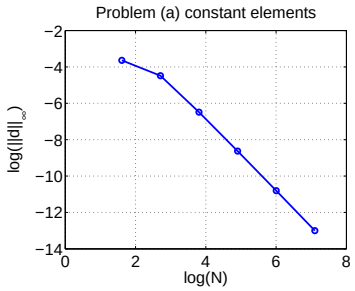

Figure 4.10: Local errors Problem (a) using constant elements.

Example 4.6.2 (Dirichlet Problem (a) using linear elements) *The problem in Example 3.7.1 is solved using linear elements. The results are shown in Figure 4.11.*

N	$\|\mathbf{d}\|_\infty$	error ratios
5	1.57E-02	1.17
15	1.34E-02	7.07
45	1.90E-03	8.48
135	2.24E-04	8.84
405	2.53E-05	8.94
1215	2.83E-06	

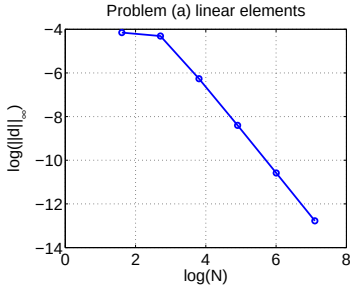

Figure 4.11: Local errors Problem (a) using linear elements.

Example 4.6.3 (Neumann Problem (c) using constant elements) *The problem in Example 3.7.3 is solved using constant elements. The results are shown in Figure 4.12.*

N	$\|\mathbf{d}\|_\infty$	error ratios
5	5.17E-02	3.72
15	1.39E-02	8.40
45	1.65E-03	8.98
135	1.84E-04	9.01
405	2.04E-05	9.01
1215	2.27E-06	-

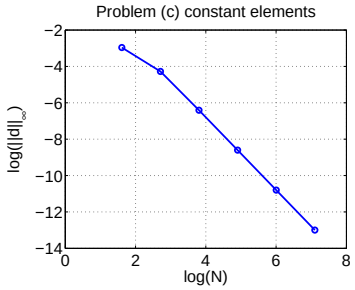

Figure 4.12: Local errors Problem (c) using constant elements.

Example 4.6.4 (Neumann Problem (c) using linear elements) *The problem in Example 3.7.3 is solved using linear elements. The results are shown in Figure 4.13.*

N	$\|\mathbf{d}\|_\infty$	error ratios
5	2.92E-02	2.54
15	1.16E-02	6.39
45	1.82E-03	8.24
135	2.21E-04	8.76
405	2.52E-05	8.92
1215	2.82E-06	-

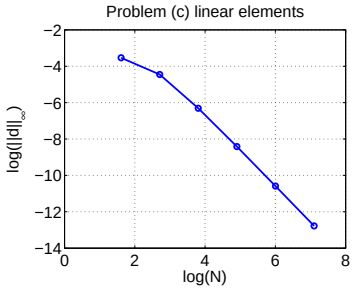

Figure 4.13: Local errors Problem (c) using linear elements.

All the results, for both the Dirichlet and the Neumann problem, show a similar error trend with respect to grid size. As we can see by taking ratios of consecutive errors, each time we refine by about a factor three, the local error goes down by about a factor of nine. The behaviour is the same for both constant and linear elements. This shows that the local error is indeed of second order convergence with respect to grid size for both constant and linear elements as our findings have revealed.

4.7 Equidistribution

For problems with localised regions of rapid variation, choosing a good mesh is essential if sufficiently accurate solutions are to be obtained as cheaply as possible. This is more important in BEM which has full matrices and uniform fine grids will drastically increase the cost of computation. Instead we would like to have a mesh that reflects the activity of the solution. That is the choice of mesh considered is based on controlling the discretisation error. The procedure discussed here is similar to that developed by [79, p. 65]. In contrast to this approach, the quantity we intend to equidistribute is not just some quantity related to the local error of the BEM solution but rather its asymptotically correct estimate as developed in Section 4.2.1.

Generally the following *mesh selection problem* is addressed [4, p. 359]: Given a boundary value problem and an error tolerance TOL, find a mesh

$$\mathcal{M} : 0 = \theta_1 < \theta_2 < \cdots < \theta_n = 2\pi \tag{4.7.1}$$

with

$$l = \max_{1 \le i \le N} l_i, \quad l_i = \theta_{i+1} - \theta_i \tag{4.7.2}$$

such that N is small and the error in $\mathbf{y}_{\mathcal{M}}(\theta)$ as an approximate solution to $\mathbf{y}(\theta)$ is less than TOL. On the other hand, for a give number of elements N, find a mesh

$$\mathcal{M} : 0 = \theta_1 < \theta_2 < \cdots < \theta_n = 2\pi \tag{4.7.3}$$

such that the local error over $\mathcal{M}$ is constant. Generally the mesh must be fine in regions where the desired solution changes rapidly but can be relatively coarse elsewhere. A mesh selection strategy is more successful if it utilises the special properties of the particular numerical method being used, namely its error form [4, p. 361], [10]. However, this error form is normally based upon an asymptotic analysis that the approximation has not yet reached.

If the error we make on each element is known then the information can be used to find a mesh that distributes this error uniformly through out the mesh. This is what is called *error equidistribution*. In what is pursued here, a good mesh is obtained by (re)distributing mesh elements through local error equidistribution after an initial approximation has been obtained. The benefits of equidistributing the local error are twofold. In Chapter 5 it is shown that the global error will be equidistributed when the local error is. Besides, in [6] it is shown that local error equidistribution will minimise the average global error.

Assume a problem whose continuous solution has a small region of high activity. Then a positive *weight function* ϕ as an indicator function for the smoothness of the solution is needed, see [1, p. 77], [10], [4, p. 363]. The weight function ϕ represents some error measurement of the solution and is called a *monitor function*. Then error equidistribution is based on equidistribution of this function. Therefore the success of any mesh equidistribution strategy largely hinges on the choice of the monitor function, see [7] and the references therein.

The idea is now the following: Suppose d_i is some measure of the error on element Γ_i. The error d_i depends on the size of the element Γ_i. Let l_i be the length of Γ_i (again Γ_i is a straight line). Generally the error increases as l_i increases. More precisely let

$$d_i = C_i l_i^p \tag{4.7.4}$$

be the error on Γ_i where the constant C_i depends on the smoothness of the solution. It is convenient to consider a measure with a linear variation in l_i, that is,

$$D^i := l_i \phi_i$$

with ϕ_i independent of l_i. So from (4.7.4) we take

$$D^i = d_i^{1/p} = l_i C_i^{1/p}$$

so that $\phi_i := C_i^{1/p}$. The error is equidistributed if for some constant λ

$$l_i C_i^{1/p} = \lambda, \quad i = 1, 2, \ldots, N. \tag{4.7.5}$$

The problem we have in BEM is that the error per element is the sublocal error given by (4.3.6). However, what we can actually measure is the local error, which is a sum of all the sublocal errors and therefore it depends on all the grid element sizes. So we need to have a measure of the local error on an element that is dependent on the grid size of that particular element. The sublocal errors are given by

$$d_j(\mathbf{s}) \doteq C \frac{\partial^2 q}{\partial \tau^2}(\mathbf{r}_j) l_j^3 \log(\|\mathbf{s} - \mathbf{r}_j\|), \tag{4.7.6}$$

where $C = -1/48\pi$ in constant elements and $1/24\pi$ in linear elements. That is the local error on an element will be

$$d(\mathbf{s}) \doteq \sum_{j=1}^{N} C \frac{\partial^2 q}{\partial \tau^2}(\mathbf{r}_j) l_j^3 \log(\|\mathbf{s} - \mathbf{r}_j\|). \tag{4.7.7}$$

Since the logarithm decays to zero away from $\mathbf{s}$, the most important contributions will be those for which $\|\mathbf{s} - \mathbf{r}_j\| \to 0$, in particular the contribution from the element for which $j = i$. Thus the following approximation can be made:

$$d(\mathbf{r}_i) \approx d_i(\mathbf{r}_i) = \begin{cases} -\dfrac{1}{48\pi} \dfrac{\partial^2 q}{\partial \tau^2}(\mathbf{r}_i) l_i^3 [\log(l_i/2) - 1/3], & \text{in constant elements,} \\ \dfrac{1}{24\pi} \dfrac{\partial^2 q}{\partial \tau^2}(\tilde{\mathbf{r}}_i) l_i^3 [\ln[l_i] - 5/6], & \text{in linear elements.} \end{cases} \tag{4.7.8}$$

For the values of l that are considered here, $[\log(l_i/2) - 1/3]$ and $[\ln[l_i] - 5/6]$ are simply order one constants. Then

$$d(\mathbf{r}_i) \approx C_i \frac{\partial^2 q}{\partial \tau^2}(\mathbf{r}_i) l_i^3, \tag{4.7.9}$$

where

$$C_i = \begin{cases} C(\log(l_i/2) - 1/3), & \text{in constant elements,} \\ C(\ln[l_i] - 5/6), & \text{in linear elements.} \end{cases} \tag{4.7.10}$$

The error in (4.7.9) also depends directly on the activity of the solution and so will be large where the solution is more active and small otherwise. Therefore we equidistribute this error as the local error per element. An interesting observation from (4.7.8) is that the ratio of the error terms for constant and linear elements is a higher order term. That is

$$\frac{\text{const}}{\text{linear}} \approx -\frac{(\ln l_i - \ln 2 - 1/2)}{2(\ln l_i - 5/6)} \tag{4.7.11}$$

which will give a higher order truncation error.

Comparing with (4.3.6) and (4.3.47), the result in (4.7.9) seems to suggest that it is enough to equidistribute the sublocal errors. That is, when the sublocal error is equidistributed, then so is the local error but the reverse is not necessarily true.

Now, equidistributing the sublocal error means

$$d_j(\mathbf{r}_i) = \lambda, \text{ for all } j, \tag{4.7.12}$$

where λ is a constant. Then the local error $d(\mathbf{r}_i)$ is given by

$$d(\mathbf{r}_i) = \sum_j d_j(\mathbf{r}_i) = \sum_j d_j = \sum_j \lambda = N\lambda =: \Lambda, \quad \text{for all } i, \tag{4.7.13}$$

where Λ is a constant. Therefore the local error is also equidistributed.

On the other hand if $d(\mathbf{r}_i)$ is equidistributed, then

$$d(\mathbf{r}_i) = \beta \quad \text{for all } i, \tag{4.7.14}$$

where β is some constant. That is, in the case of rapidly varying $q(\xi)$,

$$\sum_j d_j(\mathbf{r}_i) = d(\mathbf{r}_i) = \beta \quad \text{for all } i. \tag{4.7.15}$$

This does not necessarily imply $d_j(\mathbf{r}_i)$ is equidistributed as well.

Let us now describe strategies for error equidistribution and give some examples.

Consider the problem of Example 3.7.2. The domain and exact solution on the circle of radius $R = 1.2$ are shown in Figure 4.14. Now, using (4.7.8), define

$$d(\mathbf{r}_i) = C_i \frac{\partial^2 q}{\partial \tau^2}(\mathbf{r}_i) l_i^3 \tag{4.7.16}$$

where C_i is defined in (4.7.10). Then we have

$$D^i = \left(C_i \frac{\partial^2 q}{\partial \tau^2}(\mathbf{r}_i) \right)^{1/3} l_i. \tag{4.7.17}$$

Therefore we take the monitor function ϕ_i to be

$$\phi_i = \left(C_i \frac{\partial^2 q}{\partial \tau^2}(\mathbf{r}_i) \right)^{1/3} \tag{4.7.18}$$

where C_i is defined in (4.7.10). We see that ϕ_i is a measure of the variation of q on Γ_i and depends on the second order tangential derivative $\partial^2 q/\partial \tau^2$. For

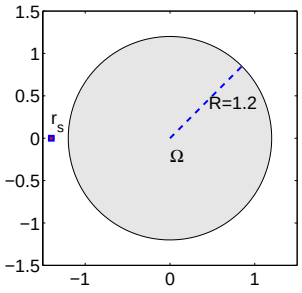

(a) Disc domain.

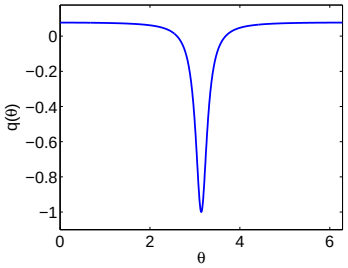

(b) Solution on circle with high activity around $\theta = \pi$

Figure 4.14: A disc domain and solution to Example 3.7.2 with $\mathbf{r}_s = (-1.4, 0)$ on the circular boundary of radius $R = 1.2$.

a BEM solution of (4.14a), we describe the equidistribution of the error in the solution obtained by using constant elements. The strategy described is such that given a number of elements N, we want a grid that ensures that

$$\phi_i l_i = \lambda, \quad i = 1, 2, \ldots, N, \tag{4.7.19}$$

for some constant λ. However, in order to use (4.7.18), we need to estimate the second order tangential derivatives $\partial^2 q/\partial\tau^2$. We can use finite difference formulas and the initial BEM approximations to do this. Suppose for each element Γ_i we have the constant element solution q_i^0 and the linear element solutions q_i^1 and q_i^2 as shown in Figure 4.15. The second order derivatives are

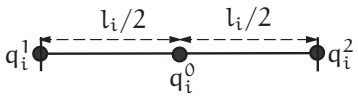

Figure 4.15: Constant element solution q_i^0 and linear element solutions q_i^1 and q_i^2 on an element Γ_i.

estimated as

$$\frac{\partial^2 q}{\partial\tau^2}(\mathbf{r}_i) \approx \frac{1}{(0.5 l_i)^2}(q_i^1 - 2q_i^0 + q_i^2). \tag{4.7.20}$$

The monitor function ϕ_i is then given by

$$\phi_i = \left(\frac{C_i}{0.25 l_i^2}(q_i^1 - 2q_i^0 + q_i^2)\right)^{1/3}. \tag{4.7.21}$$

Then from (4.7.19) we have

$$\sum_{i=1}^{N} \phi_i l_i = N\lambda \Rightarrow \lambda = \frac{1}{N} \sum_{i=1}^{N} \phi_i l_i. \tag{4.7.22}$$

So a new grid is obtained that ensures that

$$l_j^{new} \phi_j = \lambda = \frac{1}{N} \sum_{i=1}^{N} \phi_i l_i. \tag{4.7.23}$$

Therefore we have a new grid l_j^{new} given by

$$l_j^{new} = \left(\frac{1}{N} \sum_{i=1}^{N} \phi_i l_i \right) / \phi_j. \tag{4.7.24}$$

Figure 4.16b shows the solution on a uniform grid of 15 elements. We see that the deviation from the exact solution is large in the active region than in the rest of the boundary. Figure 4.17a shows the grid obtained by equidistributing the error using 15 elements. As expected the grid is small in the active region and coarse elsewhere. The solution on this grid is shown in Figure 4.17b. Figure 4.18 shows the results of equidistribution using 45 elements. Likewise we see that the grid is fine in the active region and coarses out as the activity of q reduces.

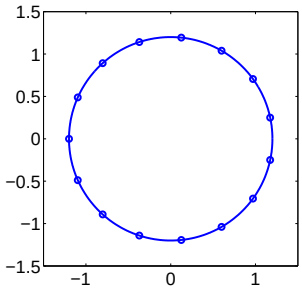

(a) A 15 elements uniform grid.

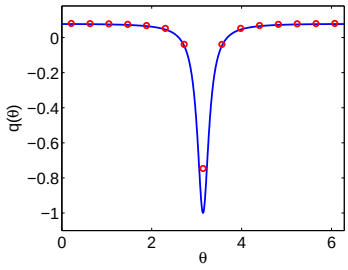

(b) Solution on a 15 elements uniform grid

Figure 4.16: A starting uniform grid of $N = 15$ elements and the corresponding solution using constant elements. The continuous line in 4.16b is the exact continuous solution and the circles are the BEM solution.

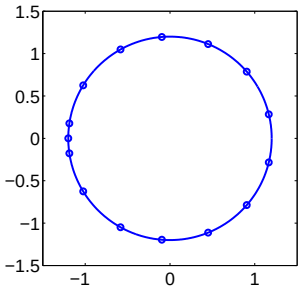

(a) A 15 elements equidistributing grid.

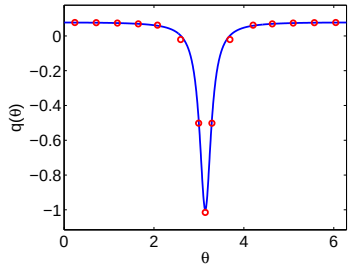

(b) Solution on a 15 elements equidistributing grid

Figure 4.17: An equidistributing grid of N = 15 elements and the corresponding solution using constant elements. The continuous line in 4.17b is the exact continuous solution and the circles are the BEM solution.

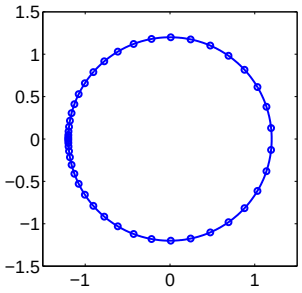

(a) A 45 elements equidistributing grid.

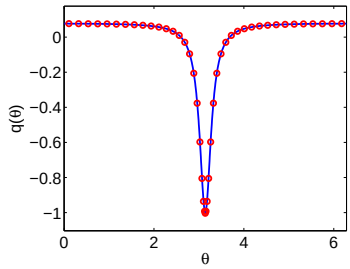

(b) Solution on a 45 elements equidistributing grid

Figure 4.18: An equidistributing grid of N = 45 elements and the corresponding solution using constant elements. The continuous line in 4.18b is the exact continuous solution and the circles are the BEM solution.

"It sounds paradoxical to say the attainment of scientific truth has been effected, to a great extent, by the help of scientific errors." – Thomas Henry Huxley.

Chapter 5

Global errors

5.1 Introduction

In Chapter 4 an analysis of local errors was given. Also the behaviour of local errors was discussed and the concept of sublocal errors introduced. However, what is really needed in practice is the *global error*. In this chapter we asses this in particular by investigating the relationship between the global error and the local error for the Neumann and Dirichlet problems. We would like to show that the global error behaves the same way as the local error. This is important because it means that if we have information about one of the errors then we can know what to expect of the other. For instance if the local error is equidistributed, then we may hope the global error is as well.

In Section 2.5 it was noted that both the single layer operator $\mathcal{K}^{\mathrm{s}}(\mathbf{r};\mathbf{r}')$ and the double layer operator $\mathcal{K}^{\mathrm{d}}(\mathbf{r};\mathbf{r}')$ for the model problem on a circle have the same eigenfunctions, being sines and cosines. This provides us with a good opportunity to study and compare solutions to integral equations of the single and double layer operators. We can employ Fourier series for the unknown functions and a spectral expansion of the operators to write general solutions to the equations. This technique is used to show that, indeed, the global error is of the same order as the local error, moreover it will be equidistributed when the local error is equidistributed.

The type of operator in a BEM formulation will depend on whether the problem has Dirichlet, Neumann or mixed boundary conditions. It is therefore rather too general to say that we are looking at errors in BEM. To be more specific, the different problems, that is, the Dirichlet, Neumann and mixed problems, are looked at separately. In Section 5.2 we consider a Dirichlet problem and examine the global error for different cases of local error distribution. In Section 5.4

we look at Neumann problems and then mixed problems in Section 5.5. We illustrate the theory presented with results from numerical experiments. The results show that the global errors are second order indeed.

5.2 Spectral decomposition

It was seen in Section 2.5 that a Dirichlet problem leads to a Fredholm integral equation of the first kind,

$$\mathcal{K}^s(\mathbf{r};\mathbf{r}')q(\mathbf{r}') = h(\mathbf{r}), \tag{5.2.1}$$

where $h(\mathbf{r})$ is a given function and the operator $\mathcal{K}^s(\mathbf{r};\mathbf{r}')$ is defined in (2.4.5). Let us discretise (5.2.1) using a grid formally indicated by size L. Then we have the approximation, say

$$\mathcal{K}^{sL}(\mathbf{r};\mathbf{r}')q^L(\mathbf{r}') = h^L(\mathbf{r}), \tag{5.2.2}$$

where superscript L is a grid parameter denoting a numerical approximation on the grid. If we were to use the exact function $q(\mathbf{r}')$ in (5.2.2) in place of $q^L(\mathbf{r}')$ we would obtain

$$\mathcal{K}^{sL}(\mathbf{r};\mathbf{r}')q(\mathbf{r}') = h^L(\mathbf{r}) + d^L(\mathbf{r}), \tag{5.2.3}$$

where the residual $d^L(\mathbf{r})$ is the *local discretisation error*. Subtracting (5.2.2) from (5.2.3) we get

$$\mathcal{K}^{sL}(\mathbf{r};\mathbf{r}')e^L(\mathbf{r}') = d^L(\mathbf{r}), \tag{5.2.4}$$

where

$$e^L(\mathbf{r}') := q(\mathbf{r}') - q^L(\mathbf{r}'), \tag{5.2.5}$$

is the *global error*. To obtain (5.2.3) we have in fact substituted the exact solution into the approximate integral equation. We can also consider the converse, that is, substitute an approximate solution into the exact continuous integral equation. Thus, suppose $q^L(\mathbf{r})$ is an approximation of $q(\mathbf{r})$ on a grid of size L, then we would have

$$\mathcal{K}^s(\mathbf{r};\mathbf{r}')q^L(\mathbf{r}') = h(\mathbf{r}) + d(\mathbf{r}), \tag{5.2.6}$$

where again $d(\mathbf{r})$ is a local error . Likewise subtracting (5.2.1) from (5.2.6) gives

$$\mathcal{K}^s(\mathbf{r};\mathbf{r}')e(\mathbf{r}') = d(\mathbf{r}), \tag{5.2.7}$$

where

$$e(\mathbf{r}) := q^L(\mathbf{r}) - q(\mathbf{r}), \tag{5.2.8}$$

is a global error. Therefore given a local error $d(\mathbf{r})$, the global error is the solution of the integral equation (5.2.7) with the local error as the right hand side.

From the spectral theory of $\mathcal{K}^s$, let λ_k be the eigenvalues of $\mathcal{K}^s$ and ϕ_k the corresponding eigenfunctions. Then we have

$$\mathcal{K}^s e(\mathbf{r}) = \sum_k \lambda_k (e, \phi_k)\phi_k(\mathbf{r}). \tag{5.2.9}$$

where the inner product $(\cdot,\cdot)$ is defined in (2.5.4). We can then formally conveniently solve (5.2.7) by using an expansion of d in eigenfunctions. Note that the eigenvalues of $\mathcal{K}^s$ have an accumulation point at zero. Using (5.2.9) in (5.2.7) we have

$$\sum_k \lambda_k (e, \phi_k)\phi_k(\mathbf{r}) = d(\mathbf{r}). \tag{5.2.10}$$

Systematically taking the inner product with ϕ_k (5.2.10) gives

$$\lambda_k (e, \phi_k) = (d, \phi_k), \tag{5.2.11}$$

where (e, ϕ_k) are the *expansion coefficients* of e and (d, ϕ_k) are the expansion coefficients of d. Solving the global error is now equivalent to solving (5.2.11) for its coefficients (e, ϕ_k). This formally yields

$$(e, \phi_k) = \frac{1}{\lambda_k}(d, \phi_k), \tag{5.2.12}$$

where we assume that $\lambda_k \neq 0$. So

$$e(\mathbf{r}) = \sum_k (e, \phi_k)\phi_k(\mathbf{r}). \tag{5.2.13}$$

From (5.2.12) we see that since the eigenvalues λ_k go to zero for increasing k, the global error coefficients might grow unboundedly large depending on the local error coefficients. We now have the following

Theorem 5.2.1 *If* d *is such that* $\left|\frac{(d, \phi_k)}{\lambda_k}\right| \leq \mathcal{O}\left(\left(\frac{1}{k}\right)^{\alpha+1}\right)$, $\alpha > 0$, *then* $\sum_k \frac{1}{\lambda_k} |(d, \phi_k)|$ *is a finite bound for* $\|e\|_\infty$.

Proof. Substituting (5.2.12) into (5.2.13) gives

$$e(\mathbf{r}) = \sum_k \frac{1}{\lambda_k}(d, \phi_k)\phi_k(\mathbf{r}). \tag{5.2.14}$$

Since the basis functions are orthonormal, we then find

$$\|e\|_\infty \leq \sum_k \frac{1}{\lambda_k} |(d, \phi_k)| . \tag{5.2.15}$$

■

Corollary 5.2.1 *Under the assumptions of Theorem 5.2.1 both the constant and the linear elements schemes are convergent.*

It is therefore important to have information about the λ_k to assess (5.2.12). The case for a general boundary is very complicated and therefore we restrict ourselves to a circular domain. We conjecture that the general case then follows using conformal mapping. In [16, p. 26], it has been established that, in the case of a Dirichlet problem on a circle, the eigenvalues λ_k are $\mathcal{O}(1/k)$. From (5.2.12) we therefore conclude that to have convergence in the coefficients of the global error the coefficients of the local error must be $\mathcal{O}(1/k^{2+\alpha})$ where $\alpha > 0$. It is this phenomenon that is the subject of investigation in the following subsections for different forms of d.

In order to do this we need to have the eigensolutions of the problem. We still restrict ourselves to a Dirichlet problem on a circle, in which case the eigenfunctions are sines and cosines and expansions of functions are just Fourier series. We begin with a problem where the local error is constant and then will show how this can be used for almost constant problems, that is, where the local error is properly equidistributed.

5.3 Dirichlet problems

A more detailed investigation of the global error requires assessing the Fourier coefficients (d, ϕ_k). As we fix our thought on a circular domain, we can use trigonometric functions for a basis. Recall from Section 2.5.1 that the single layer operator $\mathcal{K}^s$ for the Dirichlet problem has cosines and sines as eigen functions. On a circle of radius R, $R/2k$ is an eigenvalue for $\mathcal{K}^s$ with eigenfunctions $\cos k\theta$ and $\sin k\theta$ where θ is the polar angle. Also, for a symmetric kernel K with orthonormal eigenfunctions y_k, the Fourier coefficients of an arbitrary function h are given by $h_k = (h, y_k)$, see [41, p. 324]. Basically, for a function f of period 2π that is integrable over the period, the Fourier series of f is the trigonometric series, see [39, p. 532],

$$a_0 + \sum_{n=1}^{\infty} (a_n \cos n\chi + b_n \sin n\chi), \tag{5.3.1}$$

where $a_n,\ b_n,\ n = 1, 2, \ldots$ are the Fourier coefficients of f given by

$$a_0 := \frac{1}{2\pi} \int_{-\pi}^{\pi} f(\chi)\, d\chi, \tag{5.3.2a}$$

$$a_n := \frac{1}{\pi} \int_{-\pi}^{\pi} f(\chi) \cos n\chi\, d\chi, \quad n = 1, 2, \ldots, \tag{5.3.2b}$$

$$b_n := \frac{1}{\pi} \int_{-\pi}^{\pi} f(\chi) \sin n\chi\, d\chi, \quad n = 1, 2, \ldots. \tag{5.3.2c}$$

We note here that since we focus ourselves on a circular boundary, the natural arc length coordinate χ is given by $\chi = R\theta$. In what follows we use Fourier series analysis to relate global error to local error.

Theorem 5.3.1 *If the local error* d *is constant over* $\partial\Omega$*, say* $d \equiv C$ *over* $\partial\Omega$*, then* e *is also constant over* $\partial\Omega$*, that is,*

$$e(\mathbf{r}) = C_0, \tag{5.3.3}$$

for some constant $C_0 \in \mathbb{R}$*.*

Proof. This result follows directly from Theorem 5.2.1 noting that all Fourier coefficients of d are zero except the one for the constant function. ■

Corollary 5.3.1 *If we use constant elements and* $l_j^2 \frac{\partial^2 q}{\partial \chi^2})(\chi_j)$ *is equidistributed, that is,* $l_j^2 \frac{\partial^2 q}{\partial \chi^2})(\chi_j) = C_0$ *a constant, then the global error has the same order as the local error and is given by*

$$\|e_0\|_\infty \doteq \frac{1}{48\pi} C_0 (2\pi R) \log(1/R), \tag{5.3.4}$$

where R *is the radius of the circle.*

Proof. Recall from Lemma 4.3.2, $l_j^2 \frac{\partial^2 q}{\partial \chi^2})(\chi_j) = C_0$ results in

$$d_0(\mathbf{s}) = \frac{1}{48\pi} C_0 (2\pi R) \log(1/R), \tag{5.3.5}$$

where C_0 is second order in grid size. This result is independent of $\mathbf{s}$ since the contour integral in (4.3.40) gives the same result for all positions $\mathbf{s}$. So using Theorem 5.2.1, only the Fourier coefficient for the constant mode survives to give the result. ■

Corollary 5.3.2 *If we use linear elements and* $l_j^2 \frac{\partial^2 q}{\partial \chi^2})(\chi_j)$ *is equidistributed, that is,* $l_j^2 \frac{\partial^2 q}{\partial \chi^2})(\chi_j) = C_1$ *a constant, then the global error has the same order as the local error and is given by*

$$\|e_1\|_\infty \doteq \frac{1}{24\pi} C_1 (2\pi R) \log R, \tag{5.3.6}$$

where R *is the radius of the circle.*

Proof. Again, from Lemma 4.3.5, $l_j^2 \frac{\partial^2 q}{\partial \chi^2})(\chi_j) = C_1$ results in

$$d_1(\mathbf{s}) = \frac{1}{48\pi} C_1 (2\pi R) \log(1/R), \tag{5.3.7}$$

where C_1 is second order in grid size. The result is independent of $\mathbf{s}$ since the contour integral in (4.3.40) gives the same result for all positions $\mathbf{s}$. So using the results of Theorem 5.2.1, only the Fourier coefficient for the constant mode survives to give the result. ■

For a more general result we can proceed along two lines. First one may wonder what is the effect of neglecting higher order terms in local error estimates. For this we have

Theorem 5.3.2 *Let* $q \in C^2(\partial\Omega)$ *and define* $l := \max_{i=1,\ldots,N} l_i$. *Then* $\|e\|_\infty = \mathcal{O}(l^2)$.

Proof. From Theorem 4.3.1 we conclude that

$$d_0(\mathbf{s}) = -\frac{1}{24\pi} C_1 \int \frac{\partial r}{\partial \chi} \frac{1}{r} \, d\chi - \frac{1}{48\pi} C_2 \int \log(\|\mathbf{s} - \mathbf{r}(\chi)\|) \, d\chi + \mathcal{O}(l^3), \tag{5.3.8}$$

where

$$\min \left| \frac{\partial q}{\partial \chi}(\chi_j) l_j \right| \leq C_1 \leq \max \left| \frac{\partial q}{\partial \chi}(\chi_j) l_j \right|,$$

$$\min \left| \frac{\partial^2 q}{\partial \chi^2}(\chi_j) l_j^2 \right| \leq C_2 \leq \max \left| \frac{\partial^2 q}{\partial \chi^2}(\chi_j) l_j^2 \right|.$$

Let

$$M(\chi) := -\frac{1}{24\pi} C_1 \int \frac{\partial r}{\partial \chi} \frac{1}{r} \, d\chi - \frac{1}{48\pi} C_2 \int \log(\|\mathbf{s} - \mathbf{r}(\chi)\|) \, d\chi, \tag{5.3.9}$$

and

$$\delta(\chi) := \mathcal{O}(l^3), \tag{5.3.10}$$

that is $\delta(\chi)$ is the order three terms. Thus we have

$$d_0(\mathbf{s}) = M(\chi) + \delta(\chi). \tag{5.3.11}$$

We can expand the δ formally in a Fourier expansion. Before doing that we note that they can be approximated by a periodic higher order approximation polynomial of degree less than or equal to $N - 1$, which means that the coefficients for frequencies larger that N are zero. Hence

$$\delta(\chi) = \sum_{j=0}^{N-1} (\alpha_j \cos j\chi + \beta_j \sin j\chi), \tag{5.3.12}$$

where $|\alpha_j|,\ |\beta_j| = \mathcal{O}(\frac{1}{j})$. We now find that

$$e(\chi) = M + \sum_{j=0}^{N-1} \left(\frac{j}{2\pi}\alpha_j \cos j\chi + \frac{j}{2\pi}\beta_j \sin j\chi \right) \tag{5.3.13}$$

Since $\alpha_j,\ \beta_j$ are $\mathcal{O}(l^3)$ and we sum over N terms $N = \mathcal{O}(\frac{1}{l})$ and, finally, since $M = \mathcal{O}(l^2)$ we thus have proven the result. ■

In Table 5.1 we have the infinity norm of the global errors in the solution of Example 3.7.1. We see that each time we increase the number of elements N by three the error goes down by a factor of nine. The behaviour is the same for both constant and linear elements as shown in Tables 5.1(a) and (b) respectively. Thus the error is second order in grid size as is the local error.

N	$\|\mathbf{e}\|_\infty$	error ratios
5	1.02E-01	2.63
15	3.87E-02	7.58
45	5.12E-03	8.56
135	5.98E-04	8.85
405	6.75E-05	8.92
1215	7.57E-06	-

(a)Constant elements

N	$\|\mathbf{e}\|_\infty$	error ratios
5	7.14E-02	1.50
15	4.74E-02	7.46
45	6.37E-03	8.53
135	7.46E-04	8.85
405	8.44E-05	8.92
1215	9.45E-06	

(b) Linear elements

Table 5.1: Global errors in the solution of Dirichlet Example 3.7.1 using constant elements in (a), and linear elements in (b).

5.4 Neumann problems

A Neumann problem leads to a Fredholm integral equation of the second kind given by

$$\left(\frac{1}{2}\mathcal{I} + \mathcal{K}^d \right) u = f. \tag{5.4.1}$$

Since we restrict ourselves to a circular domain, we have a relatively simple spectral decomposition. Indeed, from (2.5.16) we obtain for the operator $\mathcal{K} = \frac{1}{2}\mathcal{I} + \mathcal{K}^d$ that

$$\lambda_0 = 0, \quad \lambda_j = \frac{1}{2},\ \ j \geq 1, \tag{5.4.2}$$

with corresponding eigenfunctions 1, and $\cos j\chi$ and $\sin j\chi$ for $j \geq 1$ respectively. Following the same approach as in obtaining (5.2.7), we have

$$\left(\frac{1}{2}\mathcal{I} + \mathcal{K}^d\right) e = d. \tag{5.4.3}$$

Theorem 5.4.1 *The global error $e(\mathbf{r})$ of the solution to a Neumann problem is second order in grid size, that is, the same order as the local error $d(\mathbf{r})$. That is*

$$e(\mathbf{r}) = Cd(\mathbf{r}), \tag{5.4.4}$$

for some $C \in \mathbb{R}$.

Proof. For a given d we look for solutions of (5.4.3) in the space W_1 introduced in Section 2.5. In this space the operator $\mathcal{K} = \left(\frac{1}{2}\mathcal{I} + \mathcal{K}^d\right)$ has all eigenvalues equal to $1/2$ with sines and cosines as eigenfunctions. So we have

$$\sum_k \lambda_k(e, \phi_k)\phi_k(\mathbf{r}) = d(\mathbf{r}), \quad \lambda_k = 1/2, \tag{5.4.5}$$

for all k. Taking the inner product with a ϕ_k we obtain

$$(e, \phi_k) = 2(d, \phi_k), \tag{5.4.6}$$

for all k. Thus we expect the global error to be of the same order as the local error since its Fourier coefficients are only a scalar multiple of the local error coefficients. ■

The behaviour is the same for Neumann problems as shown in Table 5.2 and as expected the error order is the same as that for the local error.

N	$\|\mathbf{e}\|_\infty$	error ratios
5	5.93E-01	9.56
15	6.20E-02	9.38
45	6.61E-03	9.70
135	6.81E-04	9.36
405	7.28E-05	9.16
1215	7.95E-06	-

(a) Constant elements

N	$\|\mathbf{e}\|_\infty$	error ratios
5	1.33E-01	4.00
15	3.32E-02	5.38
45	6.16E-03	8.08
135	7.63E-04	8.74
405	8.73E-05	8.92
1215	9.78E-06	-

(b) Linear elements

Table 5.2: Global errors in the solution of Neumann Example 3.7.3 using constant elements in (a) and linear elements in (b).

5.5 Mixed problem

The mixed problem requires some additional analysis. Suppose $u(\mathbf{r}) = g(\mathbf{r})$ on a part $\partial\Omega^1$ of the boundary and $q(\mathbf{r}) = h(\mathbf{r})$ on a part $\partial\Omega^2$, see Figure 5.1.

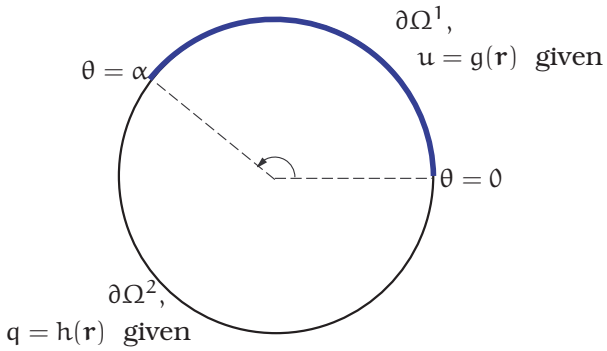

Figure 5.1: Boundary with mixed boundary conditions.

The integral equation for such a mixed problem can be written as

$$\frac{1}{2}u + \mathcal{K}^{d}_{\partial\Omega^2} u - \mathcal{K}^{s}_{\partial\Omega^1} q = f \tag{5.5.1}$$

where

$$f := -\mathcal{K}^{d}_{\partial\Omega^1} g + \mathcal{K}^{s}_{\partial\Omega^2} h. \tag{5.5.2}$$

So we have

$$\mathcal{K}^{d}_{\partial\Omega^2} u - \mathcal{K}^{s}_{\partial\Omega^1} q = f - \frac{1}{2}g, \quad \mathbf{r} \in \partial\Omega^1, \tag{5.5.3a}$$

$$\frac{1}{2}u + \mathcal{K}^{d}_{\partial\Omega^2} u - \mathcal{K}^{s}_{\partial\Omega^1} q = f, \quad \mathbf{r} \in \partial\Omega^2. \tag{5.5.3b}$$

Consider

$$\mathcal{K}^{d} u - \mathcal{K}^{s} q = f. \tag{5.5.4}$$

Now let

$$u(\theta) = \sum (\alpha_k \sin k\theta + \beta_k \cos k\theta) \quad \text{on} \quad \partial\Omega^2, \tag{5.5.5}$$

$$q(\theta) = \sum (\gamma_k \sin k\theta + \delta_k \cos k\theta) \quad \text{on} \quad \partial\Omega^1, \tag{5.5.6}$$

where as

$$f(\theta) = \sum (\xi_k \sin k\theta + \eta_k \cos k\theta) \quad \text{on} \quad \partial\Omega^1, \tag{5.5.7}$$

$$f(\theta) = \sum (\pi_k \sin k\theta + \rho_k \cos k\theta) \quad \text{on} \quad \partial\Omega^2. \tag{5.5.8}$$

Let

$$\mathcal{L}(u, q) = \mathcal{K}^d_{\partial\Omega^2} u - \mathcal{K}^s_{\partial\Omega^1} q.$$

Then we have

$$\mathcal{L}(1, 1) = \sum \left(\tilde{a}_j \cos j\theta + \tilde{b}_j \sin j\theta\right). \tag{5.5.9}$$

Similarly

$$\mathcal{L}(\cos k\cdot, \cos k\cdot) = a_k + b_k \sin k\theta + c_k \cos k\theta \tag{5.5.10}$$

and

$$\mathcal{L}(\sin k\cdot, \sin k\cdot) = \hat{a}_k + \hat{b}_k \sin k\theta + \hat{c}_k \cos k\theta. \tag{5.5.11}$$

Then on $\partial\Omega_1$

$$\begin{aligned}\mathcal{L}(u, q) = \sum_k \big\{ &\alpha_k \hat{a}_k + \alpha_k \hat{b}_k \sin k\theta + \alpha_k \hat{c}_k \cos k\theta \\ &+ \beta_k a_k + \beta_k b_k \sin k\theta + \beta_k c_k \cos k\theta + \beta_0 \tilde{a}_k \cos k\theta + \beta_0 \tilde{b}_k \sin k\theta \big\}.\end{aligned} \tag{5.5.12}$$

So

$$\eta_0 = \sum (\alpha_k \hat{a}_k + \beta_k a_k), \tag{5.5.13a}$$

$$\eta_k = \sum (\alpha_k \hat{c}_k + \beta_k c_k) + \beta_0 \tilde{a}_k, \tag{5.5.13b}$$

$$\xi_k = \sum \left(\alpha_k \hat{b}_k + \beta_k b_k\right) + \beta_0 \tilde{b}_k. \tag{5.5.13c}$$

If β_0 were known, we would find α_k and β_k from (5.5.13b) and (5.5.13c) since η_0, η_k and ξ_k are known from the right hand side of (5.5.4) which is given. In fact we have to solve a sparse system. If we truncate the series in (5.5.13) we have a sparse system from which we can solve for $\beta_1, \beta_2, \ldots, \beta_N$ and $\alpha_1, \alpha_2, \ldots, \alpha_N$.

Now, for the mixed problem, the integrals in (2.5.11), (2.5.12) and (2.5.14) are valid only on part of the circle. Thus, suppose $\partial\Omega^1$ is the arc $\theta \in [0, \alpha]$ and $\partial\Omega^2$ is the arc $\theta \in [\alpha, 2\pi]$, see Figure 5.1. Then we have, for the $\cos k\theta$ eigenfunctions,

$$\begin{aligned}(\mathcal{K}^s \cos k\theta)_{\partial\Omega^1} = &-\frac{R}{2\pi} \log R \int_0^\alpha \cos(k\theta')\, d\theta' + \frac{R}{2\pi k} \int_0^\alpha \cos(k\theta) \cos^2(k\theta')\, d\theta' \\ &+ \frac{R}{2\pi k} \int_0^\alpha \sin(k\theta) \sin(k\theta') \cos(k\theta')\, d\theta'.\end{aligned} \tag{5.5.14}$$

Evaluating the integrals we get

$$(\mathcal{K}^s \cos k\theta)_{\partial\Omega^1} = -\frac{R}{2\pi}\log R\frac{\sin k\alpha}{k} + \frac{R}{2\pi k}\cos(k\theta)\left(\frac{\alpha}{2} + \frac{\sin(2k\alpha)}{4k}\right) + \frac{R}{2\pi k}\frac{\sin k\theta}{2k}\sin^2 k\alpha. \quad (5.5.15)$$

For the $\sin k\theta$ eigenfunctions we have

$$(\mathcal{K}^s \sin k\theta)_{\partial\Omega^1} = -\frac{R}{2\pi}\log R\int_0^\alpha \sin(k\theta')\,d\theta' + \frac{R}{2\pi k}\int_0^\alpha \cos(k\theta)\cos(k\theta')\sin(k\theta')\,d\theta' + \frac{R}{2\pi k}\int_0^\alpha \sin(k\theta)\sin^2(k\theta')\,d\theta', \quad (5.5.16)$$

which yields

$$(\mathcal{K}^s \sin k\theta)_{\partial\Omega^1} = -\frac{R}{2\pi k}\log R(1-\cos k\alpha) + \frac{R}{2\pi k}\frac{\cos k\theta}{2k}\sin^2 k\alpha + \frac{R}{2\pi k}\sin(k\theta)\left(\frac{\alpha}{2} - \frac{\sin 2k\alpha}{4k}\right). \quad (5.5.17)$$

For well conditioning of (5.5.13b) and (5.5.13c), we have to look at the system

$$\begin{bmatrix} \hat{c}_k & c_k \\ \hat{b}_k & b_k \end{bmatrix} = \begin{bmatrix} \frac{R}{2k\pi}\frac{\sin^2 k\alpha}{2k} & \frac{R}{2k\pi}\left(\frac{\alpha}{2} + \frac{\sin 2k\alpha}{4k}\right) \\ \frac{R}{2k\pi}\left(\frac{\alpha}{2} - \frac{\sin 2k\alpha}{4k}\right) & \frac{R}{2k\pi}\frac{\sin^2 k\alpha}{2k} \end{bmatrix} =: \mathbf{A}, \quad (5.5.18)$$

which is obtained by comparing (5.5.15) and (5.5.17) with (5.5.10) and (5.5.11). So,

$$\det \mathbf{A} = \frac{R^2}{4k^2\pi^2}\left[\frac{\sin^4 k\alpha}{4k^2} - \frac{\alpha^2}{4} + \frac{\sin^2 2k\alpha}{16k^2}\right], \quad (5.5.19)$$

which is not zero unless $\alpha = 0$. We are therefore able to obtain the coefficients α_k and β_k. A similar process as above will show that we are able to compute the coefficients γ_k and δ_k. So we deduce that $u(\theta)$ can be found as an infinite Fourier series (5.5.5), and likewise $q(\theta)$ in (5.5.6). In computing the global error, the unknowns $u(\theta)$ on $\partial\Omega^2$ and $q(\theta)$ on $\partial\Omega^1$ are instead the local errors in these functions. So we have the following theorem

Theorem 5.5.1 *If we use linear elements and* $l_j^2\frac{\partial^2 q}{\partial\chi^2}(\chi_j)$ *is constant over* $\partial\Omega^1$ *and* $l_j^2\frac{\partial^2 u}{\partial\chi^2}(\chi_j)$ *is constant over* $\partial\Omega^2$*, then the expansion coefficients* $\alpha_k,\ \beta_k$ *of the global error are second order in grid size, that is* $\alpha_k,\ \beta_k = \mathcal{O}(l^2)$.

Proof. The coefficients α_k, β_k are obtained from solving the system (5.5.13). In (5.5.19) we have shown that the system is well conditioned. Since the right hand side is from the local error, which in Corollary 4.5.2 we have shown that it is second order, then the coefficients will also be second order. ■

Corollary 5.5.1 *For a mixed problem, if we use linear elements and have equidistribution, then the global error is* $\mathcal{O}(l)$.

Proof. Since the global error is a sum over the expansion coefficients α_k, β_k which are second order, we expect this error to be of first order. ■

“A good scientist is a person in whom the childhood quality of perennial curiosity lingers on. Once he gets an answer, he has other questions. – Frederick Seitz.

Chapter 6

Local Defect Correction for BEM

6.1 Introduction

Often boundary value problems have small localised regions of high activity where the solution varies very rapidly compared to the rest of the domain. This behaviour is due to boundary conditions or due to an irregular boundary. One therefore has to use relatively fine meshes to capture the high activity. Since the activity is localised, one may also choose to solve on a uniform structured grid. That is, instead of a uniform global grid, the solution is approximated using several uniform grids with different grid sizes that cover different parts of the domain. The size of each grid is chosen in agreement with the activity of the solution in that part of the domain. This refinement strategy is called *local uniform grid refinement* [19]. The solution is approximated on a composite grid which is the union of the various uniform local grids. One way of approximating this composite grid solution that is simple and less complex is by *Local Defect Correction* (LDC).

In LDC, at least one grid, the *global coarse grid*, covers the entire domain. Then a uniform *local fine grid* is used in a small part of the domain containing the high activity. In [19, 23] LDC has been shown to be a useful way of approximating the composite grid solution in which a global coarse grid solution is improved by a local fine grid solution through a process whereby the right hand side of the global coarse grid problem is *corrected* by the *defect* of a local fine grid approximation. This method has been well explored for numerical methods such as finite differences and finite volumes, see [1, 19, 23, 51].

In this chapter we explore potential analogues and develop an LDC strategy for BEM. The first attempt on LDC for BEM was in [32] and [34] where an algebraic approach was suggested and studied. Since in BEM we discretise the boundary, we will be concerned with problems in which the high activity occurs at the boundary. In Section 6.2 we develop an LDC strategy for BEM alongside an example. In Section 6.5 we will show that indeed LDC is a fixed point iterative method and discuss some convergence properties of the algorithm.

6.2 LDC formulation with an introductory example: A Neumann problem

Consider the Neumann problem of Example 3.7.4. Let the domain be a unit square in two dimension, that is, $\Omega = [0,\ 1] \times [0,\ 1]$ and the fixed point $\mathbf{r}_s = (0.5, -0.02)$. So we have the problem

$$\begin{cases} \nabla^2 u(\mathbf{r}) = 0, & \mathbf{r} \in \Omega := [0,\ 1] \times [0,\ 1], \\ \\ q(\mathbf{r}) = h(\mathbf{r}), & \mathbf{r} \in \Gamma, \end{cases} \tag{6.2.1}$$

where

$$h(\mathbf{r}) = \frac{(\mathbf{r} - \mathbf{r}_s) \cdot \mathbf{n}(\mathbf{r})}{\|\mathbf{r} - \mathbf{r}_s\|^2},\ \mathbf{r}_s = (0.5, -0.02). \tag{6.2.2}$$

The solution in Ω, shown in Figure 6.1, has a small area close to the boundary where it changes rapidly. As a result, the solution $u(\mathbf{r})$ in the boundary has a region of high activity in a small part of the boundary, see Figure 6.1.

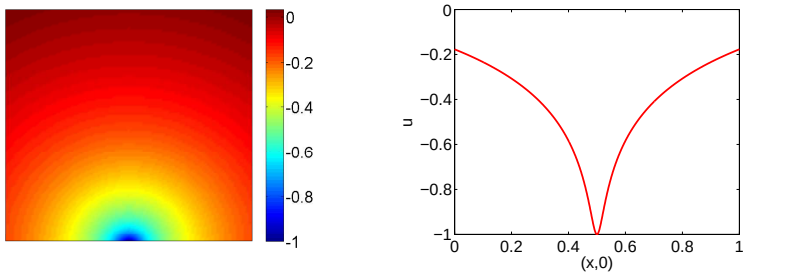

(a) Solution in Ω with small region of high activity.

(b) The solution $u(\mathbf{r})$ in part of $\partial\Omega$ that borders the high activity.

Figure 6.1: Solution in the domain and part of the solution $u(\mathbf{r})$ at the boundary for Example (3.7.4) on a unit square with $\mathbf{r}_s$ in $h(\mathbf{r})$ equal to $(0.5, -0.02)$.

Therefore we can identify a small region inside Ω which contains the high activity. This region we call the *local domain* and denote it by Ω_{local}, see Figure 6.2.

Its boundary Γ_{local}, the *local boundary*, consists of two parts: a part Γ_{active} that is also part of the global boundary and a part Γ_{inside} that is contained in the global domain Ω, Figure 6.2b. We will call the part Γ_{active} the *local active boundary*. For instance in the problem corresponding to the solutions shown in Figure 6.1, the boundary Γ_{active}, may be identified as $\Gamma_{\text{active}} = \{(x, y) : y = 0, x \in [0.2, 0.8]\}$. The part of the global boundary Γ that is outside the active region Γ_{active} will be denoted Γ_c, that is, $\Gamma_c := \Gamma \backslash \Gamma_{\text{active}}$.

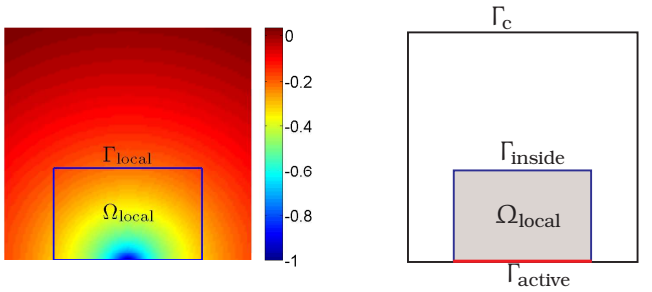

(a) Identify local activity area Ω_{local}. (b) A local domain Ω_{local}

Figure 6.2: An example of a multiscaled solution with localised high activity in 6.2a and in 6.2b, an illustration of a local problem domain. The boundary of Ω_{local} is $\Gamma_{\text{local}} := \Gamma_{\text{active}} \cup \Gamma_{\text{inside}}$.

The interest in BEM is to compute a numerical approximation of $u(\mathbf{r})$ as accurately as possible. For such kind of multiscaled variations one is faced with the option of using a global uniform grid with a mesh of relatively small size l in order to capture the high activity. This would result in very large systems which are computationally expensive since BEM matrices are full matrices. Besides, outside the local active boundary Γ_{active}, the variation of the solution is smooth and a relatively coarse grid would suffice. The other option is to use a uniform structured grid designed to capture the different activities. This would be a composite grid with a relatively fine mesh of size l in the local active region and a coarse grid of size L elsewhere.

With LDC we approximate the solution on a composite grid in an iterative way that involves solving a so called *local problem* which is a boundary value problem defined on the local domain. The local problem is solved on a fine mesh whose size is chosen in agreement with the local activity. The solution on the local fine grid is combined with the solution on the global coarse grid through defect correction to obtain a composite grid solution on Γ.

The advantage of this approach is that instead of solving a large composite grid system, two smaller systems; a global coarse grid system and a local fine grid system, are solved independently. For problems with various local activities the local problems can be solved separately in parallel giving a tremendously

cheaper way of obtaining a composite grid solution other than solving directly on the composite grid.

As introduced in Section 3.1, let Γ be the numerical representation of $\partial\Omega$ in BEM. The *global coarse grid* Γ^L is a uniform mesh of N elements each of size L covering the whole of Γ, that is,

$$\Gamma^L := \{\Gamma_1^L, \Gamma_2^L, \ldots, \Gamma_N^L\} \tag{6.2.3}$$

where $|\Gamma_j^L| = L$ for all j. The *local fine grid* Γ_{local}^l is a uniform mesh of N_l elements each of size l covering Γ_{local}, that is,

$$\Gamma_{local}^l := \{\Gamma_{local,1}^l, \Gamma_{local,2}^l, \ldots, \Gamma_{local,N_{local}}^l\} \tag{6.2.4}$$

where $|\Gamma_{local,i}^l| = l$ for all i. The size of the local fine grid l is chosen in agreement

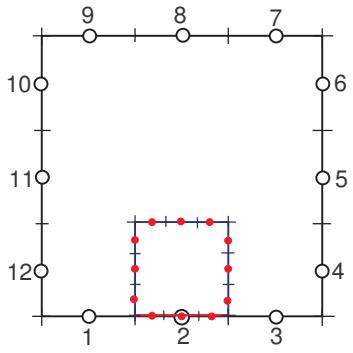

Figure 6.3: Global coarse and local fine grids. The small dots are the nodes $\mathbf{r}_{local}^l$ of the local fine grid Γ_{local}^l and the big circles are the nodes $\mathbf{r}^L$ of the global coarse grid Γ^L. Node 2 belongs to $\mathbf{r}^L \cap \mathbf{r}_{active}^l$.

with the activity of the solution in Γ_{active}. Since the solution varies much more rapidly in Γ_{active} than elsewhere, we expect l to be much smaller than L. Part of the grid Γ_{local}^l belongs to Γ_{active} and part belongs to Γ_{inside}. The part that belongs to Γ_{active} is denoted Γ_{active}^l and that that belongs to Γ^{inside} is denoted Γ_{inside}^l. That is

$$\Gamma_{active}^l := \{\Gamma_{active,1}^l, \Gamma_{active,2}^l, \ldots, \Gamma_{active,N_{active}}^l\}, \tag{6.2.5a}$$

$$\Gamma_{inside}^l := \{\Gamma_{inside,1}^l, \Gamma_{inside,2}^l, \ldots, \Gamma_{inside,N_{inside}}^l\}, \tag{6.2.5b}$$

where $\Gamma_{active}^l \cup \Gamma_{inside}^l = \Gamma_{local}^l$ and $N_{active} + N_{inside} = N_{local}$. In constant elements that we discuss here, the collocation nodes are the midpoints of the elements,

where the solution is computed. Let us denote the nodes of the coarse grid as $\mathbf{r}^L$,

$$\mathbf{r}^L := \{\mathbf{r}_1^L, \mathbf{r}_2^L, \ldots, \mathbf{r}_N^L\}. \tag{6.2.6}$$

Similarly we denote the nodes of the local fine grid as $\mathbf{r}^l_{\text{local}}$,

$$\mathbf{r}^l_{\text{local}} := \{\mathbf{r}^l_{\text{local},1}, \mathbf{r}^l_{\text{local},2}, \ldots, \mathbf{r}_{\text{local},N_{\text{local}}}\}, \tag{6.2.7}$$

and consist of $\mathbf{r}^l_{\text{active}}$ and $\mathbf{r}^l_{\text{inside}}$ that are analogously defined.

We assume that all the grid nodes of $\mathbf{r}^L \cap \mathbf{r}^l_{\text{active}}$ belong to $\mathbf{r}^l_{\text{active}}$, see Figure 6.3. The composite grid nodes $\mathbf{r}^{l,L}$ are the union $\mathbf{r}^L \cup \mathbf{r}^l_{\text{active}}$ of the global coarse grid nodes $\mathbf{r}^L$ and the active local fine grid nodes $\mathbf{r}^l_{\text{active}}$. The composite grid $\Gamma^{l,L}$ consists of the finest elements that correspond to $\mathbf{r}^{l,L}$.

First we discretise the BIE on Γ^L to yield

Step (i)

$$\frac{1}{2}u_i^L + \sum_{j=1}^{N} u_j^L \int_{\Gamma_j^L} \frac{\partial \nu}{\partial n}(\mathbf{r}_i; \mathbf{r}(\chi))\, d\chi = \sum_{j=1}^{N} \int_{\Gamma_j^L} q(\mathbf{r}(\chi))\nu(\mathbf{r}_i; \mathbf{r}(\chi))\, d\chi, \tag{6.2.8}$$

which gives the global coarse grid system of equations

$$\mathbf{A}^L\mathbf{u}_0^L = \mathbf{b}^L. \tag{6.2.9}$$

Once we have solved (6.2.9), the next step is to use the solution $\mathbf{u}_0^L$ to formulate a local problem on Ω_{local}. This local problem on Ω_{local} satisfies the same operator as in the global problem. The boundary conditions on Γ_{active} are the same as those in the global problem that is $q(\mathbf{r}) = h(\mathbf{r})$, since $\Gamma_{\text{active}} \subset \Gamma$. On Γ_{inside} we prescribe an artificial boundary condition $\tilde{g}(\mathbf{r})$ defined below. So we have

$$\begin{cases} \nabla^2 u(\mathbf{r}) = 0, & \mathbf{r} \in \Omega_{\text{local}}, \\ q(\mathbf{r}) = h(\mathbf{r}), & \mathbf{r} \in \Gamma_{\text{active}}, \\ u(\mathbf{r}) = \tilde{g}(\mathbf{r}), & \mathbf{r} \in \Gamma_{\text{inside}}, \end{cases} \tag{6.2.10}$$

where $\tilde{g}(\mathbf{r})$ is a piecewise constant function given by

$$\tilde{g}(\mathbf{r}) := u_{\text{inside}}(\mathbf{r}_i), \quad \mathbf{r} \in \Gamma^l_{\text{inside},i} \subset \Gamma_{\text{inside}}, \tag{6.2.11}$$

and

Step (ii)

$$u_{\text{inside}}(\mathbf{r}_i) := \sum_{j=1}^{N} \int_{\Gamma_j^L} q(\mathbf{r}(\chi))\nu(\mathbf{r}_i; \mathbf{r}(\chi))\, d\chi - \sum_{j=1}^{N} u_j^L \int_{\Gamma_j^L} \frac{\partial \nu}{\partial n}(\mathbf{r}_i; \mathbf{r}(\chi))\, d\chi, \quad \mathbf{r}_i \in \Gamma_{\text{inside}}. \tag{6.2.12}$$

Step (iii) Then a BIE for (6.2.10) on Γ_{local} is, for $\mathbf{r},\ \mathbf{r}(\chi) \in \Gamma_{\text{local}}$,

$$\frac{1}{2}u(\mathbf{r}) + \int_{\Gamma_{\text{active}}} u(\mathbf{r}(\chi))\frac{\partial v}{\partial n}(\mathbf{r};\mathbf{r}(\chi))\,d\chi + \int_{\Gamma_{\text{inside}}} \tilde{g}(\mathbf{r}(\chi))\frac{\partial v}{\partial n}(\mathbf{r};\mathbf{r}(\chi))\,d\chi = \int_{\Gamma_{\text{active}}} q(\mathbf{r}(\chi))v(\mathbf{r};\mathbf{r}(\chi))\,d\chi + \int_{\Gamma_{\text{inside}}} q(\mathbf{r}(\chi))v(\mathbf{r};\mathbf{r}(\chi))\,d\chi. \quad (6.2.13)$$

Discretising (6.2.13) on a local fine grid defined in (6.2.4) and (6.2.5) we have

$$\frac{1}{2}u^l_{\text{local},i} + \sum_j u^l_{\text{active},j}\int_{\Gamma^l_{\text{active},j}} \frac{\partial v}{\partial n}(\mathbf{r}_i;\mathbf{r}(\chi))\,d\chi + \sum_j u^l_{\text{inside},j}\int_{\Gamma^l_{\text{inside},j}} \frac{\partial v}{\partial n}(\mathbf{r}_i;\mathbf{r}(\chi))\,d\chi =$$

$$\sum_j q^l_{\text{active},j}\int_{\Gamma^l_{\text{active},j}} v(\mathbf{r}_i;\mathbf{r}(\chi))\,d\chi + \sum_j q^l_{\text{inside},j}\int_{\Gamma^l_{\text{inside},j}} v(\mathbf{r};\mathbf{r}(\chi))\,d\chi. \quad (6.2.14)$$

In (6.2.14) we have two vectors on Γ^l_{local}: $\mathbf{u}^l_{\text{local}}$ and $\mathbf{q}^l_{\text{local}}$, where

$$\mathbf{u}^l_{\text{local}} = \begin{bmatrix} \mathbf{u}^l_{\text{active}} \\ \mathbf{u}^l_{\text{inside}} \end{bmatrix}, \quad \mathbf{q}^l_{\text{local}} = \begin{bmatrix} \mathbf{q}^l_{\text{active}} \\ \mathbf{q}^l_{\text{inside}} \end{bmatrix}. \quad (6.2.15)$$

The vector $\mathbf{u}^l_{\text{inside}}$ is known through (6.2.12) and the vector $\mathbf{q}^l_{\text{active}}$ is known because $q(\mathbf{r}(\chi))$ is given on Γ_{active}. So if we repeat (6.2.14) for all the local nodes we obtain an algebraic system of N_{local} equations. We rearrange the system in matrix by putting the known quantities on one side to obtain the local problem system

$$\mathbf{A}^l_{\text{local}}\mathbf{x}^l_{0\text{local}} = \mathbf{b}^l_{0\text{local}} \quad (6.2.16)$$

where

$$\mathbf{x}^l_{0\text{local}} = \begin{bmatrix} \mathbf{u}^l_{0\text{active}} \\ \mathbf{q}^l_{0\text{inside}} \end{bmatrix}.$$

The formation of the system (6.2.16) will further be detailed in Section 6.5.

The solution $\mathbf{u}^l_{0\text{active}}$ is expected to be more accurate than the coarse grid solution $\mathbf{u}^L_0$ in Γ_{active}. The next step of LDC is to use the local fine grid solution to update the global coarse grid problem. In updating, the right hand side of the global coarse grid problem is corrected by the defect of the local fine grid approximation, we will call this step the *defect correction* step. The two approximations are then used to define a composite grid approximation of $u(\mathbf{r})$.

The question now is: how do we compute the defect? Consider the coarse grid discretisation (6.2.8). If we knew the exact continuous function $u(\mathbf{r})$ and hence the exact solution $u_j := u(\mathbf{r}_j)$ in the nodes we would use it in (6.2.8) to obtain

$$\frac{1}{2}u_i + \sum_{j=1}^{N} u_j \int_{\Gamma^L_j} \frac{\partial v}{\partial n}(\mathbf{r}_i;\mathbf{r}(\chi))\,d\chi = \sum_{j=1}^{N}\int_{\Gamma^L_j} q(\mathbf{r}(\chi))v(\mathbf{r}_i;\mathbf{r}(\chi))\,d\chi + d^L_i. \quad (6.2.17)$$

where d_i is the local defect for the i-th equation introduced in (4.2.9). We also have the exact BIE as

$$\frac{1}{2}u_i + \sum_{j=1}^{N} \int_{\partial\Omega_j} u(\mathbf{r}(\chi)) \frac{\partial v}{\partial n}(\mathbf{r}_i;\mathbf{r}(\chi))\, d\chi = \sum_{j=1}^{N} \int_{\partial\Omega_j} q(\mathbf{r}(\chi)) v(\mathbf{r}_i;\mathbf{r}(\chi))\, d\chi. \quad (6.2.18)$$

Subtracting (6.2.18) from (6.2.17) gives

$$\sum_{j=1}^{N} u_j \int_{\Gamma_j^L} \frac{\partial v}{\partial n}(\mathbf{r}_i;\mathbf{r}(\chi))\, d\chi - \sum_{j=1}^{N} \int_{\partial\Omega_j} u(\mathbf{r}(\chi)) \frac{\partial v}{\partial n}(\mathbf{r}_i;\mathbf{r}(\chi))\, d\chi = d_i^L. \quad (6.2.19)$$

From (6.2.19) we define the local defect per element j as

$$d_{ij}^L := u_j \int_{\Gamma_j^L} \frac{\partial v}{\partial n}(\mathbf{r}_i;\mathbf{r}(\chi))\, d\chi - \int_{\partial\Omega_j} u(\mathbf{r}(\chi)) \frac{\partial v}{\partial n}(\mathbf{r}_i;\mathbf{r}(\chi))\, d\chi, \quad (6.2.20)$$

so that the total defect at $\mathbf{r}_i$ is given by

$$d_i^L := \sum_j d_{ij}^L, \quad i = 1, 2, \ldots, N. \quad (6.2.21)$$

Therefore if we would know the exact continuous function $u(\mathbf{r})$ we could compute the local defect d_i^L, add it to the right hand side of (6.2.8) and solve for the exact solution u_j on each element. However $u(\mathbf{r})$ is not known and therefore we cannot compute the defect using (6.2.20). All we can do is estimate d_{ij}^L as accurately as possible using the best solution available, which is

Step (iv)

$$u_{\text{best},j}^L = \begin{cases} u_j^L, & \Gamma_j^L \subset \Gamma_c, \\ u_{\text{active},j}^l, & \Gamma_j^L \subset \Gamma_{\text{active}}. \end{cases} \quad (6.2.22)$$

So for elements in the high activity region we have the fine grid solution which we can use to estimate the local defect as follows.

Let us consider the case of a square where $\Gamma_j^L \equiv \partial\Omega_j$. Suppose that in the local fine grid Γ_{active}^l a global coarse grid element Γ_j^L is divided into k fine elements $\Gamma_{\text{active},j_k}^l$ such that $\Gamma_j^L = \bigcup_k \Gamma_{\text{active},j_k}^l$, see an illustration in Figure 6.4 for $k = 3$.

Then the best approximations of the integrals in (6.2.20) are

$$u_j \int_{\Gamma_j^L} \frac{\partial v}{\partial n}(\mathbf{r}_i;\mathbf{r}(\chi))\, d\chi \approx u_{\text{active},j}^l \int_{\Gamma_j^L} \frac{\partial v}{\partial n}(\mathbf{r}_i;\mathbf{r}(\chi))\, d\chi, \quad (6.2.23a)$$

$$\int_{\Gamma_j^L} u(\mathbf{r}(\chi)) \frac{\partial v}{\partial n}(\mathbf{r}_i;\mathbf{r}(\chi))\, d\chi \approx \sum_k u_{\text{active},j_k}^l \int_{\Gamma_{\text{active},j_k}} \frac{\partial v}{\partial n}(\mathbf{r}_i;\mathbf{r}(\chi))\, d\chi. \quad (6.2.23b)$$

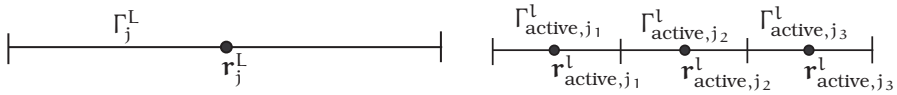

a coarse element Γ_j^L a refined coarse element Γ_j^L

Figure 6.4: A coarse element that is refined into three elements in the local fine grid $\Gamma_j^L = \bigcup_{k=1}^{3} \Gamma^l_{\text{active},j_k}$.

Step (v) Therefore we have the following best approximation of the defect per element

$$d_{ij}^L \approx u^l_{\text{active},j} \int_{\Gamma_j} \frac{\partial \nu}{\partial n}(\mathbf{r}_i;\mathbf{r}(\chi))\,d\chi - \sum_k u^l_{\text{active},j_k} \int_{\Gamma_{\text{active},j_k}} \frac{\partial \nu}{\partial n}(\mathbf{r}_i;\mathbf{r}(\chi))\,d\chi, \quad (6.2.24)$$

for $\Gamma_j^L \subset \Gamma_{\text{active}}$ and

$$d_{ij}^L \approx 0$$

for $\Gamma_j^L \subset \Gamma_c$. We can then compute the defect

$$d_i^L \approx \sum_j d_{ij}^L, \quad \Gamma_j^L \subset \Gamma_{\text{active}}, \quad \text{for all } i = 1,2,\ldots,N. \quad (6.2.25)$$

By default integration in the BIE is global. Each node of the global coarse grid communicates with the active region through integration. So although the activity is local, its effect is global. The defect d_i^L is therefore computed for all nodes of the global coarse grid.

Step (vi) The next step now is the updating step. The global coarse grid discretisation is updated with the defect of the local fine grid solution. So we have

$$\mathbf{A}^L\mathbf{u}_1^L = \mathbf{b}^L + \mathbf{d}^L. \quad (6.2.26)$$

Solving (6.2.26) gives the updated coarse grid solution $\mathbf{u}_1^L$.

At this stage we use the fine grid solution on Γ^l_{active} and the global coarse grid solution to form a composite grid solution $u^{l,L}$ as

$$u^{l,L}_{0,1}(\mathbf{r}) = \begin{cases} u^l_{0\,\text{active}}(\mathbf{r}), & \mathbf{r} \in \Gamma_{\text{active}}, \\ u^L_1(\mathbf{r}), & \mathbf{r} \in \Gamma_c. \end{cases} \quad (6.2.27)$$

The composite grid solution (6.2.27) can now be used to compute better boundary conditions on Γ_{inside} and then form and solve the updated fine grid problem

$$\mathbf{A}^l_{\text{local}}\mathbf{x}^l_{1\,\text{local}} = \mathbf{b}^l_{1\,\text{local}}. \quad (6.2.28)$$

Step (vii) Thus we obtain the updated composite grid solution given by

$$u_{1,1}^{l,L}(\mathbf{r}) = \begin{cases} u_{1\,\text{active}}^{l}(\mathbf{r}), & \mathbf{r} \in \Gamma_{\text{active}}, \\ u_{1}^{L}(\mathbf{r}), & \mathbf{r} \in \Gamma_{c}. \end{cases} \tag{6.2.29}$$

In Figures 6.5 and 6.6 we have the results at each of the above stages of local defect correction for the problem (6.2.1) with boundary conditions (6.2.2). Figure 6.7 shows how fast the global error converges. Basically the algorithm has converged already in the first iteration since the error reduction between successive iterations after the first one is small compared to that in the first iteration.

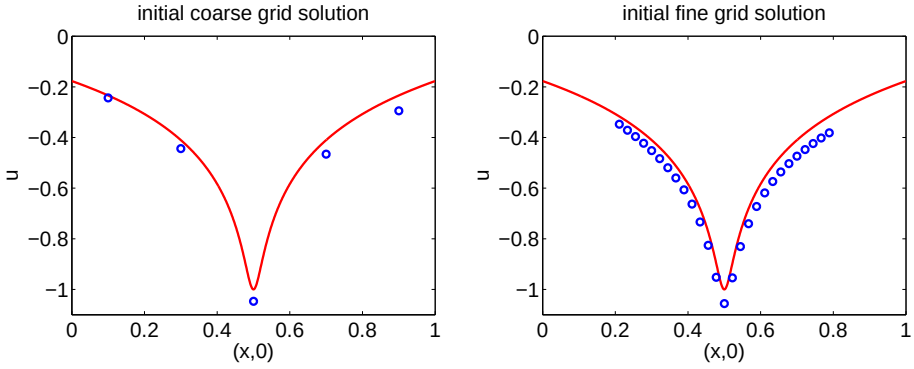

(a) Initial coarse grid solution (b) Initial fine grid solution

Figure 6.5: Results of a typical LDC process for a Neumann problem in one iteration.

The process of defect correction can be repeated generating a composite grid solution at the end of Step (vii) of each cycle. In the next section we show that this process is a fixed point iterative process for computing the solution on a composite grid. The solution is obtained by solving separate global coarse and local fine grid problems.

6.3 LDC formulation: A Dirichlet problem

The process of LDC formulation for a Dirichlet problem is completely the same as that for a Neumann problem. The only differences will be in the operators involved. The global operator will be a single layer operator. In the case of a Neumann problem, the local problem is a mixed problem with q given on Γ_{active} and u on Γ_{inside} prescribed through the use of the global solution. For a Dirichlet

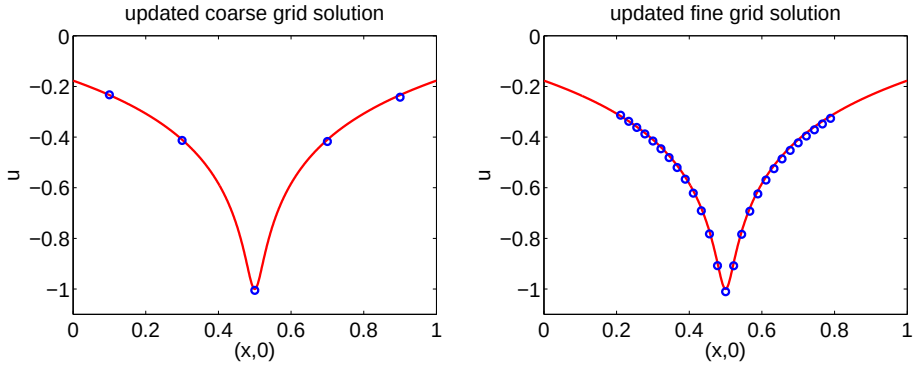

(a) Updated coarse grid solution (b) Updated fine grid solution

Figure 6.6: Results of a typical LDC process for a Neumann problem in one iteration.

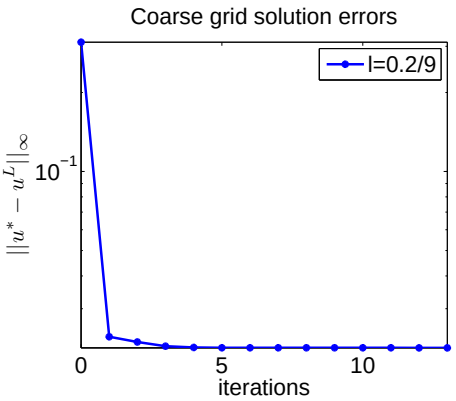

Figure 6.7: Convergence of the global coarse grid error.

problem, the local problem will be a completely Dirichlet with u given on Γ_{active} and u on Γ_{inside} prescribed through the use of the global solution.

6.4 Complexity of the algorithm

In brief, the LDC iterative process can be summarised as follows:

Algorithm 6.1
LDC iteration summary

(I) Solve the global coarse grid problem on Γ.

(II) Compute u on Γ_{inside}.

(III) Solve a fine grid problem on Γ_{local}.

(IV) Update the global coarse grid problem.

Suppose we have p locally active small regions and thus p local problems. Let, for each local problem, M^l be the number of elements Γ_{local} and M^{in} the number of elements on Γ_{inside}. Then the size of the local problem is $M = M^l + M^{\text{in}}$. Let M^{in} be so small that $M \approx M^l$. Let N be the size of the global problem and N^L_{local} the number of global elements in Γ_{local}. We assume Γ_{local} is such a small part of the global boundary that $N - N^L_{\text{local}} \approx N$. Then the equivalent size of the composite grid would be $pM + N$. The operational count for LU-decomposition is $N^3/3$ for a size N matrix. So the complexity of the equivalent composite grid problem would be

$$\frac{1}{3}(pM + N)^3 \approx \frac{(p+1)^3}{3}N^3 \text{ if } M \approx N. \tag{6.4.1}$$

The BEM-LDC algorithm converges in one step which involves solving two coarse grid problems and p local problems and so has total complexity

$$2 \cdot \frac{1}{3}N^3 + \frac{p}{3}M^3 \approx \frac{N^3}{3}(2+p). \tag{6.4.2}$$

So when we compare (6.4.1) with (6.4.2) we see that the composite problem is $(p+1)^3/(2+p)$ times more expensive than BEM-LDC. Suppose instead we were to refine globally to a grid of size equal to that of the local problems. Then if the refinement ratio is say α, that is, $L/l = \alpha$, the resulting problem would be of complexity $\frac{1}{3}\alpha^3 N^3$. So the resulting problem would be $\alpha^3/(p+2)$ times more complex than using LDC. For instance in the modes case of $\alpha = 2$, this factor is more than one for up to $p = 5$ local problems. Thus BEM-LDC is cheaper

than both of its obvious alternatives of either composite gridding or refining uniformly.

Another advantage of LDC over solving on direct composite or fine uniform grids is the memory required. LDC requires less memory than the equivalent composite or uniform grid problems. This is because instead of handling large matrices and vectors of sizes say $(M + N)$ or αN, it handles smaller vectors of sizes N and M at a time.

6.5 LDC algorithm as a fixed point iteration

In BEM, Dirichlet and Neumann problems have different properties because they result in different integral operators. However the LDC process is the same for both the Neumann and Dirichlet problems, with the only differences being in the operators involved. In this chapter we consider the Neumann problem and show that the LDC algorithm is a fixed point iterative process. The case of a Dirichlet problem is developed along the same lines.

In general the LDC process can be summarised in the following algorithm:

Algorithm 6.2
LDC algorithm for BEM

Initialisation

(1) Solve a global coarse grid problem

$$\mathbf{A}^L \mathbf{x}_0^L = \mathbf{b}^L \quad \text{on} \quad \Gamma^L.$$

(2) Compute the potential $u(\mathbf{r})$ on Γ_{inside} using $\mathbf{x}_0^L$ and the boundary integral relation for a point inside Ω.

(3) Solve a local fine grid problem

$$\mathbf{A}^l_{\text{local}} \mathbf{x}^l_{0\,\text{local}} = \mathbf{b}^l_{0\,\text{local}} \quad \text{on} \quad \Gamma^l_{\text{local}}.$$

Iterations i=1,2,...

(4) Compute the defect $\mathbf{d}^L_{i-1}$.

(5) Solve the global coarse grid problem.

$$\mathbf{A}^L \mathbf{x}_i^L = \mathbf{b}^L + \mathbf{d}^L_{i-1} \quad \text{on} \quad \Gamma^L$$

(6) Assemble the partly updated composite grid solution $\mathbf{x}^{l,L}_{i-1,i}$.

(7) Compute the potential $u(\mathbf{r})$ on Γ_{inside} using $\mathbf{x}^{l,L}_{i-1,i}$ and the boundary integral relation for points inside Ω.

(8) Solve the local fine grid problem

$$\mathbf{A}^l_{\text{local}} \mathbf{x}^l_{i\,\text{local}} = \mathbf{b}^l_{i\,\text{local}} \quad \text{on} \quad \Gamma^l_{\text{local}}.$$

(9) Assemble the updated composite grid solution $\mathbf{x}^{l,L}_{i,i}$.

In the sequel we will formulate the above algorithm as a fixed point iteration for a Neumann problem.

Consider the Neumann problem

$$\begin{cases} \nabla^2 u(\mathbf{r}) = 0, & \mathbf{r} \in \Omega, \\ q(\mathbf{r}) = h(\mathbf{r}), & \mathbf{r} \in \partial\Omega. \end{cases} \tag{6.5.1}$$

To formulate the LDC algorithm as a fixed point iteration, we need a vector formulation for the steps in Algorithm 6.2. The first step of the Algorithm 6.2 is to solve a global coarse grid problem

$$\mathbf{A}^L \mathbf{x}_0^L = \mathbf{b}^L, \tag{6.5.2}$$

for an initial solution $\mathbf{x}_0^L$ and this involves "inversion" of the coefficient matrix $\mathbf{A}^L$. The coefficient matrix for a Neumann problem is singular. In order to obtain a unique solution we prescribe $u(\mathbf{r})$ at a point at the boundary as explained in Section 2.5.2. In particular, we prescribe Dirichlet boundary conditions in the last node of the grid. So we use $\mathbf{x}_0^L$ to denote the solution vector in (6.5.2) which is a vector of u's except the last entry which is a q. Using $\mathbf{u}_0^L$, the boundary conditions and the boundary integral relation (2.4.1), we compute the potential $u(\mathbf{r})$ on Γ_{inside}. That is,

$$u_{\text{inside}}(\mathbf{r}_i) = \int_\Gamma v(\mathbf{r}_i;\mathbf{r}(\chi)) q(\mathbf{r}(\chi)) d\chi - \sum_j u_{0j}^L \int_{\Gamma_j} \frac{\partial v}{\partial n}(\mathbf{r}_i;\mathbf{r}(\chi)) d\chi, \quad \mathbf{r}_i \in \mathbf{r}_{\text{inside}}^l. \tag{6.5.3}$$

Let us introduce a vector $\mathbf{g}$ and a matrix $\tilde{\mathbf{H}}^L$ such that

$$g_i := \int_\Gamma q(\mathbf{r}(\chi)) v(\mathbf{r}_i;\mathbf{r}(\chi))\, d\chi, \quad \mathbf{r}_i \in \Gamma_{\text{inside}}, \tag{6.5.4}$$

$$\tilde{H}_{ij}^L := \int_{\Gamma_j^L} \frac{\partial v}{\partial n}(\mathbf{r}_i;\mathbf{r}(\chi))\, d\chi, \mathbf{r}_i \in \Gamma_{\text{inside}}. \tag{6.5.5}$$

Then we can write (6.5.3) as

$$\mathbf{u}_{0\,\text{inside}} = \mathbf{g} - \tilde{\mathbf{H}}^L \mathbf{u}_0^L. \tag{6.5.6}$$

Using (6.5.6) we obtain Dirichlet boundary conditions on Γ_{inside}. The boundary conditions on Γ_{active} are the given Neumann boundary conditions since $\Gamma_{\text{active}} \subset \Gamma$. Using (3.2.10) we can then write the equations on Γ_{local}^l in vector form as

$$\mathbf{H}_{\text{local}}^l \begin{bmatrix} \mathbf{u}_{0\,\text{active}}^l \\ \mathbf{u}_{0\,\text{inside}}^l \end{bmatrix} = \mathbf{G}_{\text{local}}^l \begin{bmatrix} \mathbf{q}_{\text{active}} \\ \mathbf{q}_{0\,\text{inside}}^l \end{bmatrix}, \tag{6.5.7}$$

where $\mathbf{H}_{\text{local}}^l$ and $\mathbf{G}_{\text{local}}^l$ are matrices on Γ_{local}^l, $\mathbf{u}_{\text{active}}^l$ and $\mathbf{q}_{\text{active}}^l$ are vectors on Γ_{active}^l and $\mathbf{u}_{0\,\text{inside}}^l$ and $\mathbf{q}_{0\,\text{inside}}^l$ are vectors on Γ_{inside}^l. The vector $\mathbf{u}_{0\,\text{inside}}^l$ is known through (6.5.6) and the vector $\mathbf{q}_{\text{active}}$ is known through the boundary conditions. So we rearrange (6.5.7) as

$$[\mathbf{H}_{\text{active}}^l \quad -\mathbf{G}_{\text{inside}}^l] \begin{bmatrix} \mathbf{u}_{\text{active}}^l \\ \mathbf{q}_{0\,\text{inside}}^l \end{bmatrix} = [\mathbf{G}_{\text{active}}^l \quad -\mathbf{H}_{\text{inside}}^l] \begin{bmatrix} \mathbf{q}_{\text{active}} \\ \mathbf{u}_{0\,\text{inside}}^l \end{bmatrix} \tag{6.5.8}$$

The matrix $\mathbf{H}^l_{\text{active}}$ is a block of $\mathbf{H}^l$ for which the column index corresponds to nodes in Γ^l_{active}. Similarly $\mathbf{H}^l_{\text{inside}}$ is a block of $\mathbf{H}^l$ for which the column index corresponds to nodes in Γ^l_{inside}. The blocks $\mathbf{G}^l_{\text{active}}$ and $\mathbf{G}^l_{\text{inside}}$ are defined analogously. The quantities on the right hand side of (6.5.8) are all known. Let

$$\mathbf{B}^l_{\text{local}} := [\mathbf{G}^l_{\text{active}} \quad -\mathbf{H}^l_{\text{inside}}], \tag{6.5.9}$$

$$\mathbf{A}^l_{\text{local}} := [\mathbf{H}^l_{\text{active}} \quad -\mathbf{G}^l_{\text{inside}}], \tag{6.5.10}$$

$$\mathbf{b}^l_{0\text{local}} := \mathbf{B}^l_{\text{local}} \begin{bmatrix} \mathbf{q}_{\text{active}} \\ \mathbf{u}^l_{0\text{inside}} \end{bmatrix}, \tag{6.5.11}$$

$$\mathbf{x}^l_{0\text{local}} := \begin{bmatrix} \mathbf{u}^l_{0\text{active}} \\ \mathbf{q}^l_{0\text{inside}} \end{bmatrix}. \tag{6.5.12}$$

Then we have

$$\mathbf{A}^l_{\text{local}}\mathbf{x}^l_{0\text{local}} = \mathbf{b}^l_{0\text{local}}. \tag{6.5.13}$$

The solution of (6.5.13) gives us another solution $\mathbf{u}^l_{0\text{active}}$ in Γ_{active} which should be a better approximation of $u(\mathbf{r})$ than $\mathbf{u}^L_0$ in Γ_{active} because of the fine grid used. Next we use this solution to compute the defect and update the global coarse grid solution. Using (6.2.24), the defect on an element Γ^L_j when the collocation node is i is given by

$$d_{0ij} \approx \sum_k u^l_{0\text{active},j_k} \int_{\Gamma^l_{\text{active},j_k}} \frac{\partial \nu}{\partial n}(\mathbf{r}_i;\mathbf{r}(\chi))\,d\chi - u^l_{0\text{active},j}\int_{\Gamma^L_j}\frac{\partial \nu}{\partial n}(\mathbf{r}_i;\mathbf{r}(\chi))\,d\chi, \tag{6.5.14}$$

where $\bigcup_k \Gamma^l_{\text{active},j_k} = \Gamma^L_j$, see Figure 6.4. The integration in (6.5.14) is computed at all the global elements that lie in Γ_{active} so that the total defect for the i-th collocation node is

$$d_{0i} = \sum_{j,\Gamma^L_j \subset \Gamma_{\text{active}}} d_{0ij}. \tag{6.5.15}$$

Since each collocation node communicates with the local active region through integration, the defect d_{0i} is computed for all the collocation nodes.

Let us introduce a matrix $\bar{\mathbf{H}}$ as

$$\bar{H}_{ik} = \int_{\Gamma_k} \frac{\partial \nu}{\partial n}(\mathbf{r}_i;\mathbf{r}(\chi))\,d\chi, \quad \mathbf{r}_i \in \mathbf{r}^L, \quad \Gamma_k \in \Gamma^l_{\text{active}}.$$

Let $\mathbf{P}^{L,l}$ be a restriction from the fine grid Γ^l_{active} to the coarse grid Γ^L_{active} in Γ_{active}. Then we can write the defect $\mathbf{d}_0$ as

$$\mathbf{d}_0 = \bar{\mathbf{H}}\mathbf{u}^l_{0\text{active}} - \hat{\mathbf{H}}^L\mathbf{P}^{L,l}\mathbf{u}^l_{0\text{active}} = (\bar{\mathbf{H}} - \hat{\mathbf{H}}^L\mathbf{P}^{L,l})\mathbf{u}^l_{0\text{active}}, \tag{6.5.16}$$

where the matrix $\hat{\mathbf{H}}$ is as defined in (3.2.5) with the superscript L indicating on a coarse grid of size L. Now we have the defect for all the coarse grid nodes. We update the coarse grid system (6.5.2) to obtain the updated coarse grid solution $\mathbf{x}_1^L$. That is

$$\mathbf{A}^L\mathbf{x}_1^L = \mathbf{b}^L - (\bar{\mathbf{H}} - \hat{\mathbf{H}}^L\mathbf{P}^{L,l})\mathbf{u}_{0\,\text{active}}^l. \tag{6.5.17}$$

At this stage we can assemble a composite grid solution on $\Gamma^{l,L}$ that consists of the initial fine grid solution and the updated coarse grid solution. So

$$\mathbf{u}_{0,1}^{l,L} := \begin{bmatrix} \mathbf{u}_{0\,\text{active}}^l \\ \mathbf{u}_{1\,c}^L \end{bmatrix}, \tag{6.5.18}$$

where $\mathbf{u}_{1\,c}^L$ is the updated coarse grid solution on Γ_c outside the active region Γ_{active}. To complete the updated composite grid solution, we need to solve a new local problem. To this end we use the solution in (6.5.18) to compute another approximation of $u(\mathbf{r})$ on Γ_{inside}. Thus we have

$$\mathbf{u}_{1\,\text{inside}} = \mathbf{g} - \tilde{\mathbf{H}}^{l,L}\mathbf{u}_{0,1}^{l,L}, \tag{6.5.19}$$

where the matrix $\tilde{\mathbf{H}}^{l,L}$ is as defined in (6.5.6) but on the composite grid, that is,

$$\tilde{H}_{ij}^{l,L} = \begin{cases} \int_{\Gamma_{c,j}^L} \dfrac{\partial v}{\partial n}(\mathbf{r}_i;\mathbf{r}(\chi))\,d\chi, \ \mathbf{r}(\chi) \in \Gamma_c, \\ \\ \int_{\Gamma_{\text{active},j}^l} \dfrac{\partial v}{\partial n}(\mathbf{r}_i;\mathbf{r}(\chi))\,d\chi, \ \mathbf{r}(\chi) \in \Gamma_{\text{active}}, \end{cases} \tag{6.5.20}$$

and $\mathbf{r}_i \in \Gamma_{\text{inside}}$. Then we formulate an updated local problem system

$$\mathbf{A}_{\text{local}}^l\mathbf{x}_{1\,\text{local}}^l = \mathbf{b}_{1\,\text{local}}^l, \tag{6.5.21a}$$

where

$$\mathbf{b}_1^l = \mathbf{B}_{\text{local}}^l \begin{bmatrix} \mathbf{q}_{\text{active}}^l \\ \mathbf{u}_{1\,\text{inside}} \end{bmatrix}. \tag{6.5.21b}$$

Solving (6.5.21) gives us an updated solution $\mathbf{u}_{1\,\text{active}}^l$ of $u(\mathbf{r})$ on Γ_{active}. At this stage we have a completely updated composite grid solution given by

$$\mathbf{u}_{1,1}^{l,L} = \begin{bmatrix} \mathbf{u}_{1\,\text{active}}^l \\ \mathbf{u}_{1\,c}^L \end{bmatrix}. \tag{6.5.22}$$

This completes the first iteration that gives us the first updated composite grid solution. The process can be repeated till there is no more change in the solution. In what follows we formulate the above process as a fixed point iterative process.

Let $\mathbf{I}_{\text{active}}^l$ be an identity of size N_{active}. Then the part of the local solution in Γ_{active} is given by, for the i-th iteration,

$$\mathbf{u}_{i\,\text{active}}^l = [\mathbf{I}_{\text{active}}\ \mathbf{O}]\mathbf{x}_{i\,\text{local}}^l. \tag{6.5.23}$$

Consider the updated composite grid solution (6.5.22) for iteration $i+1$. Using (6.5.21) and (6.5.23), we have

$$\mathbf{u}^{l,L}_{i+1,i+1} = \begin{bmatrix} \mathbf{u}^{l}_{i+1\,\text{active}} \\ \\ \mathbf{u}^{L}_{i+1\,c} \end{bmatrix} = \begin{bmatrix} [\mathbf{I}_{\text{active}}\ \mathbf{O}]\mathbf{A}^{l^{-1}}_{\text{local}}\mathbf{B}^{l}_{\text{local}} \begin{bmatrix} \mathbf{q}^{l}_{\text{active}} \\ \mathbf{u}^{l}_{i+1\,\text{inside}} \end{bmatrix} \\ \\ [\mathbf{O}\ \ \mathbf{I}_c]\,\mathbf{u}^{L}_{i+1} \end{bmatrix}. \tag{6.5.24}$$

From the second block row of (6.5.24) we have

$$\mathbf{u}^{L}_{i+1\,c} = [\mathbf{O}\ \ \mathbf{I}_c]\,\mathbf{u}^{L}_{i+1}.$$

This is the global coarse grid solution outside the active region. For a Neumann problem we prescribe Dirichlet boundary conditions in the last node in order to obtain a unique solution. Thus the last value of the solution vector will be a q value. So in general let us write

$$\mathbf{x}^{L}_{i+1\,c} = [\mathbf{O}\ \ \mathbf{I}_c]\,\mathbf{x}^{L}_{i+1}. \tag{6.5.25}$$

Using (6.5.17) we have

$$\begin{aligned} \mathbf{x}^{L}_{i+1\,c} &= [\mathbf{O}\ \ \mathbf{I}_c]\mathbf{A}^{L^{-1}}\left(\mathbf{b}^{L} - (\bar{\mathbf{H}} - \hat{\mathbf{H}}^{L}\mathbf{P}^{L,l})\mathbf{u}^{l}_{i\,\text{active}}\right), \\ &= \mathbf{x}^{L}_{0\,c} - [\mathbf{O}\ \ \mathbf{I}_c]\mathbf{A}^{L^{-1}}\left(\bar{\mathbf{H}} - \hat{\mathbf{H}}^{L}\mathbf{P}^{L,l}\right)\mathbf{u}^{l}_{i\,\text{active}}, \end{aligned} \tag{6.5.26}$$

where

$$\mathbf{x}^{L}_{0} = \mathbf{A}^{L^{-1}}\mathbf{b}^{L}.$$

Let us introduce a matrix $\mathbf{M}$ as

$$\mathbf{M} := [\mathbf{I}_{\text{active}}\ \mathbf{O}]\mathbf{A}^{l^{-1}}_{\text{local}}\mathbf{B}^{l}_{\text{local}}.$$

Then from the first block row of (6.5.24) we have

$$\mathbf{u}^{l}_{i+1\,\text{active}} = \mathbf{M}\begin{bmatrix} \mathbf{q}^{l}_{\text{active}} \\ \mathbf{u}^{l}_{i+1\,\text{inside}} \end{bmatrix} \tag{6.5.27}$$

Note that the matrix $\mathbf{M}$ is rectangular in size. Let us break it into two blocks: a square block $\mathbf{M}_{\text{active}}$ that operates on $\Gamma^{l}_{\text{active}}$ and a block $\mathbf{M}_{\text{inside}}$ that operates on $\Gamma^{l}_{\text{inside}}$. Then we can write (6.5.27) as

$$\mathbf{u}^{l}_{i+1\,\text{active}} = [\mathbf{M}_{\text{active}}\ \ \mathbf{M}_{\text{inside}}]\begin{bmatrix} \mathbf{q}^{l}_{\text{active}} \\ \mathbf{u}^{l}_{i+1\,\text{inside}} \end{bmatrix} = \mathbf{M}_{\text{active}}\mathbf{q}^{l}_{\text{active}} + \mathbf{M}_{\text{inside}}\mathbf{u}^{l}_{i+1\,\text{inside}}. \tag{6.5.28}$$

From (6.5.19) we see that

$$\mathbf{u}_{i+1\,\text{inside}} = \mathbf{g} - \tilde{\mathbf{H}}^{l,L}\mathbf{u}^{l,L}_{i,i+1}. \tag{6.5.29}$$

Let us also break down the operator $\tilde{\mathbf{H}}^{l,L}$ in (6.5.29) into a part that operates on Γ^l_{active} and another that operates on Γ^L_c, so that we can write (6.5.29) as

$$\mathbf{u}_{i+1\,\text{inside}} = \mathbf{g} - \tilde{\mathbf{H}}^{l,L}_{\text{active}}\mathbf{u}^l_{i\,\text{active}} - \tilde{\mathbf{H}}^{l,L}_{c}\mathbf{u}^L_{i+1\,c}. \tag{6.5.30}$$

Using (6.5.30) in (6.5.28) we have

$$\begin{aligned}\mathbf{u}^l_{i+1\,\text{active}} &= \mathbf{M}_{\text{active}}\mathbf{q}^l_{\text{active}} + \mathbf{M}_{\text{inside}}\left(\mathbf{g} - \tilde{\mathbf{H}}^{l,L}_{\text{active}}\mathbf{u}^l_{i\,\text{active}} - \tilde{\mathbf{H}}^{l,L}_{c}\mathbf{u}^L_{i+1\,c}\right),\\ &= \mathbf{M}_{\text{active}}\mathbf{q}^l_{\text{active}} + \mathbf{M}_{\text{inside}}\mathbf{g} - \mathbf{M}_{\text{inside}}\tilde{\mathbf{H}}^{l,L}_{\text{active}}\mathbf{u}^l_{i\,\text{active}} - \mathbf{M}_{\text{inside}}\tilde{\mathbf{H}}^{l,L}_{c}\mathbf{u}^L_{i+1\,c}.\end{aligned} \tag{6.5.31}$$

We introduce the following operators

$$\mathbf{R} := -\mathbf{M}_{\text{inside}}\tilde{\mathbf{H}}^{l,L}_{\text{active}},$$

$$\mathbf{T} := -\mathbf{M}_{\text{inside}}\tilde{\mathbf{H}}^{l,L}_{c},$$

so that we can write (6.5.31) as

$$\mathbf{u}^l_{i+1\,\text{active}} = \mathbf{M}_{\text{active}}\mathbf{q}^l_{\text{active}} + \mathbf{M}_{\text{inside}}\mathbf{g} + \mathbf{R}\mathbf{u}^l_{i\,\text{active}} + \mathbf{T}\mathbf{u}^L_{i+1\,c}. \tag{6.5.32}$$

In (6.5.32) the updated solution on the active grid Γ^l_{active} is expressed in terms of the previous solution there and the updated solution outside the active grid. To have an expression for the iteration that takes place on the active region alone, we use (6.5.26) to replace $\mathbf{u}^L_{i+1,c}$. So,

$$\mathbf{u}^L_{i+1\,c} = \mathbf{D}_1\mathbf{x}^L_{i+1\,c} + \mathbf{D}_2\mathbf{b}_c, \tag{6.5.33}$$

where $\mathbf{b}_c$ is the vector of boundary conditions outside the active region. Because the last entry of $\mathbf{x}^L_{i+1\,c}$ is a q-value and that of $\mathbf{b}_c$ is a u-value, the matrices $\mathbf{D}_1$ and $\mathbf{D}_2$ are the projections

$$\mathbf{D}_1 := \begin{bmatrix}\mathbf{I} & \mathbf{0}\\ \mathbf{0}^T & 0\end{bmatrix}, \quad \mathbf{D}_2 := \begin{bmatrix}\mathbf{O} & \mathbf{0}\\ \mathbf{0}^T & 1\end{bmatrix}. \tag{6.5.34}$$

So we have

$$\mathbf{u}^L_{i+1\,c} = \mathbf{D}_1(\mathbf{x}^L_{0\,c} - [\mathbf{O}\ \ \mathbf{I}_c]\mathbf{A}^{L-1}\left(\bar{\mathbf{H}} - \hat{\mathbf{H}}^L\mathbf{P}^{L,l}\right)\mathbf{u}^l_{i\,\text{active}}) + \mathbf{D}_2\mathbf{b}_c. \tag{6.5.35}$$

Let us introduce the following notation

$$\mathbf{W} := [\mathbf{O}\ \ \mathbf{I}_c]\mathbf{A}^{L-1}(\bar{\mathbf{H}} - \hat{\mathbf{H}}^L\mathbf{P}^{L,l}) \tag{6.5.36}$$

so that we can write(6.5.35) as

$$\mathbf{u}^L_{i+1\,c} = \mathbf{D}_1\mathbf{x}^L_{0\,c} - \mathbf{D}_1\mathbf{W}\mathbf{u}^l_{i\,\text{active}} + \mathbf{D}_2\mathbf{b}_c. \tag{6.5.37}$$

Now we use (6.5.37) in (6.5.32) to obtain

$$\mathbf{u}^l_{i+1\,\text{active}} = \mathbf{M}_{\text{active}}\mathbf{q}^l_{\text{active}} + \mathbf{M}_{\text{inside}}\mathbf{g} + \mathbf{R}\mathbf{u}^l_{i\,\text{active}} + \mathbf{T}(\mathbf{D}_1\mathbf{x}^L_{0\,c} - \mathbf{D}_1\mathbf{W}\mathbf{u}^l_{i\,\text{active}} + \mathbf{D}_2\mathbf{b}_c)$$

which can be rearranged as

$$\mathbf{u}^l_{i+1\,\text{active}} = (\mathbf{R}-\mathbf{T}\mathbf{D}_1\mathbf{W})\mathbf{u}^l_{i\,\text{active}}+\mathbf{T}\mathbf{D}_1\mathbf{x}^L_{0\,c}+\mathbf{M}_{\text{active}}\mathbf{q}^l_{\text{active}}+\mathbf{M}_{\text{inside}}\mathbf{g}+\mathbf{T}\mathbf{D}_2\mathbf{b}_c. \quad (6.5.38)$$

We introduce a vector $\mathbf{v}$ as

$$\mathbf{v} := \mathbf{T}\mathbf{D}_1\mathbf{x}^L_{0\,c} + \mathbf{M}_{\text{active}}\mathbf{q}^l_{\text{active}} + \mathbf{M}_{\text{inside}}\mathbf{g} + \mathbf{T}\mathbf{D}_2\mathbf{b}_c.$$

We can now write equation (6.5.38) as

$$\mathbf{u}^l_{i+1\,\text{active}} = (\mathbf{R} - \mathbf{T}\mathbf{D}_1\mathbf{W})\mathbf{u}^l_{i\,\text{active}} + \mathbf{v}. \quad (6.5.39)$$

The vector $\mathbf{v}$ remains fixed throughout the iteration since $\mathbf{q}^l_{\text{active}}$, $\mathbf{g}$, $\mathbf{b}_c$, remain fixed and $\mathbf{x}^L_{0\,c} = [\mathbf{O}\ \mathbf{I}_c]\mathbf{A}^{L^{-1}}\mathbf{b}^L$ remains the same throughout the iteration. Equation (6.5.39) expresses the iteration that takes place on the fine grid Γ^l_{active} as a fixed point iteration with iteration matrix $\mathbf{Q}$ defined as

$$\mathbf{Q} := \mathbf{R} - \mathbf{T}\mathbf{D}_1\mathbf{W}. \quad (6.5.40)$$

Thus we have

$$\mathbf{u}^l_{i+1\,\text{active}} = \mathbf{Q}\mathbf{u}^l_{i\,\text{active}} + \mathbf{v}. \quad (6.5.41)$$

This iteration will converge if the spectral radius of the iteration matrix $\mathbf{Q}$ is less than unity. In Tables 6.1 and 6.2 we have the spectral radii of $\mathbf{Q}$ for different combinations of L and l.

	l				
L	0.2	0.2/3	0.2/9	0.2/27	0.2/81
0.2	2.137E-01	2.308E-01	2.402E-01	2.457E-01	2.492E-01
0.2/3		2.253E-01	2.342E-01	2.399E-01	2.436E-01
0.2/9			2.316E-01	2.367E-01	2.401E-01
0.2/27				2.357E-01	2.388E-01
0.2/81					2.385E-01

Table 6.1: Spectral radius of the iteration matrix $\mathbf{Q}$ for a Neumann problem for different combinations of fine and coarse grid sizes l and L respectively. The local problem domain is the rectangle $[0.2,\ 0.8] \times [0,\ 0.4]$ and $\Omega = [0,\ 1] \times [0,\ 1]$.

Recall again the problem of Example 3.7.4 on page 31 with $\Omega = [0,\ 1] \times [0,\ 1]$ and $\mathbf{r}_s = (0.5, -0.02)$ as summarised in (6.2.1). We identify Ω_{local} as $\Omega_{\text{local}} := [0.2,\ 0.8] \times [0,\ 0.4]$, see Figure 6.8. LDC is then used with various sizes of coarse grid size L and fine grid size l. We also expect the ratios $\|\mathbf{u}^l_{i+1} - \mathbf{u}^l_i\|/\|(\mathbf{u}^l_i - \mathbf{u}^l_{i-1})\|$ to be a measure of the convergence speed. In Table 6.3 we have computed these ratios for five iterations and different combinations of grid sizes. The results in Tables 6.1, 6.2 and 6.3 all indicate that the spectral radius of the LDC algorithm iteration matrix is smaller than one and therefore we expect the algorithm to converge.

	l				
L	0.2	0.2/3	0.2/9	0.2/27	0.2/81
0.2	1.756E-01	2.165E-01	2.338E-01	2.426E-01	2.476E-01
0.2/3		2.086E-01	2.255E-01	2.349E-01	2.405E-01
0.2/9			2.219E-01	2.306E-01	2.361E-01
0.2/81					2.341E-01

Table 6.2: Spectral radius of the iteration matrix $\mathcal{G}$ for a Neumann problem for different combinations of grid sizes L and l. The local problem domain is the rectangle $[0.4,\ 0.6] \times [0,\ 0.2]$ and $\Omega = [0,\ 1] \times [0,\ 1]$.

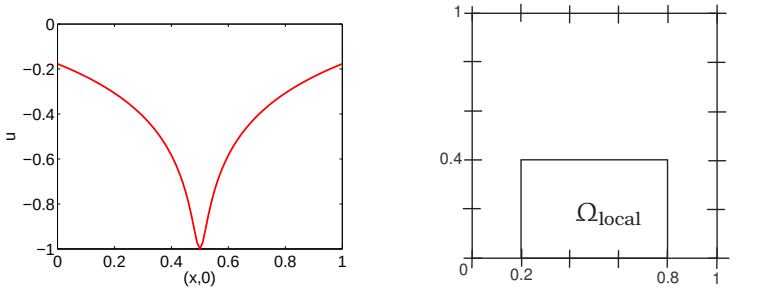

(a) The solution $u(\mathbf{r})$ in part of $\partial\Omega$

(b) Domain demarcations for LDC

Figure 6.8: Part of the solution at the boundary and the LDC domain demarcations.

L	l	i	ρ_i
0.2	0.2/3	1	0.1574
		2	0.1848
		3	0.1883
		4	0.1886
		5	0.1886

L	l	i	ρ_i
0.2	0.2/9	1	0.2024
		2	0.2228
		3	0.2295
		4	0.2312
		5	0.2316

L	l	i	ρ_i
0.2	0.2/27	1	0.2177
		2	0.2334
		3	0.2393
		4	0.2416
		5	0.2425

L	l	i	ρ_i
0.2	0.2/81	1	0.2226
		2	0.2372
		3	0.2428
		4	0.2452
		5	0.2463

Table 6.3: The ratios $\rho_i = \|\mathbf{u}_{i+1}^l - \mathbf{u}_i^l\|_2 / \|(\mathbf{u}_i^l - \mathbf{u}_{i-1}^l)\|_2$ when we use LDC to solve the problem in (6.2.1).

6.6 Continuous formulation of the LDC steps

The integral operators $\mathcal{K}^s$ and $\mathcal{K}^d$ have somewhat been extensively studied in continuous form. We can make use of this available information to draw an analysis for our LDC algorithm if we can have its equivalent formulation in continuous form. That is the focus of this section.

Basically we would like to study the error convergence during the iteration process. So we develop a continuous formulation of the LDC algorithm in terms of the error. For this purpose we need the equations which the initial and converged solutions satisfy. The Algorithm 6.2 can be summarised in the following six steps:

Step (i) Initialisation: solve the global coarse grid problem

$$\frac{1}{2}u^L_{0\,i} + \sum_{j=1}^{N} u^L_{0\,j} \int_{\Gamma^L_j} \frac{\partial \nu}{\partial n}(\mathbf{r}_i;\mathbf{r}(\chi))\,d\chi = b^L_i. \tag{6.6.1}$$

Step (ii) After discretisation of Γ_{local} into $\Gamma^l_{\text{local}} = \Gamma^l_{\text{inside}} \cup \Gamma^l_{\text{active}}$, see (6.2.4), (6.2.5) and Figure (6.3), compute $u(\mathbf{r})$ on Γ^l_{inside} using the integral relation

$$u^l_{0\,\text{inside},i} = \int_\Gamma \nu(\mathbf{r}_i;\mathbf{r}(\chi))q(\mathbf{r}(\chi))\,d\chi - \sum_{j=1}^{N} u^L_{0\,j} \int_{\Gamma^L_j} \frac{\partial \nu}{\partial n}(\mathbf{r}_i;\mathbf{r}(\chi))\,d\chi, \quad \mathbf{r}_i \in \mathbf{r}^l_{\text{inside}}. \tag{6.6.2}$$

This gives a vector $\mathbf{u}^l_{\text{inside}}$ of u's on Γ_{inside} as introduced in (6.2.15).

Step (iii) Now we have Dirichlet boundary conditions on Γ_{inside}. On Γ_{active} $q(\mathbf{r})$ is known. Next is to solve the local problem:

$$\begin{aligned}
&\frac{1}{2}u^l_{0\,\text{local},i} + \sum_j u^l_{0\,\text{active},j} \int_{\Gamma^l_{\text{active},j}} \frac{\partial \nu}{\partial n}(\mathbf{r}_i;\mathbf{r}(\chi))\,d\chi + \\
&\sum_j u^l_{0\,\text{inside},j} \int_{\Gamma^l_{\text{inside},j}} \frac{\partial \nu}{\partial n}(\mathbf{r}_i;\mathbf{r}(\chi))\,d\chi = \\
&\qquad \int_{\Gamma_{\text{active}}} \nu(\mathbf{r}_i;\mathbf{r}(\chi))q_{\text{active}}(\mathbf{r}(\chi))\,d\chi + \sum_j q^l_{0\,\text{inside},j} \int_{\Gamma^l_{\text{inside},j}} \nu(\mathbf{r}_i;\mathbf{r}(\chi))\,d\chi.
\end{aligned} \tag{6.6.3}$$

Here $q_{\text{active}}(\mathbf{r})$ is known from the boundary conditions of the global problem since $\Gamma_{\text{active}} \subset \Gamma$. Also u^l_{inside} is known through (6.6.2). Solving (6.6.3) gives $\mathbf{q}^l_{0\,\text{inside}}$ and $\mathbf{u}^l_{0\,\text{active}}$.

Step (iv) We need to compute the defect. First we need the best solution available, which is:

$$u^L_{0\,\mathrm{best},j} = \begin{cases} u^L_{0\,c,j}, & \Gamma^L_j \subset \Gamma_c, \\ u^l_{0\,\mathrm{active},j}, & \Gamma^L_j \subset \Gamma_{\mathrm{active}}. \end{cases} \tag{6.6.4}$$

Step (v) Using the fine grid solution, we estimate the defect per element $d^L_{0\,ij}$ in (6.2.24) as

$$d^L_{0\,ij} \doteq \begin{cases} u^l_{0\,\mathrm{active},j} \int_{\Gamma^L_j} \dfrac{\partial v}{\partial n}(\mathbf{r}_i;\mathbf{r}(\chi))\,d\chi - \\ \qquad \displaystyle\sum_k u^l_{0\,\mathrm{active},j_k} \int_{\Gamma^l_{\mathrm{active},j_k}} \dfrac{\partial v}{\partial n}(\mathbf{r}_i;\mathbf{r}(\chi))\,d\chi, & \Gamma^L_j \subset \Gamma_{\mathrm{active}}, \\ 0 & \Gamma_j \subset \Gamma_c. \end{cases} \tag{6.6.5a}$$

Then the defect d^L_i for each equation is estimated as

$$\begin{aligned} d^L_{0\,i} &= \sum_j d^L_{0\,ij} \\ &\doteq \sum_j \left(u^l_{0\,\mathrm{active},j} \int_{\Gamma^L_j} \frac{\partial v}{\partial n}(\mathbf{r}_i;\mathbf{r}(\chi))\,d\chi - \sum_k u^l_{0\,\mathrm{active},j_k} \int_{\Gamma^l_{\mathrm{active},j_k}} \frac{\partial v}{\partial n}(\mathbf{r}_i;\mathbf{r}(\chi))\,d\chi \right) \end{aligned} \tag{6.6.5b}$$

for all $\mathbf{r}_i$. Here $\bigcup_k \Gamma^l_{\mathrm{active},j_k} = \Gamma^L_j$ for $\Gamma^L_j \subset \Gamma_{\mathrm{active}}$, see Figure 6.4.

Step (vi) Defect correction: add the defect to the right hand side of the coarse grid equation and solve for the updated global coarse grid solution u^L_1. That is

$$\frac{1}{2}u^L_{1,i} + \sum_{j=1}^{N} u^L_{1,j} \int_{\Gamma^L_j} \frac{\partial v}{\partial n}(\mathbf{r}_i;\mathbf{r}(\chi))\,d\chi = b^L_i + d^L_{0\,i}. \tag{6.6.6}$$

Step (vii) Assemble the composite grid solution and go back to step (ii), replace $\mathbf{u}^L_0$ with $\mathbf{u}^L_1$ and continue.

We assume that the algorithm (i) to (vi) converges. Let the unknowns in steps (ii) to (vi) converge to their respective fixed points denoted by an asterisk, namely $\mathbf{u}^{*L}$, $\mathbf{u}^{*l}_{\mathrm{inside}}$, $\mathbf{u}^{*l}_{\mathrm{active}}$ and $\mathbf{q}^{*l}_{\mathrm{inside}}$. The fixed point should satisfy the equations in (6.6.2) to (6.6.6). So we have:

Step (ii) Computing $u(\mathbf{r})$ on Γ_{inside}:

$$u^*_{\text{inside},i} = \int_\Gamma v(\mathbf{r}_i;\mathbf{r}(\chi))q(\mathbf{r}(\chi))\,d\chi - \sum_{j=1}^{N}\int_{\Gamma_j^L} u_j^{*L}\frac{\partial v}{\partial n}(\mathbf{r}_i;\mathbf{r}(\chi))\,d\chi, \quad \mathbf{r}_i \in \mathbf{r}^l_{\text{inside}}. \tag{6.6.7}$$

Step (iii) The local problem equations for $\mathbf{u}^l_{\text{active}}$ and $\mathbf{q}^l_{\text{inside}}$:

$$\begin{aligned}\frac{1}{2}u^{*l}_{\text{local},i} + \sum_j u^{*l}_{\text{active},j}\int_{\Gamma_{\text{active},j}}\frac{\partial v}{\partial n}(\mathbf{r}_i;\mathbf{r}(\chi))\,d\chi \\ + \sum_j u^{*l}_{\text{inside},j}\int_{\Gamma_{\text{inside},j}}\frac{\partial v}{\partial n}(\mathbf{r}_i;\mathbf{r}(\chi))\,d\chi = \\ \int_{\Gamma_{\text{active}}} v(\mathbf{r}_i;\mathbf{r}(\chi))q_{\text{active}}(\mathbf{r}(\chi))\,d\chi + \sum_j q^{*l}_{\text{inside},j}\int_{\Gamma_{\text{inside},j}} v(\mathbf{r}_i;\mathbf{r}(\chi))\,d\chi.\end{aligned} \tag{6.6.8}$$

Step (iv) Computing the defect; Best solution available:

$$u^{*L}_{\text{best},j} = \begin{cases} u^{*L}_{c,j}, & \Gamma_j^L \subset \Gamma_c, \\ u^{*l}_{\text{active},j}, & \Gamma_j^L \subset \Gamma_{\text{active}}. \end{cases} \tag{6.6.9}$$

Step (v) Fixed point for the defect:

$$\begin{aligned}d_i^{*L} \approx \sum_j \Bigg(u^{*l}_{\text{active},j}\int_{\Gamma_j^L}\frac{\partial v}{\partial n}(\mathbf{r}_i;\mathbf{r}(\chi))\,d\chi - \\ \sum_k u^{*l}_{\text{active},j_k}\int_{\Gamma^l_{\text{active},j_k}}\frac{\partial v}{\partial n}(\mathbf{r}_i;\mathbf{r}(\chi))\,d\chi\Bigg)\end{aligned} \tag{6.6.10a}$$

for all i, $\Gamma_j^L \subset \Gamma_{\text{active}}$.

Step (vi) The fixed point for the updated global coarse grid equations:

$$\frac{1}{2}u_i^{*L} + \sum_{j=1}^{N} u_j^{*L}\int_{\Gamma_j^L}\frac{\partial v}{\partial n}(\mathbf{r}_i;\mathbf{r}(\chi))\,d\chi = b_i^L + d_i^{*L}. \tag{6.6.11}$$

Let us define the errors:

$$\begin{aligned}&\delta u_j^L := u_j^{*L} - u_j^L,\\ &\delta u^l_{\text{active},j} := u^{*l}_{\text{active},j} - u^l_{\text{active},j},\\ &\delta u^l_{\text{inside},j} := u^{*l}_{\text{inside},j} - u^l_{\text{inside},j},\\ &\delta q^l_{\text{inside},j} := q^{*l}_{\text{inside},j} - q^l_{\text{inside},j},\\ &\delta d_i^L := d_i^{*L} - d_i^L.\end{aligned}$$

Then subtracting equations (6.6.2) to (6.6.6) from (6.6.7) to (6.6.11) yields the following equations for the errors:

Step (ii) In computing u on Γ_{inside} :

$$\delta u^l_{\text{inside},i} = -\sum_{j=1}^{N} \delta u^L_j \int_{\Gamma^L_j} \frac{\partial v}{\partial n}(\mathbf{r}_i;\mathbf{r}(\chi))\,d\chi, \quad \mathbf{r}_i \in \mathbf{r}^l_{\text{inside}}. \tag{6.6.13}$$

Step (iii) In solving the local problem:

$$\begin{aligned}\frac{1}{2}\delta u^l_i + \sum_j \delta u^l_{\text{active},j} \int_{\Gamma^l_{\text{active},j}} \frac{\partial v}{\partial n}(\mathbf{r}_i;\mathbf{r}(\chi))\,d\chi \\ + \sum_j \delta u^l_{\text{inside},j} \int_{\Gamma^l_{\text{inside},j}} \frac{\partial v}{\partial n}(\mathbf{r}_i;\mathbf{r}(\chi))\,d\chi = \\ \sum_j \delta q^l_{\text{inside},j} \int_{\Gamma^l_{\text{inside},j}} v(\mathbf{r}_i;\mathbf{r}(\chi))\,d\chi.\end{aligned} \tag{6.6.14}$$

Step (iv) In the best solution available:

$$\delta u^L_{\text{best},j} = \begin{cases} \delta u^L_{c,j}, & \Gamma^L_j \subset \Gamma_c, \\ \delta u^l_{\text{active},j}, & \Gamma^L_j \subset \Gamma_{\text{active}}. \end{cases} \tag{6.6.15}$$

Step (v) In computing the defect:

$$\begin{aligned}\delta d^L_i \approx \sum_j \Bigg(\delta u^l_{\text{active},j} \int_{\Gamma^L_j} \frac{\partial v}{\partial n}(\mathbf{r}_i;\mathbf{r}(\chi))\,d\chi - \\ \sum_k \delta u^l_{\text{active},j_k} \int_{\Gamma^l_{\text{active},j_k}} \frac{\partial v}{\partial n}(\mathbf{r}_i;\mathbf{r}(\chi))\,d\chi \Bigg).\end{aligned} \tag{6.6.16}$$

Step (vi) In updating the global solution:

$$\frac{1}{2}\delta u^L_i + \sum_{j=1}^{N} \delta u^L_j \int_{\Gamma^L_j} \frac{\partial v}{\partial n}(\mathbf{r}_i;\mathbf{r}(\chi))\,d\chi = \delta d^L_i. \tag{6.6.17}$$

Like we did in investigating global errors in Chapter 5, we can also model the above error equations in continuous form. Then we can use the available properties of the operators to derive some convergence properties for the LDC algorithm.

Consider the exact BIE on Γ

$$\frac{1}{2}u(\mathbf{r}) + \int_\Gamma u(\mathbf{r}(\chi))\frac{\partial v}{\partial n}(\mathbf{r};\mathbf{r}(\chi))\,d\chi = \int_\Gamma q(\mathbf{r}(\chi))v(\mathbf{r};\mathbf{r}(\chi))\,d\chi \tag{6.6.18}$$

Let $u_0(\mathbf{r})$ be a BEM solution of (6.6.18) on Γ with error $\delta u_0(\mathbf{r})$. That is

$$\frac{1}{2}u_0(\mathbf{r}) + \int_\Gamma u_0(\mathbf{r}(\chi))\frac{\partial v}{\partial n}(\mathbf{r};\mathbf{r}(\chi))\,d\Gamma = \int_\Gamma q(\mathbf{r}(\chi))v(\mathbf{r};\mathbf{r}(\chi))\,d\Gamma + f_0(\mathbf{r}).$$

where $f_0(\mathbf{r})$ is a source term incorporating discretisation errors. Since

$$u(\mathbf{r}) = u_0(\mathbf{r}) + \delta u_0(\mathbf{r}), \tag{6.6.19}$$

we can write

$$\frac{1}{2}(u_0(\mathbf{r})+\delta u_0(\mathbf{r})) + \int_\Gamma (u_0(\mathbf{r}(\chi))+\delta u_0(\mathbf{r}(\chi)))\frac{\partial v}{\partial n}(\mathbf{r};\mathbf{r}(\chi))\,d\chi = \int_\Gamma q(\mathbf{r}(\chi))v(\mathbf{r};\mathbf{r}(\chi))\,d\chi. \tag{6.6.20}$$

So the error term $f_0(\mathbf{r})$ is given by

$$f_0(\mathbf{r}) := \frac{1}{2}\delta u_0(\mathbf{r}) + \int_\Gamma \delta u_0(\mathbf{r}(\chi))\frac{\partial v}{\partial n}(\mathbf{r};\mathbf{r}(\chi))\,d\chi, \quad \mathbf{r},\ \mathbf{r}(\chi) \in \Gamma. \tag{6.6.21}$$

Theorem 6.6.1 *For points on Γ^{in}, if we eliminate the error in integration, the error in u is bounded by the error in u on Γ.*

Proof. Let $u_0(\mathbf{r})$ be the global solution on Γ. Let $u_{inside}(\mathbf{r})$ be u on Γ^{in} computed using the solution $u_0(\mathbf{r})$. Then

$$u_{inside}(\mathbf{r}) = \int_\Gamma q(\mathbf{r}(\chi))v(\mathbf{r};\mathbf{r}(\chi))\,d\chi - \int_\Gamma u_0(\mathbf{r}(\chi))\frac{\partial v}{\partial n}(\mathbf{r};\mathbf{r}(\chi))\,d\chi, \quad \mathbf{r} \in \Gamma^{in},\ \ \mathbf{r}(\chi) \in \Gamma. \tag{6.6.22}$$

If $\delta u_{inside}(\mathbf{r})$ is the error in $u_{inside}(\mathbf{r})$ and $\delta u_0(\mathbf{r})$ is the error in $u_0(\mathbf{r})$, then

$$u_{inside}(\mathbf{r})+\delta u_{inside}(\mathbf{r}) = \int_\Gamma q(\mathbf{r})v(\mathbf{r};\mathbf{r}(\chi))\,d\chi - \int_\Gamma (u_0(\mathbf{r}(\chi))+\delta u_0(\mathbf{r}(\chi)))\frac{\partial v}{\partial n}(\mathbf{r};\mathbf{r}(\chi))\,d\chi. \tag{6.6.23}$$

So the error $\delta u_{inside}(\mathbf{r})$ is given by

$$\delta u_{inside}(\mathbf{r}) = -\int_\Gamma \delta u_0(\mathbf{r}(\chi))\frac{\partial v}{\partial n}(\mathbf{r};\mathbf{r}(\chi))\,d\chi, \quad \mathbf{r} \in \Gamma^{in},\ \ \mathbf{r}(\chi) \in \Gamma. \tag{6.6.24}$$

In (6.6.24) we have a continuous equivalent of (6.6.13). Taking the maximum norm (6.6.24) gives

$$\begin{aligned}\|\delta u_{\text{inside}}(\mathbf{r})\|_\infty &= \max\left|\int_\Gamma \delta u_0(\mathbf{r}(\chi))\frac{\partial v}{\partial n}(\mathbf{r};\mathbf{r}(\chi))\,d\chi\right| \\ &\le \int_\Gamma \|\delta u_0(\mathbf{r}(\chi))\|_\infty \|\frac{\partial v}{\partial n}(\mathbf{r};\mathbf{r}(\chi))\|_\infty\,d\chi, \\ &\le \|\delta u_0(\mathbf{r}(\chi))\|_\infty, \end{aligned} \tag{6.6.25}$$

since $\partial v/\partial n$ does not change sign over Γ and the integral of $\partial v/\partial n$ over Γ is 1 for source points inside the domain. ■

Now, let u_{local} and q_{local} be functions on Γ_{local}. Let $u_{0\text{local}}$ and q_{local} be the initial BEM solutions on Γ_{local}. The functions $u_{0\text{local}}$ and q_{local} can also be divided into $u_{0\text{active}}$ and $u_{0\text{inside}}$ and $q_{0\text{active}}$ and $q_{0\text{inside}}$ respectively. Then we have

$$\begin{aligned}&\frac{1}{2}u_{0\text{local}}(\mathbf{r}) + \int_{\Gamma_{\text{active}}} u_{0\text{active}}(\mathbf{r}(\chi))\frac{\partial v}{\partial n}(\mathbf{r};\mathbf{r}(\chi))\,d\chi + \int_{\Gamma_{\text{inside}}} u_{0\text{inside}}(\mathbf{r}(\chi))\frac{\partial v}{\partial n}(\mathbf{r};\mathbf{r}(\chi))\,d\chi = \\ &\int_{\Gamma_{\text{active}}} q_{\text{active}}(\mathbf{r}(\chi))v(\mathbf{r};\mathbf{r}(\chi))\,d\chi + \int_{\Gamma_{\text{inside}}} q_{0\text{inside}}(\mathbf{r}(\chi))v(\mathbf{r};\mathbf{r}(\chi))\,d\chi;\quad \mathbf{r},\ \mathbf{r}(\chi)\in\Gamma_{\text{local}}.\end{aligned} \tag{6.6.26}$$

Again using δf to denote a perturbation of a function f, we have

$$\begin{aligned}&\frac{1}{2}\left(u_{0\text{local}}(\mathbf{r}) + \delta u_{0\text{local}}(\mathbf{r})\right) + \int_{\Gamma_{\text{active}}} \left(u_{0\text{active}}(\mathbf{r}(\chi)) + \delta u_{0\text{active}}(\mathbf{r}(\chi))\right)\frac{\partial v}{\partial n}(\mathbf{r};\mathbf{r}(\chi))\,d\chi + \\ &\int_{\Gamma_{\text{inside}}} \left(u_{0\text{inside}}(\mathbf{r}(\chi)) + \delta u_{0\text{inside}}(\mathbf{r}(\chi))\right)\frac{\partial v}{\partial n}(\mathbf{r};\mathbf{r}(\chi))\,d\chi = \int_{\Gamma_{\text{active}}} q_{\text{active}}(\mathbf{r}(\chi))v(\mathbf{r};\mathbf{r}(\chi))\,d\chi + \\ &\int_{\Gamma_{\text{inside}}} \left(q_{0\text{inside}}(\mathbf{r}(\chi)) + \delta q_{0\text{inside}}(\mathbf{r}(\chi))\right)v(\mathbf{r};\mathbf{r}(\chi))\,d\chi;\quad \mathbf{r},\ \mathbf{r}(\chi)\in\Gamma_{\text{local}}.\end{aligned} \tag{6.6.27}$$

Comparing (6.6.27) with (6.6.26) gives a BIE for the error:

$$\begin{aligned}&\frac{1}{2}\delta u_{0\text{local}}(\mathbf{r}) + \int_{\Gamma_{\text{active}}} \delta u_{0\text{active}}(\mathbf{r}(\chi))\frac{\partial v}{\partial n}(\mathbf{r};\mathbf{r}(\chi))\,d\chi + \int_{\Gamma_{\text{inside}}} \delta u_{0\text{inside}}(\mathbf{r}(\chi))\frac{\partial v}{\partial n}(\mathbf{r};\mathbf{r}(\chi))\,d\chi = \\ &\int_{\Gamma_{\text{inside}}} \delta q_{0\text{inside}}(\mathbf{r}(\chi))v(\mathbf{r};\mathbf{r}(\chi))\,d\chi;\quad \mathbf{r},\ \mathbf{r}(\chi)\in\Gamma_{\text{local}}.\end{aligned} \tag{6.6.28}$$

Theorem 6.6.2 *The fine grid solution error* $\delta u_{0\text{active}}(\mathbf{r})$ *on* Γ_{active} *is bounded by the error committed on* Γ_{inside}*, that is,*

$$\|\delta u_{0\text{active}}(\mathbf{r}(\chi))\|_{\infty(\Gamma_{\text{active}})} \le \|\delta u_{0\text{inside}}(\mathbf{r}(\chi))\|_{\infty(\Gamma_{\text{inside}})}. \tag{6.6.29}$$

Proof. Equation (6.6.28) is a BIE for an error function $\delta u_{0\text{local}}(\mathbf{r})$ on Γ_{local}, the boundary of Ω_{local}, with homogeneous Neumann boundary conditions on Γ_{active}. According to the weak maximum principle, the maximum of $\delta u_{0\text{local}}(\mathbf{r})$ occurs at the boundary. That is, there is an $\mathbf{r}_0 \in \Gamma_{\text{local}}$ such that

$$\delta u_{0\text{local}}(\mathbf{r}) \leq \delta u_{0\text{local}}(\mathbf{r}_0) = \max_{\overline{\Omega}_{\text{local}}} \delta u_{0\text{local}}(\mathbf{r}). \tag{6.6.30}$$

We suppose that the maximum $\delta u_{0\text{local}}(\mathbf{r}_0)$ is on Γ_{inside}. Suppose $\mathbf{r}_0 \in \Gamma_{\text{active}}$. According to Hopf's boundary point lemma, see [61, p43], if

- $\delta u_{0\text{local}}(\mathbf{r}_0)$ is continuous at $\mathbf{r}_0$,
- $\delta u_{0\text{local}}(\mathbf{r}) < \delta u_{0\text{local}}(\mathbf{r}_0) \ \ \forall \ \ \mathbf{r} \in \Omega_{\text{local}}$,
- there is a ball B_R of radius R, $B_R \subset \Omega_{\text{local}}$, with $\mathbf{r}_0 \in \partial B_R$,

then $\dfrac{\partial}{\partial n}\delta u_{0\text{local}}(\mathbf{r}_0) > 0$. This is a contradiction since we have homogeneous Neumann boundary conditions on Γ_{active}. If $\delta u_{0\text{local}}(\mathbf{r})$ is a negative function then starting with the weak minimum principle would give a similar result. So we have

$$\|\delta u_{0\text{active}}(\mathbf{r})\|_\infty \leq \max_{\overline{\Omega}_{\text{local}}} |\delta u_{0\text{local}}(\mathbf{r})| = |\delta u_{0\text{local}}(\mathbf{r}_0)| = \|\delta u_{0\text{inside}}(\mathbf{r})\|_\infty. \tag{6.6.31}$$

However we note that Hopf's lemma does not rule out the corner points. ■

The next step in the LDC algorithm is to compute the defect. The defect $d(\mathbf{r})$ is the integral of the double layer with a perturbation in the exact u, that is

$$d_0(\mathbf{r}) = \int_\Gamma \delta u_0(\mathbf{r}(\chi)) \frac{\partial \nu}{\partial n}(\mathbf{r}; \mathbf{r}(\chi))\, d\chi, \quad \mathbf{r}, \mathbf{r}(\chi) \in \Gamma. \tag{6.6.32}$$

In our simulations $\delta u_0(\mathbf{r}(\chi))$ is the difference between the local problem and global problem solutions. Once we have the defect then we apply defect correction to the initial BIE and solve for the updated solution. Let u_1 denote the updated solution on Γ, then

$$\frac{1}{2}u_1(\mathbf{r}) + \int_\Gamma u_1(\mathbf{r}(\chi)) \frac{\partial \nu}{\partial n}(\mathbf{r}; \mathbf{r}(\chi))\, d\chi + d_0(\mathbf{r}) = \int_\Gamma q(\mathbf{r}(\chi)) \nu(\mathbf{r}; \mathbf{r}(\chi))\, d\Gamma + f_1(\mathbf{r}); \quad \mathbf{r}, \mathbf{r}(\chi) \in \mathbf{r}(\chi). \tag{6.6.33}$$

Using notations already introduced above, we have

$$\frac{1}{2}(u_1(\mathbf{r}) + \delta u_1(\mathbf{r})) + \int_\Gamma (u_1(\mathbf{r}(\chi)) + \delta u_1(\mathbf{r}(\chi))) \frac{\partial \nu}{\partial n}(\mathbf{r}; \mathbf{r}(\chi))\, d\chi + d_0(\mathbf{r}) = \int_\Gamma q(\mathbf{r}(\chi)) \nu(\mathbf{r}; \mathbf{r}(\chi))\, d\chi. \tag{6.6.34}$$

Comparing (6.6.34) with (6.6.33) we have

$$\frac{1}{2}\delta u_1(\mathbf{r}) + \int_\Gamma \delta u_1(\mathbf{r}(\chi))\frac{\partial v}{\partial n}(\mathbf{r};\mathbf{r}(\chi))\,d\chi + d_0(\mathbf{r}) = 0. \tag{6.6.35}$$

That is,

$$\left(\frac{1}{2}\mathcal{I} + \frac{\partial v}{\partial n}(\mathbf{r};\mathbf{r}(\chi))\right)\,\delta u_1(\mathbf{r}) = -d_0(\mathbf{r}), \quad \mathbf{r}\in\Gamma. \tag{6.6.36}$$

Theorem 6.6.3 (The combined process) *The combined LDC process will converge since the error of the updated solution is bounded by the error of old solution provided the shifted double layer operator inverse is bounded by a constant not more than 2 in absolute size.*

Proof. Let the error in the initial global coarse grid solution be $\delta u_0(\mathbf{r})$, that is,

$$u(\mathbf{r}) = u_0(\mathbf{r}) + \delta u_0(\mathbf{r}). \tag{6.6.37}$$

Then (6.6.24) implies that the error in u on Γ^{in} is given by

$$\delta u_{\text{inside}}(\mathbf{r}) = \int_\Gamma \delta u_0(\mathbf{r}(\chi))\frac{\partial v}{\partial n}(\mathbf{r};\mathbf{r}(\chi))\,d\chi, \quad \mathbf{r}\in\Gamma^{in}\subset\Omega,\ \mathbf{r}(\chi)\in\Gamma. \tag{6.6.38}$$

In the space W_1 defined in (2.5.19), equation (6.6.36) has a unique solution. Thus the operator $(0.5\mathcal{I}+\mathcal{K}^d)$ is invertible in that space. Using (6.6.36) we have

$$\delta u_1(\mathbf{r}) = -\left(\frac{1}{2}\mathcal{I}+\mathcal{K}^d\right)^{-1} d_0(\mathbf{r}), \quad \mathbf{r}\in\Gamma. \tag{6.6.39}$$

Also recall that the defect is given by

$$d_0(\mathbf{r}) = \int_\Gamma \delta u_0(\mathbf{r}(\chi))\frac{\partial v}{\partial n}(\mathbf{r};\mathbf{r}(\chi))\,d\chi = \int_{\Gamma_{\text{active}}} \delta u_{0\,\text{active}}(\mathbf{r}(\chi))\frac{\partial v}{\partial n}(\mathbf{r};\mathbf{r}(\chi))\,d\chi, \quad \mathbf{r}\in\Gamma. \tag{6.6.40}$$

So we have,

$$\delta u_1(\mathbf{r}) = -\left(\frac{1}{2}\mathcal{I}+\mathcal{K}^d\right)^{-1}\int_{\Gamma_{\text{active}}} u_{0\,\text{active}}(\mathbf{r}(\chi))\frac{\partial v}{\partial n}(\mathbf{r};\mathbf{r}(\chi))\,d\chi. \tag{6.6.41}$$

Let a scalar C be such that

$$\left\|\left(0.5\mathcal{I}+\mathcal{K}^d\right)^{-1}\right\|_\infty \le C. \tag{6.6.42}$$

Then

$$\|\delta u_1(\mathbf{r})\|_\infty \le C\|d_0(\mathbf{r})\|_\infty. \tag{6.6.43}$$

For the defect $d_0(\mathbf{r})$ we have

$$\begin{aligned}
\|d_0(\mathbf{r})\|_\infty &= \max \left| \int_{\Gamma_{\text{active}}} \delta u_{0\,\text{active}}(\mathbf{r}(\chi)) \frac{\partial \nu}{\partial n}(\mathbf{r};\mathbf{r}(\chi))\, d\chi \right| \\
&\leq \int_{\Gamma_{\text{active}}} |\delta u_{0\,\text{active}}(\mathbf{r}(\chi))| \left| \frac{\partial \nu}{\partial n}(\mathbf{r};\mathbf{r}(\chi)) \right| d\chi \\
&\leq \|\delta u_{0\,\text{active}}(\mathbf{r}(\chi))\|_\infty \int_{\Gamma_{\text{active}}} \left| \frac{\partial \nu}{\partial n}(\mathbf{r};\mathbf{r}(\chi)) \right| d\chi, \\
&\leq \frac{1}{2} \|\delta u_{0\,\text{active}}(\mathbf{r}(\chi))\|_\infty , \qquad (6.6.44)
\end{aligned}$$

since $\partial\nu/\partial n$ is of the same sign around Γ and the integral of $\partial\nu/\partial n$ around Γ is $1/2$ for boundary points. Using (6.6.44) in (6.6.43) yields

$$\|\delta u_1(\mathbf{r})\|_\infty \leq \frac{C}{2} \|\delta u_{0\,\text{active}}(\mathbf{r}(\chi))\|_\infty . \qquad (6.6.45)$$

Then we use (6.6.31) and (6.6.25) to obtain

$$\|\delta u_1(\mathbf{r})\|_\infty \leq \frac{C}{2} \|\delta u_0(\mathbf{r})\|_\infty . \qquad (6.6.46)$$

■

"Education is what remains after one has forgotten everything one learned in school." – Albert Einstein

Chapter 7

The potential problem for the impressed current cathodic protection system

7.1 Introduction

Usually steel structures are protected from *corrosion* by painting. But not all parts can be painted, like for instance propellers of a ship. Also, due to damage, some parts lose their paint hence creating more exposed parts of the steel. *Cathodic protection* effectively protects underground or submerged metallic structures through the use of a negative potential applied by an external source to the structure. The method is typically applied to iron or steel structures such as underground pipelines, storage tanks, submarine structures, ocean pilings, and electrical transmission towers. Cathodic protection is a proven technology for controlling corrosion on the bottoms of above ground storage tanks [40].

There are two types of cathodic protection systems used against corrosion: a *galvanic or sacrificial anode cathodic protection system* and an *impressed current cathodic protection system (ICCP)* . The galvanic *anode* system is based upon the natural potential difference which exists between the structure being protected and the auxiliary *electrode* (anode) which is installed in the *electrolyte*. The current that prevents corrosion is then due to the potential difference between the structure and the anode. Materials commonly used for galvanic anode systems are magnesium, zinc and aluminum.

The ICCP system uses anodes in conjunction with an external direct current (DC) power source. The structure to be protected is connected to the nega-

tive terminal of a direct current power source and electrical current is forced to flow from the positive terminal to the anodes through the electrolyte to the structure. This type of cathodic protection system uses long life anode materials such as high silicon chromium, cast iron, graphite, and mixed metal oxide coated titanium. In water storage tanks, cathodic protection systems are usually designed to protect the interior wetted surfaces of the tank [47, p. 40]. However, in some cases, the exterior of a tank bottom or shell is in contact with corrosive soils and in that case cathodic protection can also be used [40].

A properly designed, installed and operated cathodic protection system will eliminate the corroding areas by passing direct current to the metal surface. This therefore necessitates the solution of the ICCP potential problem. In this chapter we discuss the solution of the potential problem associated with impressed current cathodic protection (ICCP) of the external surfaces of tank bottoms which are in contact with corrosive soils. The potential problem has localised regions of high activity. These are the anodes or the *cathodes* which are the corroded parts of the surface to be protected. Because of the small regions of high activity associated with the problem, we would like to use of LDC for BEM to solve the potential problem model and that is the subject of this chapter. In the sequel we begin with a brief description of the problem. Then in Section 7.2 we introduce the model and an example of a full BEM solution and in Section 7.3 we give the BEMLDC solution.

Corrosion is an electrochemical process that involves passage of electrons from one substance, usually metallic, called the anode to another substance called the cathode. It is at the anode that the oxidation reaction which is responsible for the corrosion of the metal involved takes place according to the following ionic equation, in the case of steel

$$Fe_{(s)} \rightarrow Fe^{2+}_{(aq)} + 2e^{-}, \tag{7.1.1}$$

where Fe represents a ferrous atom, Fe^{2+} a ferrous II ion, e an electron and the subscripts s and aq imply the solid state and the aqueous state respectively. The electrons so produced pass on to the cathode where they are used up in a reduction reaction

$$2H^{+}_{(aq)} + 2e^{-} \rightarrow H_{2(g)} \tag{7.1.2}$$

in acidic solutions, or:

$$O_{2(g)} + 2H_2O_{(l)} + 4e^{-} \rightarrow 4OH^{-}_{(aq)} \tag{7.1.3}$$

in neutral solutions, see Figure 7.1. Metal II is a metal that is more electropositive than steel.
In equations (7.1.2) and (7.1.3), H^{+} represents a hydrogen ion, O_2 oxygen gas, H_2O a water molecule and OH^{-} a hydroxyl ion. The subscripts l and g imply the liquid state and the gaseous state respectively. Therefore corrosion basically occurs at the anode. Cathodic protection involves attaching an anode to the surface to be protected and supplying a direct current through it such that

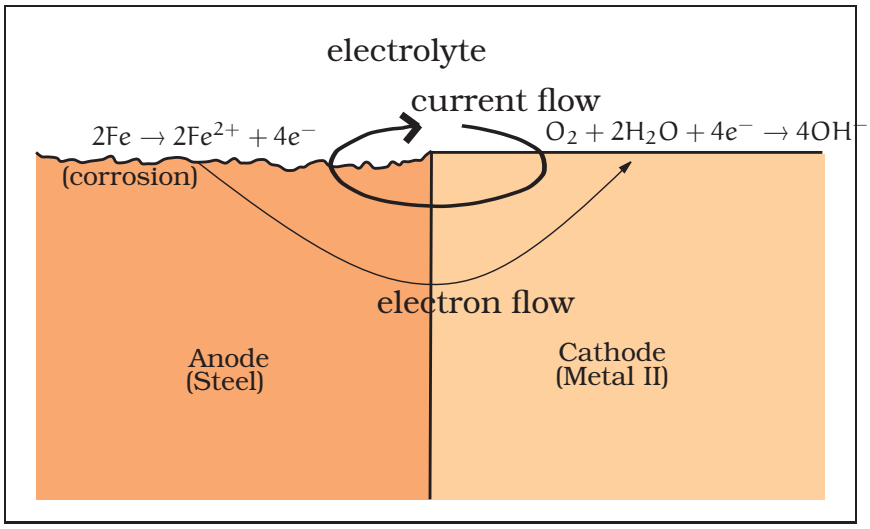

Figure 7.1: Bimetallic corrosion cell.

all the other parts of the surface become cathodic and therefore do not corrode, see Figure 7.2.

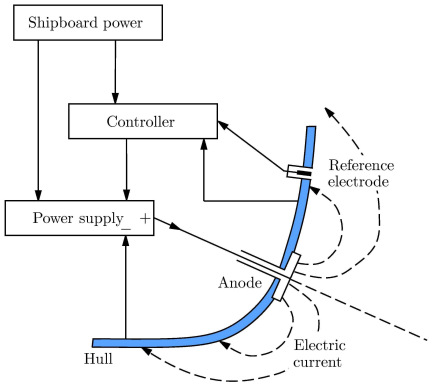

(a) ICCP system for a submarine ship, source: [31].

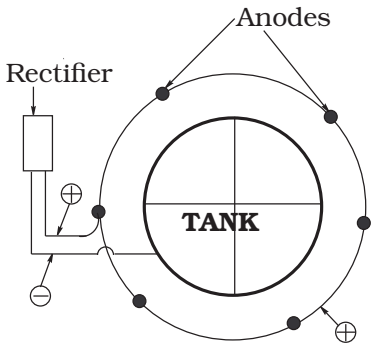

(b) ICCP system for a storage tank, source: [40].

Figure 7.2: Examples of ICCP systems for ship's hull and exterior of a water storage tank.

7.2 Modelling

We will now describe a two dimensional model for ICCP. The ICCP problem for the cathodic protection of a ship in water is an exterior problem, see [31]. For continuity of the analysis in this thesis we will solve a model for the ICCP protection of water storage tanks, which is an interior problem. One typical situation of a tank under cathodic protection is shown in Figure 7.2b. This problem can be modelled in two dimensions as shown in Figure 7.3. The domain consists of soil of electric conductivity σ. Further, the potential satisfies boundary conditions at the anode surface, cathode surface and insulating surface. The insulating surface is the perfectly (not damaged) painted tank surface and the anodes interconnectivity. The boundary conditions are derived by taking into account the electric field $\mathbf{E}$ and the electric current density $\mathbf{J}$ in the domain, which are related by

$$\mathbf{E} = -\nabla u, \qquad \mathbf{J} = \sigma \mathbf{E}, \tag{7.2.1}$$

where σ represents the soil conductivity and u is the potential. For the insulating surface we have

$$\mathbf{n} \cdot \mathbf{J} = \sigma \mathbf{n} \cdot \mathbf{E} = -\sigma \mathbf{n} \cdot \nabla u. \tag{7.2.2}$$

Since no current flows through the insulating surface, this results in the condition

$$\frac{\partial u}{\partial n}(\mathbf{r}) = \mathbf{n} \cdot \nabla u(\mathbf{r}) = 0, \tag{7.2.3}$$

at the insulating surface. At the cathode surface, the relation between current density and potential difference is given by a polarisation curve

$$\mathbf{J} \cdot \mathbf{n} = -\sigma \frac{\partial u}{\partial n} = f_{\text{cathode}}(u), \tag{7.2.4}$$

with the general shape of $f_{\text{cathode}}(u)$ determined by the oxidation and reduction currents of Iron and Oxygen, [31, p. 13]. At the anode surface, perfect contact with the domain medium is assumed. Therefore either one of the following relations may be assumed at the anode surface:

$$u(\mathbf{r}) = u_{\text{anode}}, \tag{7.2.5a}$$

$$\sigma \mathbf{n} \cdot \nabla u = -\frac{I}{A}, \tag{7.2.5b}$$

$$\mathbf{J} \cdot \mathbf{n} = -\sigma \frac{\partial u}{\partial n} = f_{\text{anode}}(u). \tag{7.2.5c}$$

The first boundary condition expresses that each point of the anode surface has the same potential, see [77]. The second boundary condition expresses a homogeneously distributed current density flowing out of the anode surface. Here I is the total current flowing through the anode surface and A is the total

surface area , see [74]. The third condition is a more general polarisation curve for anodic surfaces used by [18, 49, 52, 58]. Boundary conditions involving polarisation curves are non-linear. That is, the relation between the potential and the current density is non-linear, but it can be linearised [49, 53]. For our model, we shall use (7.2.5a). Similarly, we also assume at the cathode $f_{\text{cathode}}(u) = u_{\text{cathode}}$. The current J flows from the anode to the cathode as depicted in the illustration Figure 7.3. The domain is the soil area between

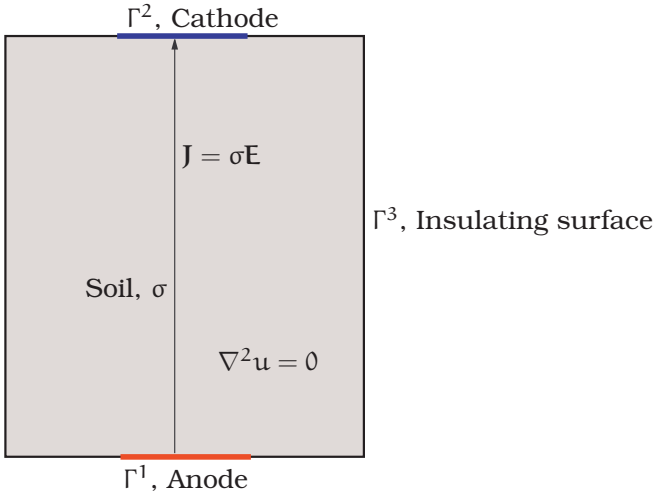

Figure 7.3: Schematic two dimension model for the ICCP of a water storage tank shown in Figure 7.2b.

the tank surface and the anodes interconnectivity. Apart from the anodes and the damaged parts, the rest of the painted surface is assumed to be a perfect insulator. Also, for simplicity we assume one anode and cathode. However, the solution process is still the same for more active regions. At the electrodes we consider the potential to be a prescribed value.

Thus, let Ω be the region between the tank surface and the anodes interconnectivity, Γ^1 the anode surface, Γ^2 the cathode surface and Γ^3 the insulating surface. Let $u(\mathbf{r})$ be the potential at a point $\mathbf{r} \in \Omega \subset \mathbb{R}^2$, then we have the following problem:

$$\begin{cases} \nabla^2 u(\mathbf{r}) = 0, & \mathbf{r} \in \Omega, \\ u(\mathbf{r}) = u_{\text{anode}}, & \mathbf{r} \in \Gamma^1, \\ u(\mathbf{r}) = u_{\text{cathode}}, & \mathbf{r} \in \Gamma^2, \\ \dfrac{\partial u}{\partial n}(\mathbf{r}) = 0, & \mathbf{r} \in \Gamma^3. \end{cases} \tag{7.2.6}$$

where $\mathbf{n}(\mathbf{r})$ is the unit normal vector at $\mathbf{r}$ pointing into Ω^c, see Figure 7.4.

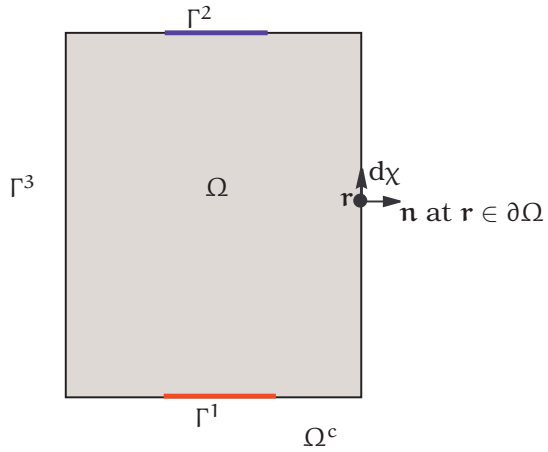

Figure 7.4: Diagram for a two dimensional mathematical model for an ICCP.

So we have the following BIE representation for the problem:

$$c(\mathbf{s})u(\mathbf{r}) = \int_\Gamma u(\mathbf{r})\frac{\partial v}{\partial n}(\mathbf{s};\mathbf{r})d\chi - \int_\Gamma \frac{\partial u}{\partial n}(\mathbf{r})v(\mathbf{s};\mathbf{r})d\chi \tag{7.2.7}$$

where $\Gamma = \Gamma^1 \cup \Gamma^2 \cup \Gamma^3$. As we will see in Section 7.3, the solution of the integral equation (7.2.7) together with the boundary conditions in (7.2.6) has rapid variation of the potential around the electrodes and the solution is smooth elsewhere. This is why the use of LDC is recommended for such a problem in order to use a grid that captures the activity well yet keeping the computational costs low. In the next section we present the application of LDC to solve this problem.

7.3 BEM-LDC for the ICCP problem

In this section we give an LDC formulation and solution for the ICCP potential problem model presented in Section 7.2. In practice the number of active regions p can be one, two, or even more, that is, several anodes and cathodes. Here we consider two active regions, that is $p = 2$, one anode and one cathode. The procedure for even more anodes and cathodes is the same and the gain in complexity for a given p is discussed on page 97. After solving a global coarse grid problem on the global boundary Γ, we formulate a local problem at each of the electrodes Γ^1_{active} and Γ^2_{active}, see Figure 7.5.

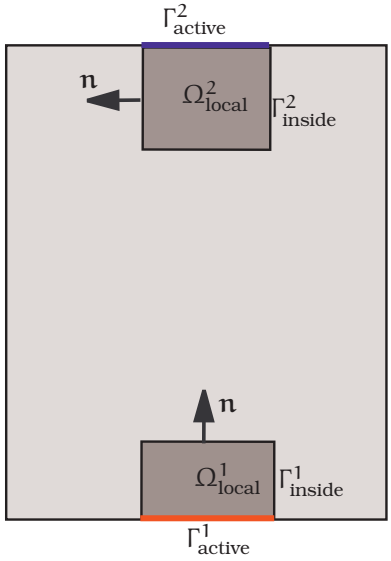

Figure 7.5: Global and local domains for a LDC formulation.

On each Ω^p_{local}, $p = 1, 2$, see Figure 7.5, we have the interior problem

$$\begin{cases} \nabla^2 u(\mathbf{r}) = 0, & \mathbf{r} \in \Omega^p_{\text{local}}, \\ u(\mathbf{r}) = u_{\text{electrode}}(\mathbf{r}), & \mathbf{r} \in \Gamma^p_{\text{active}}, \\ u(\mathbf{r}) = \tilde{g}(\mathbf{r}), & \mathbf{r} \in \Gamma^p_{\text{inside}}, \end{cases} \tag{7.3.1}$$

where $\tilde{g}(\mathbf{r})$ is a piecewise constant function given by

$$\tilde{g}(\mathbf{r}) = u_{\text{inside}}(\mathbf{r}_i), \quad \mathbf{r} \in \mathbf{r}^l_{\text{inside}} \subset \Gamma^p_{\text{inside}}, \quad \mathbf{r} = \mathbf{r}_i, \tag{7.3.2}$$

and

$$u_{\text{electrode}}(\mathbf{r}) = \begin{cases} u_{\text{anode}}, & \mathbf{r} \in \Gamma^1_{\text{active}}, \\ u_{\text{cathode}} & \mathbf{r} \in \Gamma^2_{\text{active}}. \end{cases} \tag{7.3.3}$$

The LDC process is what has been described in Section 6.2. Here we only add in the twist of having more than one local problem. So we have the following process:

(i) Initialisation: we solve the global coarse grid problem on Γ using a grid of

size L to obtain the initial solution $\mathbf{q}_0^L$, $\mathbf{u}_0^L$;

$$\frac{1}{2}u_{0,i}^L = \sum_{j=1}^{N} u_{0,j}^L \int_{\Gamma_j^L} \frac{\partial \nu}{\partial n}(\mathbf{r}_i;\mathbf{r}(\chi))d\chi - \sum_{j=1}^{N} q_{0,j}^L \int_{\Gamma_j^L} \nu(\mathbf{r}_i;\mathbf{r}(\chi))d\chi. \tag{7.3.4}$$

(ii) For each local problem, after discretisation of Γ_{local}^p into $\Gamma_{\text{local}}^{p,l} = \Gamma_{\text{inside}}^{p,l} \cup \Gamma_{\text{active}}^{p,l}$, compute $u(\mathbf{r})$ on $\Gamma_{\text{inside}}^{p,l}$ using the global coarse grid solution and the integral relation

$$u_{\text{inside},i}^{p,l} = \sum_{j=1}^{N} u_j^L \int_{\Gamma_j^L} \frac{\partial \nu}{\partial n}(\mathbf{r}_i;\mathbf{r}(\chi))d\chi - \sum_{j=1}^{N} q_j^L \int_{\Gamma_j^L} \nu(\mathbf{r}_i;\mathbf{r}(\chi))d\chi, \quad \mathbf{r}_i \in \Gamma_{\text{inside}}^p. \tag{7.3.5}$$

(iii) Now we have Dirichlet boundary conditions on Γ_{inside}^p. On Γ_{active}^p the boundary conditions are as given on the global Γ since $\Gamma_{\text{active}}^p \subset \Gamma$, $p = 1,2$. So next is to solve the local problems on Γ_{local}^p:

$$\begin{aligned}\frac{1}{2}u_{\text{local},i}^{p,l} &+ \sum_j u_{\text{active},j}^{p,l} \int_{\Gamma_{\text{active},j}^l} \frac{\partial \nu}{\partial n}(\mathbf{r}_i;\mathbf{r}(\chi))\,d\chi \\ &+ \sum_j u_{\text{inside},j}^{p,l} \int_{\Gamma_{\text{inside},j}^l} \frac{\partial \nu}{\partial n}(\mathbf{r}_i;\mathbf{r}(\chi))\,d\chi = \\ &\sum_j q_{\text{active},j}^{p,l} \int_{\Gamma_{\text{active},j}^l} \nu(\mathbf{r}_i;\mathbf{r}(\chi))\,d\chi + \sum_j q_{\text{inside},j}^{p,l} \int_{\Gamma_{\text{inside},j}^l} \nu(\mathbf{r}_i;\mathbf{r}(\chi))\,d\chi.\end{aligned} \tag{7.3.6}$$

Note that the p problems are independent of one another and can be solved in parallel.

(iv) To compute the defect: we now have a better solution on Γ_{active}^p, $p = 1,2$ and

$$u_{\text{best},j}^L = \begin{cases} u_{c,j}^L, & \Gamma_j^L \subset \Gamma_c, \\ u_{\text{active},j}^{p,l}, & \Gamma_j^L \subset \Gamma_{\text{active}}^p, \end{cases} \tag{7.3.7}$$

$$q_{\text{best},j}^L = \begin{cases} q_{c,j}^L, & \Gamma_j^L \subset \Gamma_c, \\ q_{\text{active},j}^{p,l}, & \Gamma_j^L \subset \Gamma_{\text{active}}^p. \end{cases} \tag{7.3.8}$$

Using the fine grid solution, we approximate the defect d_i for each node of

the global coarse grid as follows. We compute

$$d_{ij}^L \approx \begin{cases} \sum_{p=1}^{2} \left(q^{p,l}_{\text{active},j} \int_{\Gamma_j^L} \nu(\mathbf{r}_i;\mathbf{r}(\chi))\,d\chi - \right. \\ \qquad \left. \sum_k q^{p,l}_{\text{active},j_k} \int\limits_{\Gamma^{p,l}_{\text{active},j_k}} \nu(\mathbf{r}_i;\mathbf{r}(\chi))\,d\chi \right), & \Gamma_j^L \subset \Gamma^p_{\text{active}}, \\ 0 & \Gamma_j \subset \Gamma_c. \end{cases} \tag{7.3.9}$$

Here $\bigcup_k \Gamma^{p,l}_{\text{active},j_k} = \Gamma_j^L$, see Figure 6.4. Then

$$d_i^L = \sum_j d_{ij}^L \tag{7.3.10}$$

for $\Gamma_j^L \subset \Gamma_{\text{active}}$. The defect d_i has contributions from all the p active regions hence the summation for $p = 1, 2$, in (7.3.9).

(v) We now do the defect correction: the defect (7.3.10) is added to the right hand side of the coarse grid equation and then we solve for the updated global coarse grid solution $\mathbf{u}_1^L$, $\mathbf{q}_1^L$ on the global coarse grid,

$$\frac{1}{2}u_{1,i}^L = \sum_{j=1}^{N} u_{1,j}^L \int_{\Gamma_j^L} \frac{\partial \nu}{\partial n}(\mathbf{r}_i;\mathbf{r}(\chi))d\chi - \sum_{j=1}^{N} q_{1,j}^L \int_{\Gamma_j^L} \nu(\mathbf{r}_i;\mathbf{r}(\chi))d\chi + d_i^L. \tag{7.3.11}$$

(vi) Go back to step (ii) with $\mathbf{u}^L$ replaced by $\mathbf{u}_1^L$ and $\mathbf{q}^L$ replaced by $\mathbf{q}_1^L$.

To test this LDC formulation for more than one local problem we solve the following problem, whose continuous solution is known. We consider the function

$$f(\mathbf{r}) = \log(r_1) + \log(r_2) \tag{7.3.12}$$

where

$$r_1 = \|\mathbf{r} - \mathbf{s}_1\|_2, \quad r_2 = \|\mathbf{r} - \mathbf{s}_2\|_2 \tag{7.3.13}$$

and $\mathbf{s}_1$, $\mathbf{s}_2$ are source points just outside the square. Then we solve the problem

$$\begin{cases} \nabla^2 u(\mathbf{r}) = 0, & \mathbf{r} \in \Omega = [0\ 1] \times [0\ 1], \\ q(\mathbf{r}) = \dfrac{\partial f}{\partial n}(\mathbf{r}), & \mathbf{r} \in \Gamma. \end{cases} \tag{7.3.14}$$

The solution to (7.3.14) is shown in Figure 7.6.

Clearly the solution has two small regions, one on the lower side and another on the upper side of the square where u varies rapidly. In Figures 7.7 and 7.8

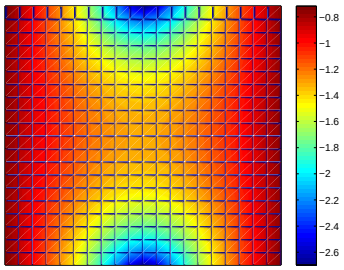

Figure 7.6: Profile of the potential u inside a unit square due to problem (7.3.14). The source points s_1 and s_2 are $(0.5, -0.02)$ and $(0.5, 1.02)$ respectively.

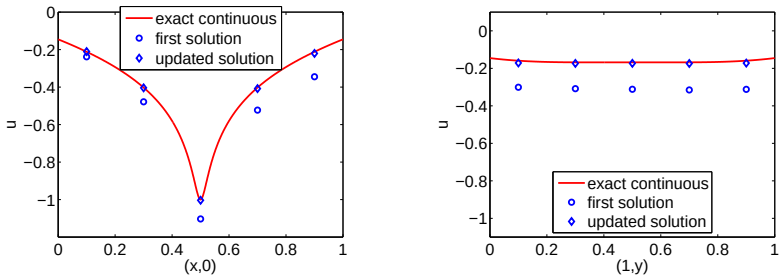

(a) Solutions on $y = 0$. (b) Solutions on $x = 1$.

Figure 7.7: LDC solutions to problem 7.3.14 on a unit square after the first iteration.

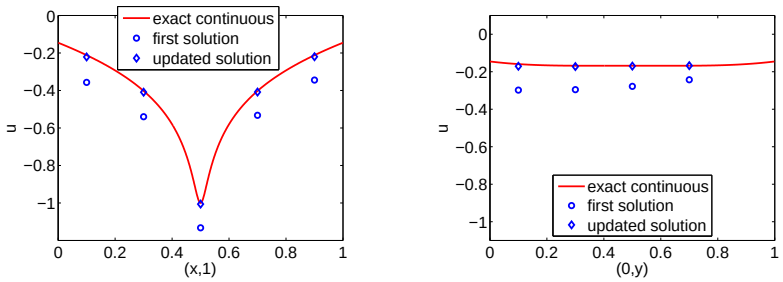

(a) Solutions on $y = 1$. (b) Solutions on $x = 0$.

Figure 7.8: LDC solutions to problem 7.3.14 on a unit square after the first iteration.

we have the BEM solutions to the problem using local defect corrections with a local problem at each active region.

The updated solution agrees with the continuous solution better than the initial problem as expected. We can therefore proceed to solve the ICCP problem whose continuous solution is not known. Once we have the potential u in Ω we use (7.2.1) to compute the electric field in Ω. Figure 7.2.6 shows the potential and the electric field lines for the ICCP potential problem (7.2.6) with $u_{\text{anode}} = 1$ and $u_{\text{cathode}} = -u_{\text{anode}}$. Now for the ICCP problem we let

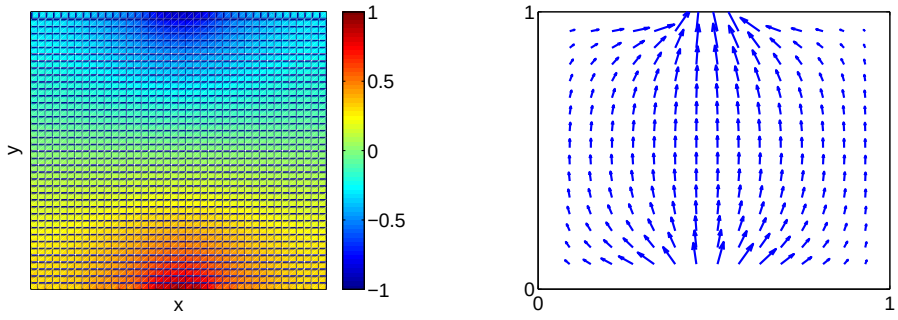

(a) Potential inside Ω.

(b) Electric field lines inside Ω.

Figure 7.9: The potential and field lines of the ICCP model 7.2.6 in a region inside Ω where $u_{\text{anode}} = 1$ and $u_{\text{cathode}} = -u_{\text{anode}}$.

$$\Gamma^1_{\text{active}} = \{(x, y) : x \in [0.4,\ 0.6], y = 0\},$$
$$\Gamma^2_{\text{active}} = \{(x, y) : x \in [0.4,\ 0.6], y = 1\}.$$

Then we set, see Figure 7.10,

$$\Omega^1_{\text{local}} = \{(x, y) \in [0.4,\ 0.6] \times [0,\ 0.4]\},$$
$$\Omega^2_{\text{local}} = \{(x, y) \in [0.4,\ 0.6] \times [0.6,\ 1]\}.$$

LDC solutions for the problem are shown in Figures 7.11 and 7.12 .

Since we do not have the exact continuous solution to (7.3.1) we cannot compute the actual error. However, assuming that the solution converges to a fixed point $\mathbf{x}_{\text{fixed}}$, we can then compute the errors $\|\mathbf{x}_i - \mathbf{x}_{\text{fixed}}\|_\infty$ where $\mathbf{x}_i$ is the solution after the i-th iteration to demonstrate how fast we reach the fixed point. The results are shown in Figure 7.13. The results indeed show that one or two iterations is just enough.

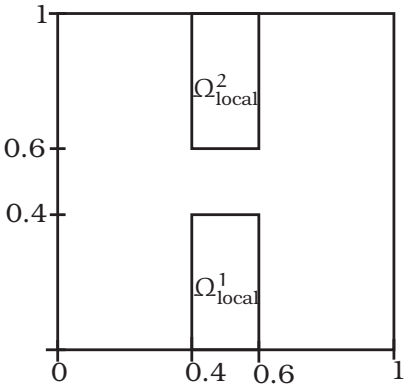

Figure 7.10: Domain demarcations for the LDC solution of the model problem.

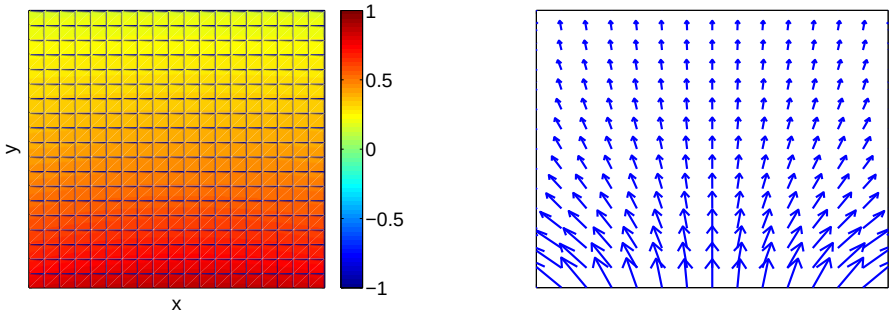

(a) Solution of local problem on Ω^1_{local}.

(b) Field lines due to potential of local problem solution on Ω^1_{local}.

Figure 7.11: LDC solutions to first local problem.

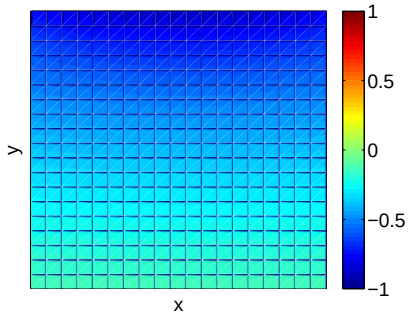

(a) Solution of local problem on Ω^2_{local}.

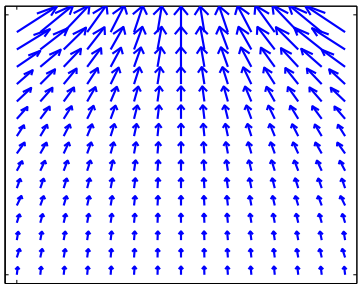

(b) Field lines due to potential of local problem solution on Ω^2_{local}.

Figure 7.12: LDC solutions to the second local problem.

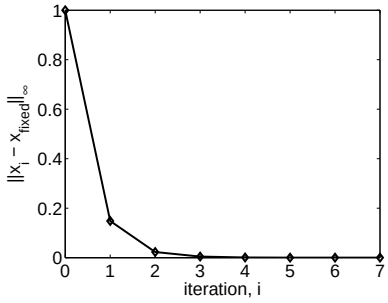

Figure 7.13: Variation of the global coarse grid solution error from the fixed point solution during iteration. The fine grid is of size $l = L/9$ and the global coarse grid of size $L = 0.2$.

Bibliography

[1] M. J. H. Anthonissen, *Local Defect Correction Techniques: Analysis and Application to Combustion*, Ph.D. thesis, Eindhoven University of Technology, Eindhoven, The Netherlands, 2001.

[2] D. N. Arnold and W. L. Wendland, *On the asymptotic convergence of collocation methods*, Math. Comp. **41** (1983), 349 – 381.

[3] D. N. Arnold and W. L. Wendland, *The convergence of spline collocation for the strongly elliptic equations on curves*, Numer. Math. **47** (1985), 317 – 341.

[4] U. M. Ascher, R. M. M. Mattheij, and Robert D. Russel, *Numerical Solution of Boundary Value Problems for Ordinary Differential Equations*, SIAM, Philadelphia, 1995.

[5] K. E. Atkinson, *The numerical solution of integral equations of the second kind*, Cambridge University Press, 1997.

[6] T. J. Baker, *Mesh adaptation strategies for problems in fluid dynamics*, Finite Elements Analysis and Design **25** (1997), 243 – 273.

[7] W. Cao, W. Huang, and R. D. Russel, *A study of monitor functions for two dimensional adaptive mesh generation.*, SIAM J. Sci. Computing. **20 No. 6** (1999), 1978–1994.

[8] C. Carsten and E. P. Stephan, *A posteriori error estimates for boundary element methods.*, Mathematics of Computation. **64** (1995), 483–500.

[9] G. Chen and J. Zhou, *Boundary Element Methods*, Academic press, London, San Diego, 1992.

[10] K. Chen, *Error equidistribution and mesh adaptation*, SIAM Journal on Scientific Computing **15, No. 4** (1994), 798–818.

[11] C. Constanda, *On the solution of the Dirichlet problem for the two-dimensional laplace equation.*, Proceedings of the American Mathematical Society. **, Vol. 119, No. 3** (Nov., 1993), 877–884.

[12] M. Costabel and M. Dauge, *Invertibility of the biharmonic single layer potential operator.*, Inter Equat Oper Th **24** (1996), 46–67.

[13] M. Costabel, M. Dauge, and S. Nicaise, *Boundary value problems and integral equations in nonsmooth domains*, Marcel Decker, INC, New York, 1995.

[14] T. A. Cruse, *Numerical solutions in three dimensional elastostatics.*, Int. J. Solids Structures. **5** (1969), 1259 – 1274.

[15] P. J. Davis and P. Rabinowitz, *Numerical integration*, Blaisdell Publishing Company, Waltham, 1967.

[16] W. Dijkstra, *Condition Numbers in the Boundary Element Method: Shape and Solvability*, Technische Universiteit Eindhoven, Eindhoven, 2008.

[17] W. Dijkstra, G. Kakuba, and R. M. M. Mattheij, *Condition numbers and local errors in the boundary element method*, In BOUNDARY ELEMENT METHODS IN ENGINEERING AND SCIENCES (Imperial College Press London, 2010), M H Aliabadi and P H Wen, COMPUTATIONAL AND EXPERIMENTAL METHODS IN STRUCTURES **4** (2010), 412.

[18] P. Doig and P.E.J. Flewitt, *A finite difference numerical analysis of galvanic corrosion for semi-infinite linear coplanar electrodes*, Journal of The Electrochemical Society **126(12)** (1979), 2057–2063.

[19] P. J. J. Ferket and A. A. Reusken, *Further Analysis of the Local Defect Correction Method*, Computing **56** (1996), 117 – 139.

[20] I. Fredholm, *Sur une classe d'equations fonctionnelles*, Acta Numer. **27** (1903), 365 – 390.

[21] M. Graziadei, *Using local defect correction for laminar flame simulation*, Ph.D. thesis, Eindhoven University of Technology, 2004.

[22] M. Guiggiani and F. Lombardi, *Self-adaptive boundary elements with* h*-Hierachical shape functions.*, Advances in Engineering Software, Special issue on error estimates and adaptive meshes for FEM/BEM. **15** (1992), 269–277.

[23] W. Hackbusch, *Local defect correction method and domain decomposition technique*, Computing [Suppl.] **5** (1984), 89 – 113.

[24] W. Hackbusch, *Integral Equations: Theory and Numerical Treatment*, Birkhauser Verlag, Basel, 1995.

[25] M. T. Heath, *Scientific computing, an introductory survey*, McGraw Hill, New York, 2002.

[26] G.C. Hsiao and W. L. Wendland, *A finite element method for some integral equations of the first kind.*, J. Math. Anal. Appl. **58** (1977), 449 – 481.

[27] M.A. Jaswon, *Integral equation methods in potential theory i, Series a*, vol. 275, 1963.

[28] M.A. Jaswon and G. Symm, *Integral Equation Methods in Potential Theory and Elastostatics*, Academic Press, London, 1977.

[29] A. B. Jorge, G. O. Ribero, and T. S. Fischer, *New approaches for error estimation and adaptivity for 2d potential boundary element methods*, Int. J. Numer. Meth. Engng **56** (2003), 177 – 144.

[30] K. Jorgens, *Linear Integral Operators*, Pitman Advanced Publishing Program, Boston, London, Melbourne, 1982.

[31] G. Kakuba, *The Impressed Current Cathodic Protection System*, Master's thesis, Eindhoven University of Technology, Eindhoven, The Netherlands, 2005.

[32] G. Kakuba and R. M. M. Mattheij, *Convergence analysis of Local Defect Correction for the BEM*, Advances in Boundary Integral Methods. Proceedings of the sixth UK conference on Boundary Integral Methods **15** (2007), 251 – 261.

[33] G. Kakuba and R. M. M. Mattheij, *Local errors in the constant and linear boundary element method for potential problems*, Advances in boundary element techniques X. Proceedings of the 10th International conference (2009), 367 – 374.

[34] G. Kakuba, R. M. M. Mattheij, and M. J. Anthonissen, *Local Defect Correction for the Boundary Element Method*, Computer Modeling in Engineering Sciences **15** (2006), 127 – 135.

[35] J. T. Katsikadelis, *Boundary elements theory and applications*, Elsevier, 2002.

[36] O. D. Kellogg, *Foundations of potential theory*, Springer, Berlin, 1929.

[37] E. Kita and N. Kamiya, *Adaptive mesh refinement in boundary element method, an overview*, Engineering Analysis with Boundary Elements **25** (2001), 479–495.

[38] R. Kress, *Linear integral equations*, Springer-Verlag, 1989.

[39] E. Kreyszig, *Advanced Engineering Mathematics*, John Wiley and Sons, New York, 1999.

[40] D. H. Kroon and M. Urbas, *Cathodic protection of above ground storage tank bottoms*, Corrpro Companies, Inc and Harco technologies corporation respectively. **http://www.corrpro.co.uk/pdf/TechnicalPapers/40CP Cathodic protection of above ground storage tank bottoms.pdf** (2010 October 7).

[41] A. Kufner and J. Kadlec, *Fourier series*, London: Iliffe Books, 1971.

[42] V. D. Kupradze, *Potential methods in theory of elasticity*, Daniel Davy, New York, 1965.

[43] P. K. Kythe and M. R. Schferkotter, *Handbook of computational methods for integration*, Chapman & Hall/CRC, Florida, 2005.

[44] M. T. Liang, J. T. Chen, and S. S. Yang, *Error estimation for boundary element method.*, Engineering analysis with boundary elements. **23** (1999), 257–265.

[45] S. Liapis, *A review of error estimation and adaptivity in the boundary element method.*, Engineering analysis with boundary elements. **14** (1994), 315–323.

[46] Z. Liu, M. D. Thoreson, A. V. Kildishev, and V. M. Shalaev, *Translation of nanoantenna hot spots by a metal-dielectric composite superlens*, Applied physics letters **95** (2009), 033114.

[47] American Water Works Association MANUAL M42, *Steel water storage tanks*, American Water Works Association, 1999.

[48] R. M. M. Mattheij, S. W. Rienstra, and J. H. M. ten Thije Boonkkamp, *Partial differential equations: Modeling, analysis, computation*, SIAM, Philadelphia, 2005.

[49] E. McCafferty, *Distribution of potential and current in circular corrosion cells having unequal polarisation parameters*, Journal of The Electrochemical Society **124(12)** (1977), 1869–1878.

[50] S. D. Mikhlin, *Integral equations*, Pregamon Press, Oxford, 1957.

[51] R. Minero, M. J. H. Anthonissen, and R. M. M. Mattheij, *A Local Defect Correction Technique for Time-Dependent Problems*, Numerical Methods for Partial Differential Equations **22** (2006), 128 – 144.

[52] R. Morris and W. Smyrl, *Galvanic interactions on periodically regular heterogeneous surfaces*, AIChE Journal **34(5)** (1988), 723–732.

[53] R. Morris and W. Smyrl, *Current and potential distribution in thin electrolyte layer galvanic cells*, Journal of The Electrochemical Society **136(11)** (1989), 3229–3236.

[54] P. Mund, E. P. Stephan, and J. W. Hannover, *Two-level mthods for the single layer potential in* $\setminus^3$., Computing **60** (1998), 243 – 266.

[55] N. I. Muskhelishvili, *Some basic problems of mthematical theory of elasticity*, Noordholl, Holland, 1953.

[56] E. T. Ong and K. M. Lim, *Three-dimensional singular boundary elements for corner and edge singularities in potential problems.*, Engineering analysis with Boundary Elements **29** (2005), 175–189.

[57] F. Paris and J. Canas, *Boundary Element Method: Fundamentals and Applications*, Oxford University Press, Oxford, 1997.

[58] R. Oltra Ph. Bucaille and T. Warner, *Theoretical and experimental studies of galvanic corrosion between aluminium and Al-Cu alloys*, Materials Science Forum **242** (1997), 207–212.

[59] C. Pozrikidis, *Boundary integral and singularity methods for linearised viscous flow*, Cambridge University Press, 1992.

[60] C. Pozrikidis, *A Practical Guide to Boundary Element Methods with the software BEMLIB*, Chapman & Hall/CRC, London, 2002.

[61] P. Pucci and J. Serrin, *The maximum principle*, Birkhauser Verlag AG, 2007.

[62] C. G. Reimbert and A. A. Minzoni, *Effect of radiation losses on hotspot formation and propagation in microwave heating*, IMA Journal of Applied Mathematics **57** (1996), 165 – 179.

[63] F. J. Rizzo, *An integral equation approach to boundary-value problems of classical elastostatics.*, Q. Applied Math. **25** (1967), 83 – 95.

[64] J. Saranen and W. L. Wendland, *On the asymptotic convergence of collocation methods with spline functions of even dgree*, Math. Comp. **45** (1985), 91 – 108.

[65] K. Schimmanz and A. Kost, *Formulation of mixed elements for the 2d-bem*, The International Journal for Computation and Mathematics in Electrical and Electronic Engineering **23 No. 4** (2004), 866–875.

[66] H. Schulz and O. Steinbach, *A new a posteriori error estimator in adaptive direct boundary element methods: the Dirichlet problem*, CALCOLO Springer-Verlag **37** (2000), 79–96.

[67] V. Sladek, J. Sladek, and M. Tanaka, *Numerical integration of logarithmic and nearly logarithmic singularity in bems*, Applied mathematical modelling **25** (2001), 901 – 992.

[68] I. H. Sloan, *Error analysis of boundary integral methods*, Acta Numerica (1991), 287–339.

[69] C. Somigliana, *Sopra l'equilibrio di un corpo elastico isotrope*, Il Nuovo Ciemento (1886), 181–185.

[70] H. Strese, *Remarks concerning the boundary element method in potential theory*, Appl. Math. Modelling **8** (1984), 40 – 44.

[71] T. Strouboulis and K. A. Hague, *Recent experiences with error estimation and adaptivity. part i: Review of error estimators for scalar elliptic problems*, Comp. Meth. Appl. Mech. Eng. **97** (1992), 399 – 436.

[72] T. Strouboulis and K. A. Hague, *Recent experiences with error estimation and adaptivity. part ii: Error estimation for h-adaptive approximation on grids of triangles and quadrilaterals.*, Comp. Meth. Appl. Mech. Eng. **100** (1992), 359 – 430.

[73] A. H. Stroud and D. Secrest, *Gaussian quadrature formulas*, Prentice-Hall, Englewood Cliffs, NJ, 1966.

[74] W. Sun and K. M. Liu, *Numerical solution of cathodic protection systems with nonlinear polarisation curves*, Journal of The Electrochemical Society **147(10)** (2000), 3687–3690.

[75] G. T. Symm, *Integral equation methods in potential theory - ii, Series a.*, Proc. Roy. Soc. Lond. **275** (1963), 33 – 46.

[76] R. Vodicka and V. Mantic, *On invertibility of elastic single-layer potential operator*, Journal of Elasticity **74** (2004), 147 – 173.

[77] J. T. Waber, *Mathematical studies on galvanic corrosion*, Journal of The Electrochemical Society **101(6)** (1954), 271–276.

[78] S. P. Walker and R. T. Fenner, *Treatment of corners in BIE analysis of potential problems.*, International journal for numerical methods in engineering. **28** (1989), 2569–2581.

[79] K. Wang, *Bem simulation for glass parisons*, Ph.D. thesis, Eindhoven University of Technology, 2002.

[80] J. A. Whitehead, *Fluid models of geological hotspots*, Annual review of Fluid Mechanics **20** (1988), 61 – 68.

[81] G. M. Wing, *A primer on integral equations of the first kind: the problem of deconvolution and unfolding.*, SIAM, Baltimore, 1991.

[82] D. J. Wu, Y. Cheng, and X. J. Liu, *Hot spots induced near-field enhancements in au nanoshell and au nanoshell dimer*, Applied Physics B: Lasers and Optics **97, Number 2** (2009), 497 – 503.

Index

Summary

Adaptive gridding methods are of fundamental importance both for industry and academia. As one of the computing methods, the *Boundary Element Method* (BEM) is used to simulate problems whose fundamental solutions are available. The method is usually characterised as *constant elements* BEM or *linear elements* BEM depending on the type of interpolation used at the elements. Its popularity is steadily growing because of its advantages over other numerical methods most important of which being that it only involves obtaining data at the boundary and computation of the solution in the domain is merely a case of post processing through the use of an identity. This results in the reduction of the problem dimension by unity.

Although there is a reduction in dimension when we use BEM, the method usually results in full matrices which can be expensive to solve. This makes the method costly for problems that require very fine grids like those with hot spots as in the example of *impressed current cathodic protection systems* (ICCP). The BEM is a global method in nature in that the solution in one node depends on the solutions in all the other nodes of the grid. Hence an error in one node can pollute the solution in all the other nodes.

In this thesis, we first focus our attention on defining and studying both the *local* and *global errors* for the BEM. This is not a completely new study as the literature suggests, however, our approach is different. We use the basic foundations of the the method to define the errors. Since the method is a global method, first we use the interpolation error on each element to define what we have called a *sublocal error*. Then using the sublocal error we have defined the local error. Understanding the local errors enabled us study the global error. Theoretical and numerical results show that these errors are second order in grid size for both the constant and linear element cases.

Then, having explored errors, we study a method for adaptive grid refinement for the BEM. Rather than using a truly nonuniform grid, we present a method called *local defect correction* (LDC) that is based on local uniform grid refinement. This method is already developed and documented for other numerical methods such as finite difference and finite volume methods but not for BEM.

In the LDC method, the discretization on a *composite grid* is based on a combination of standard discretizations on several uniform grids with different grid sizes that cover different parts of the domain. At least one grid, the uniform *global coarse grid*, should cover the entire boundary. The size of the global coarse grid is chosen in agreement with the relatively smooth behaviour of the solution outside the hot spots. Then several uniform *local fine grids* each of which covers only a (small) part of the boundary are used in the hot spots. The grid sizes of the local grids are chosen in agreement with the behaviour of the continuous solution in that part of the boundary.

The LDC method is an iterative process whereby a basic global discretisation is improved by local discretisations defined in subdomains. The update of the coarse grid solution is achieved by adding a *defect correction* term to the right hand side of the coarse grid problem. At each iteration step, the process yields a discrete approximation of the continuous solution on the corresponding composite grid. We have shown how this discretisation can be achieved for the BEM. We apply the discretisation to an academic example to demonstrate its implementation and later show how to use it for an application as the ICCP system. The results show that it is a cheaper method than solving on a truly composite grid and converges in a single step.

Curriculum vitae

The author of this thesis was born in Rwengoma, Uganda. He finished his high school at St. Leo's College, Kyegobe. He later joined Makerere University where he graduated in June 2001 with a Bachelor of Science degree in the subjects Maths, Physics and Education. In 2002 he joined and worked at the Department of Mathematics at Makerere University as a teaching assistant until September 2003 when he joined Eindhoven University of Technology in the Netherlands to pursue a masters course. In August 2005 he graduated cum laude as a master of science in computational science and engineering. His master's thesis, written under the supervision of prof.dr.ir. R. M. M. Mattheij and dr. ir. M.J. H. Anthonissen was titled *The impressed current cathodic protection system*.

Late in 2005, Godwin returned to the Netherlands, and started working as a PhD student in the Centre for Analysis and Scientific Computing group at Eindhoven University of Technology under the supervision of prof.dr. R. M. M. Mattheij, the group's chair for scientific computing. His research on boundary element methods has lead to this thesis.

Godwin is at the moment working as an assistant lecturer in the department of mathematics at Makerere University, Kampala.